Hybrid Electrospun Transcatheter Aortic Heart Valves for Tissue Engineering Applications

Jade Taylor
Submitted for the degree: MSc Biomedical Engineering

University of Cape Town

December 2021

Department of Human Biology: Division of Biomedical Engineering

In association with

Cardiovascular Research Unit

Supervisor: Professor Deon Bezuidenhout

DECLARATION

I, *Jade Taylor*, hereby declare that the work on which this dissertation/thesis is based is my original work (except where acknowledgements indicate otherwise) and that neither the whole work nor any part of it has been, is being, or is to be submitted for another degree in this or any other university.

I empower the university to reproduce for the purpose of research either the whole or any portion of the contents in any manner whatsoever.

Signature: Signed by candidate

Date: …….13/09/2022……..

Abstract

Bioprosthetic and mechanical heart valves are suboptimal due to both calcific degeneration and the need for lifelong anticoagulation treatment. Tissue engineering (TE) has the potential to overcome these and other shortcomings by providing viable valves capable of growth, remodelling, and repair. Electrospinning has gained popularity as one of the methods used to create porous, three-dimensional TE scaffolds that mimic the extracellular matrix (ECM) and allow for cellular ingrowth into the construct. The aim of the current study was to investigate the feasibility of producing electrospun scaffolds with both degradable and reinforcing, non-degradable, fibres to improve mechanical properties and allow for improved control over degradation rates to avoid catastrophic valve failure due to premature valve degradation and inadequate tissue ingrowth.

Degradable (DegraPol15®; DP15), non-degradable (Pellethane®), and hybrid (dual) scaffolds (± 1:1 mass ratio of DP15 and Pellethane®) were electrospun and characterised morphologically and mechanically before and after various periods of hydrolytic degradation. Transcatheter aortic heart valves (23 mm) with DegraPol®, Pellethane®, and hybrid leaflets respectively, were fabricated by means of bonding and suturing into balloon expandable transcatheter stents and tested in vitro at left heart conditions to determine hydrodynamic performance and durability.

Ultimate tensile strength (UTS) decreased as electrospun scaffolds degraded, with DegraPol® exhibiting a more rapid decrease in UTS than hybrid scaffolds after six weeks of incubation (57 ± 5% vs 24 ± 10%). The same trend was seen in the distinct reduction of maximum elongation of the scaffolds (35 ± 5% and 18 ± 8 %) . Pellethane® exhibited a reduction in both UTS and % elongation close to that of hybrid scaffolds (27 ± 6% and 13 ± 6% respectively) with the Young's modulus of all scaffolds remaining nearly unaffected by the hydrolytic degradation. Hybrid scaffolds had suture retention strength similar to DegraPol®, however, hybrid scaffolds unexpectedly had the lowest tear strength (4.7 ± 0.29 N/mm) with Pellethane® scaffolds displaying superior strength in both tear strength (13.53 ± 0.35 N/mm) and suture retention strength (16.13 ± 0.8 N/mm longitudinally).

In terms of valve hydrodynamic performance, all valves had an average effective orifice area (EOA) larger than 2 cm^2 and pressure gradients lower than 8mmHg with no significant difference between the groups in either of these measurements. Pellethane® and hybrid valves both had lower regurgitation fractions than DegraPol® valves (30.3 ± 5.3% 28.6 ± 1.5% and 56.4 ± 4.4% for Pellethane®, hybrid and DegraPol® valves respectively), with high (>20%) values resulting from inherent material porosity shown by water permeability tests. With regards to valve durability, DegraPol® valve leaflets failed before adequate testing conditions could be reached while Pellethane® valves lasted for ±40 million cycles and were removed before failure. Hybrid valves lasted for an intermediate average of 7.0 ± 2.3 million cycles at 100 mmHg.

The study shows that the polymers can be dual spun from degradable and non-degradable polymers to produce hybrid scaffolds which can potentially be used, with further development, in tissue engineering applications such as heart valves when the degradable component may lack sufficient physical strength.

Visual Abstract

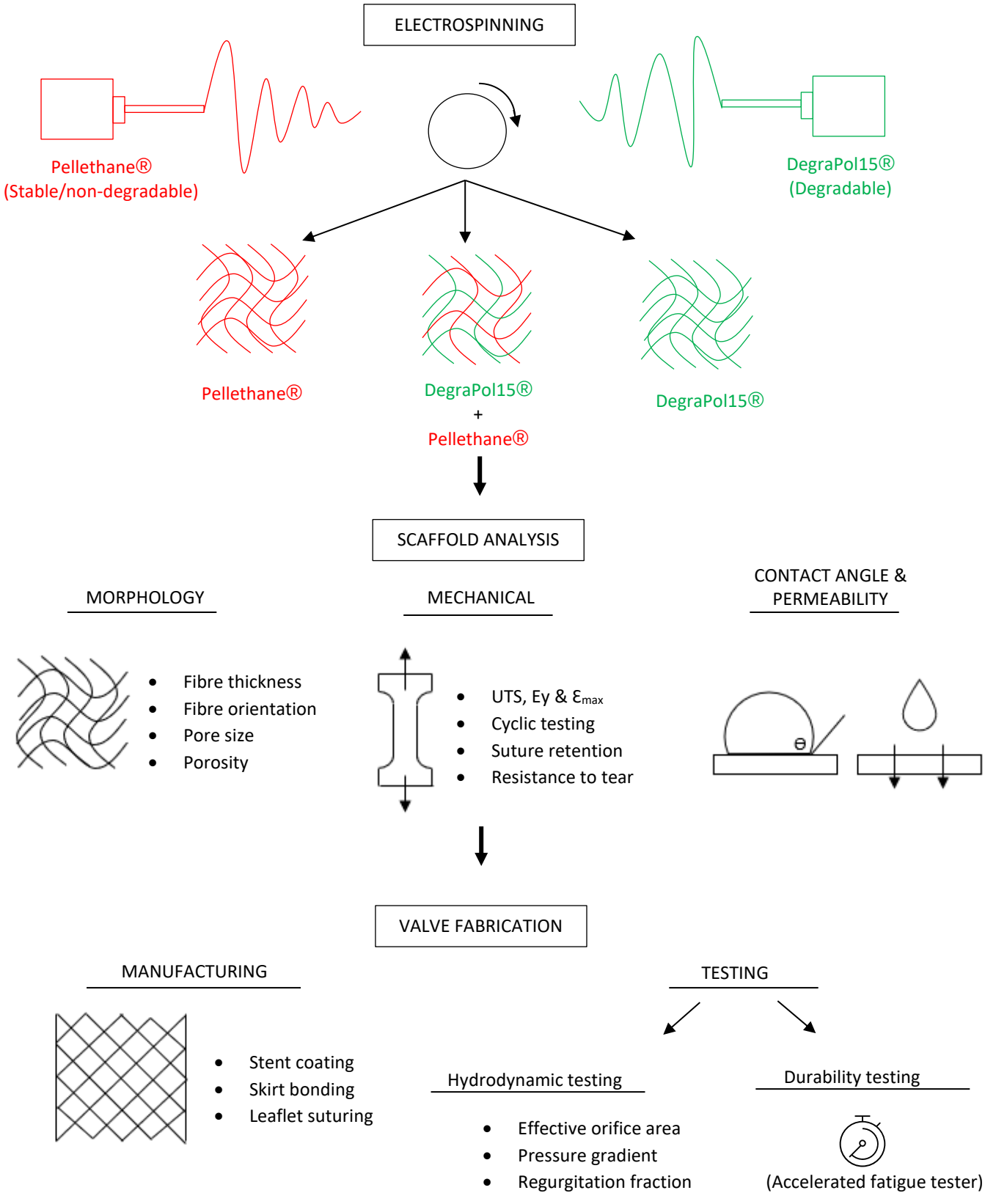

Acknowledgements

Firstly, I would like to thank Professor Deon Bezuidenhout for his guidance and mentorship over the past two years. His passion, enthusiasm and positivity throughout this journey has been a driving force and will forever be appreciated.

A special thanks to my incredible father, Byron, and mother, Pauli, for the sacrifices they have made for me to be here. I am forever grateful for their support and encouragement throughout my academic career. Thanks to my dearest partner, Stephen, for encouraging me to undertake this journey and for supporting me every step of the way.

I would like to thank the following incredible people for the hand they had in making this research possible – Anel Oosthuysen and Jandré de Villiers for patiently providing lab equipment training. Robyn Smith for selflessly conducting all pulse duplicator tests on valve prototypes and for sharing some of his vast knowledge of the field with me. Gerhard Krause, Carmen Gaffley, and Cameron Hume for keeping the moral in the laboratory high.

I would like to extend a special thanks to Straight Access Technologies (SAT) for providing the TAVR stents used during this project and to ab medica S.p.A for donating the DegraPol® material for this project.

Another special thanks to Rosslee Guess for being a sounding board and paving the way, providing me with vital information on both electrospinning and valve fabrication, without which this project would not have been possible.

I would also like to acknowledge the University of Cape Town for making funds available to support this degree.

Table of contents

Page

List of figures

Page

List of tables

Page

List of symbols

A	Area
AO	Aortic pressure
D	Diameter
Ø	Diameter
d	Thickness
F	Load
Ey	Young's modulus
k	Permeability
L	Length
m	Mass
n	Sample size
OI	Orientation index
P	Pore
p	Pressure
t	Time
V	Volume
VE	Ventricular pressure
W	Width
Q	Flow
°	Degree
△	Difference
Ɛ	Elongation
µ	Dynamic viscosity
ρ	Density

List of abbreviations

AC	Alternating current
AS	Aortic stenosis
ASTM	American society for testing and materials
AVD	Aortic valve disease
AVL	Aortic valve leaflet
BDO	Butanediol
CAVS	Calcific aortic valve stenosis
CVD	Cardiovascular disease
DC	Direct current
DI	Deionised
DMAC	Dimethylacetamide
DMF	Dimethylformamide
ECM	Extracellular matrix
EOA	Effective orifice area
FDA	Food and drug administration
HFIP	Hexafluoro isopropanol
HVTE	Heart valve tissue engineering
ISO	International standardisation organisation
LMIC	Low- and middle-income country
MDI	Methylene-di-phenyldiisocyanate
MR	Mitral Regurgitation
NSF	National Science Foundation
PBS	Phosphate-buffered saline
PCL	Polycaprolactone
PDLLA	Poly(D,L-lactic acid)
PEO	Polyethylene Oxide
PGA	3-Phosphoglyceric acid
PHA	Polyhyroxyalkanoate
PHO	poly-3-hydroxyoctanoate
PLA	polylactic acid
PLGA	polylactide-co-glycolide
PTMO	Poly-tetramethylene oxide
P4HB	Poly-4-hydroxybuterate
PU	Polyurethane
PVP	Poly(vinyl pyrrolidone)
RF	Regurgitant fraction
RHD	Rheumatic heart disease
RV	Regurgitant volume
SAVR	Surgical aortic valve replacement
SEM	Scanning electron microscope
SV	Stroke volume
TAVI	Transcatheter aortic valve implantation
TAVR	Transcatheter aortic valve replacement
TEHV	Tissue Engineered Heart Valve
THF	Tetrahydrofuran

UTS Ultimate tensile strength
VEC Valvular endothelial cell
VIC Valvular interstitial cell
VHD Valvular heart disease

1 Introduction

1.1 Background

1.1.1 Cardiovascular disease burden

Cardiovascular disease (CVD) is the leading cause of death and disability worldwide, accounting for up to 17.8 million deaths annually in 2017, corresponding to 330 million years of life lost [9-11]. Furthermore, death caused by CVD in working age individuals (35 – 64 years) is expected to increase by 41% by 2030 [9]. Heart valve replacement surgery is the second most prevalent cardiovascular surgical procedure with 300 000 valve replacement surgeries performed annually on a global scale [12]. The annual financial burden of heart valve replacement surgery in the US alone is estimated at 14 billion dollars with the number of patients affected by valvular heart diseases (VHDs) expected to increase threefold by 2050 [12, 13]. Treatment of VHDs to increase the life expectancy of patients consist of either valve repair or replacement. Valve repair is considered superior to valve replacement, however it is not a suitable option for all patients as nearly 70% of diseased valves cannot be repaired and must be replaced [12].

Currently, around 80% of the CVD burden is carried by low- and middle-income countries (LMICs)[14]. This is since pervasive diseases such as rheumatic heart disease (RHD) are still prevalent and under addressed in developing countries. The 2015 Global Burden of Disease study estimated that acute rheumatic fever and subsequent RHD affects 33.4 million people globally [11, 15]. Acute rheumatic fever occurs after a streptococcus infection of the tonsillo-pharynx, generally in children, and molecular mimicry between the streptococcal-M protein and cardiac protein initiates progressive valve inflammation, fibrosis and scarring of the valve and valve apparatus [11, 16]. Of all patients who suffer from rheumatic fever, 65% will develop RHD [16].

In 1944 Dr TD Jones developed the Jones criteria which along with subsequent revisions has laid the foundation for enhanced detection and subsequent treatment of RHD [11]. To this end, in the past RHD was the leading cause of VHD worldwide however the reduction of its burden in economically developed countries has been largely associated with improved living conditions along with the effective use of antibiotics to treat rheumatic fever [11]. Despite this reduction of RHD in developed countries, the disease still accounts for the greatest cardiovascular related loss of disability-adjusted life years among 10- to 14-year-olds and continues to plague public health in sub-Sharan Africa and other LMICs [17]. In 2015, 319 400 deaths were attributable to RHD presenting an age-standardized mortality of 4.8 deaths per 100 000. The highest age-standardized death rates were found in the regions of Oceania (14 deaths per 100 000), South Asia (12 deaths per 100 000) and sub-Saharan Africa (8 deaths per 100 000) [11, 15].

In developed high-income countries the greatest burden of VHDs is due to a degenerative disease process [11]. The most common degenerative VHD is calcific aortic valve stenosis (CAVS), which requires valve replacement and is present to some degree in 2.8% of adults over the age of 75 years [12, 18, 19]. Despite the frequency of CAVS our understanding of the disease's pathogenesis still remains incomplete. CAVD is the most common cause of Aortic stenosis (AS) which is characterised by fibrotic thickening, angiogenesis and the development of mineralised lesions throughout the bulk of the valve leaflet which reduces the ability of the aortic valve to open fully during ventricular systole [11, 18].

AS is among the most common valve diseases in Europe and North America and is present in around 25% of people older than 65 in these populations [16]. In comparison to healthy aortic valves, valves affected by CAVS have reduced elastin content and the elastin fibres are fragmented which contribute to an overall increase in valve stiffness [18]. Other common valvular diseases to take note of include mitral valve degeneration, aortic regurgitation, bicuspid aortic valve, infective endocarditis and mitral stenosis.

1.1.2 Prosthetic heart valve requirements

In the 1950's and 1960's design criteria for the ideal heart valve were outlined yet currently there still is no ideal replacement valve that is suitable for every patient [20]. The "ideal" prosthetic heart valve can be described with relative ease. Blood flow through the valve should not be turbulent and the valve should allow unimpeded forward flow while open and no regurgitation when closed. The valve should be able to function effectively over the entire lifespan of the patient without the need for further intervention. Additionally, the valve should also be easily implantable, poses native hemodynamic properties, be resistant to degradation and require no anticoagulation treatment while being fully bio-functional with physiological regeneration [20-22]. Lastly a newer goal was recently added which caters to the need of paediatric patients, where it would be beneficial if the valve was able to enlarge as the patient grows [20]. In order to work towards realising this ideal, heart valve prostheses must be designed to mimic the form and function of the native valve as closely as possible. Thus, prosthetic valves must replicate both the main structural and histological features of the native valve [21, 23].

1.1.2.1 Native heart valve anatomy

The primary function of a heart valve is to control unidirectional blood flow through the heart during a cardiac cycle. A heart valve opens and closes more than 100 000 time each day [12]. In order to maintain this level of function and efficacy there exists a complex hierarchical relationship which spans from molecular level to macroscopic tissue geometry [23]. The human heart has four valves: aortic, pulmonary, tricuspid and bicuspid (mitral) valve. The pulmonary and aortic valves are semilunar valves which regulate blood flow to the arteries leaving the heart. The tricuspid and mitral heart valves are known as atrioventricular valves and are situated on either side of the heart where they regulate blood flow between the atria and ventricles of the heart.

A heart valve leaflet consists of an extra-cellular matrix which is deposited in different locations within the valve and consequently forms three layers with a total thickness of less than 1 mm [8]. The ECM is filled with specialised cells and has the role of providing physical support to cellular components while also dictating biochemical and biomechanical signals between cells, matrix and external forces [12].

Of the three ECM layers, all depicted in Figure 1, the middle is the spongiosa layer of which its scaffold is made up of glycosaminoglycans and loose collagen [8]. On its inflow surface the spongiosa layer is covered with ventricularis in semilunar valves and atrialis in atrioventricular valves. This first valve layer consists of dense elastin fibres while the valve's outflow surface is covered with the fibrosa layer, composed mainly of dense collagen tissue [8, 21]. The ventricularis layer ensures that the valve returns to its original shape after opening while the spongiosa layer maintains valve plasticity and the fibrosa layer maintains the pressure formed by diastole [18, 21].

On a cellular level heart valves consist of two main types, valvular endothelial cells (VECs) and valvular interstitial cells (VICs). VECs line the outer surfaces of the valve while VICs are found within the bulk of the leaflet [18]. It is understood that VECs protect the valve from immune reactions, degeneration and damage [21], while VICs are the predominant cell type of valves and are responsible for the stability of the heart valve by maintaining the ECM by synthesis of proteins, matrix metalloproteinases and their inhibitors. This is possible since VICs contain characteristics of myofibroblast, fibroblasts and smooth muscle cells combined [18, 21].

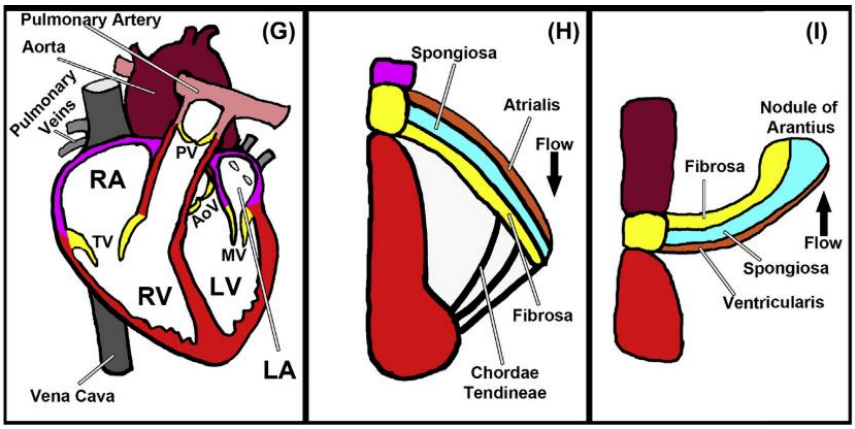

Figure 1 - (G) Depiction of a fully developed heart with all four heart valves clearly visible. (H) Atrioventricular valve composed of three layers. (I) Semilunar valves composed of three layers. Image adapted from [8]

1.1.2.2 Native aortic heart valve mechanics

Approximately 3.5 litres of blood are pumped through the valves of a heart each minute during a cardiac cycle. All of which applies cyclic, shear, tensile and flexural loading forces on the valves [12]. While aortic - and pulmonary valve leaflets share the same basic structure, the main difference is that aortic valves are significantly thicker [24]. Additionally, mechanical properties of human aortic valves differ in the radial and circumferential directions. In the circumferential direction the modulus of elasticity, ultimate stress and ultimate strain were 15.34±3.84 MPa, 1.74±0.29 MPa and 18.35±7.61%, respectively [19]. In the radial directions these values were 1.98±0.15 MPa, 0.32±0.04 MPa and 23.92±4.87%, respectively [19]. This difference in values due to direction is attributed to the circumferential alignment of collagen fibres in the fibrosa and radial alignment of elastin fibres in the ventricularis [12]. Additionally, in healthy adults, blood velocity reaches up to 1.35 ± 0.35 m/s within the aortic valve and is slightly higher at 1.5 ± 0.3 m/s in the aortic valve of children with transvalvular pressure reaching around 80 mmHg for the aortic valves in adults [12, 25].

Correct heart valve functioning relies heavily on the previously mentioned anisotropic mechanical properties. This is since too much stiffness can hinder cusp coaptation while too little stiffness can allow for distortion and regurgitation [19]. Additionally, obtaining the correct mechanical properties is also necessary as VICs are extremely sensitive to local tissue strains and respond by modulating behaviour such as collagen synthesis [19]. Thus, it may be necessary to produce scaffolds of either synthetic or biological materials with similar anisotropic mechanical properties during valve engineering.

1.1.3 Existing prosthetic heart valves

1.1.3.1 Surgical heart valve replacements

The current standard of care offers patient's a choice between mechanical and bioprosthetic heart valves. In the US approximately 50% of patients receive bioprosthetic heart valve prosthesis of which porcine and xenograft bovine pericardial valves are the most common. Furthermore, 43% of patients receive mechanical valves and 7% homographs, which are either autografts through Ross procedure or allografts from cadaveric donors [12]. Currently, there continues to be a trend towards an increasing use of bioprosthetic heart valves, which has been accelerated by the success of transcatheter aortic valve replacements (TAVR) [24]. The choice of which valve is best to implant depends on two risk factors: anticoagulation related bleeding and valve deterioration. To this end bioprosthetic valves are implanted when the risk of bleeding due to anticoagulation treatment is too high and mechanical valves are implanted when valve tissue deterioration could be accelerated [26].

1.1.3.1.1 Mechanical heart valve replacements

In 1950 the ball and cage valve was proposed as the first mechanical heart valve prosthetic [27]. Later in 1957 a cardiac surgeon Albert Star and engineer, Miles Lowell Edwards, met and created a novel mechanical valve prosthetic, the Starr-Edwards valve. In 1960 the Starr-Edwards valve became the first FDA approved mechanical valve and was successfully implanted in a human [12]. A variety of mechanical valve designs have been used since their original development, with current mechanical valve manufacturers including Edwards Lifesciences, Medtronic, St. Jude Medical and Livona among others [27].

Figure 2 depicts the three basic designs of mechanical valves: ball-in-cage, mono-leaflet and bi-leaflet with modern mechanical valves generally made in a tilting-disk formation with either one (mono-leaflet) or two (bi-leaflet) rigid leaflets which rotate on hinges [24]. These valves consist of a variety of materials such as stainless steel, pyrolytic carbon or ceramic with various configurations [26]. Furthermore, these valves are structurally robust with a theoretical service life of 25 to 30 years [26]. Currently development in this field continues to focus on improving valve hemodynamics and durability to reduce thrombus formation, hemolysis and pannus which is the ingrowth of native tissue that can compromise leaflet motion [27].

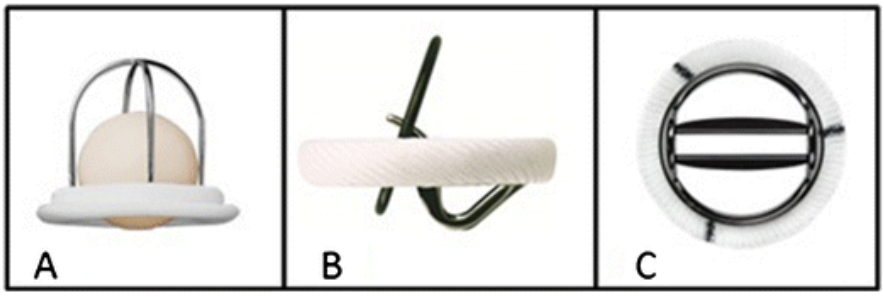

Figure 2 - Mechanical heart valves (A) Ball-in-cage-, (B) Mono-leaflet-, (C) Bi-leaflet valve [4]

A significant disadvantage of mechanical valves is the non-physiological hemodynamics which is brought about by the geometry of the valves coupled with the rigidity of the synthetic materials used to fabricate the valves. Blood flow must separate as it passes the valve leaflets which results in areas of stasis distal to the orifice and leaflets as well as regions of high shear stress, which in turn creates conditions which precipitate thrombus and require the patient to undergo lifelong anticoagulation treatment [24].

Despite decades of experience anticoagulation treatment is still considered dangerous since suboptimal anticoagulation carries the danger of clot formation which can lead to immobilization of the valve leaflets or the downstream occlusion of a blood vessel, both of which can lead to catastrophic results [28]. Anticoagulation treatment also results in the inability to live a healthy and active sports life in young individuals [12]. Furthermore, mechanical valves are subject to hemodynamic failure including the valve becoming stuck in either a fully open or closed position, a condition which can lead to death [12].

1.1.3.1.2 Bioprosthetic heart valve replacements

Currently more than 250 000 biological heart valves are being implanted annually with elderly developed-world patients making up the majority of these recipients [28]. Bioprosthetic heart valves evoked excitement upon their introduction as they do not require anticoagulation treatment however, it soon became evident that they degenerate and fail at a rapid rate with an estimated service life of 10 to 15 years [26].

This degeneration rate generally coincides with the relatively short natural life expectancy of older patients and therefor biological valves are still a suitable option for these patients. The same is not true for younger patients who will eventually have to undergo follow-up heart valve replacement surgery. Furthermore, the degradation process of these valves is also much faster in younger patients [28]. Patients who require a prosthetic heart valve due to rheumatic heart disease are often too young for a bioprosthetic valve, even if the durability of the valve could be moderately improved [28].

Biological valves can be xenogenic (bovine, porcine or from another animal source) or allogenic (homograft), stented or stentless, as shown in Figure 3 [26]. Today bioprosthetic heart valves are almost exclusively bovine pericardial valves [20]. Principally there are four phenomena which are associated with failing bioprosthetic valves: calcific degradation, mechanical damage, inflammation and pannus overgrowth, or a combination of the aforementioned [28]. Research has showed that the primary reason for bioprosthetic valve failure is tissue degeneration which leads to valve incompetence due to tears or other disruptions to the leaflet tissue which leads to stenosis or regurgitation [24, 28].

With regards to calcific degradation, techniques currently used for valve fixation are not ideal and have been shown to result in tearing of the leaflet at the free edge near the stent post [12, 24]. Additionally, glutaraldehyde is the most common preservative for bioprosthetic tissues, which has been shown to adversely affect the shear and flexural properties of the tissue leading to increased internal stressed associated with increased calcification and reduced fatigue [24]. Thus, despite being deemed the current “gold standard” in heart valve replacements, neither mechanical nor bioprosthetic heart valve replacements are ideal solutions and continue to be plagued by complications such as thrombus, calcification, structural valve degeneration, pannus and mechanical failure [24].

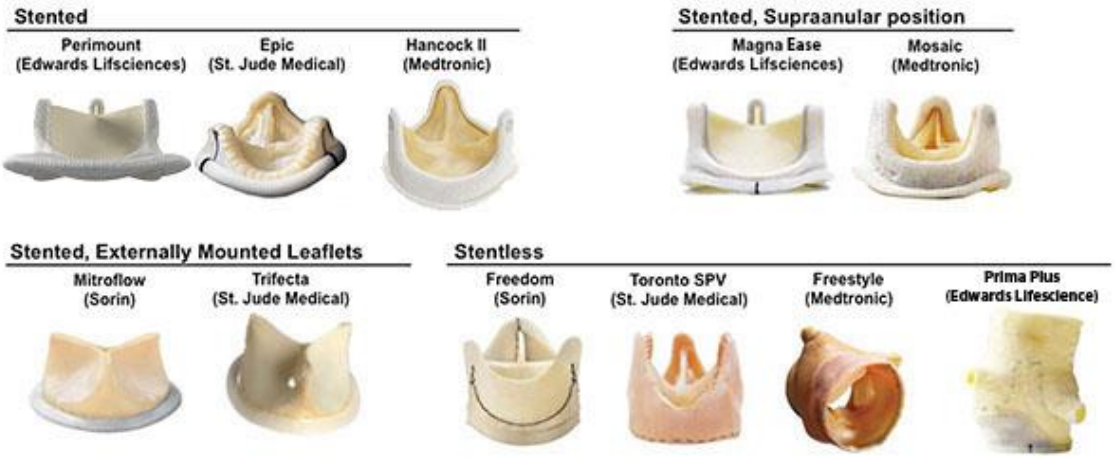

Figure 3 - Bioprosthetic valve types [29]

1.1.3.1.3 Ross procedure

An important complication present in all heart valve prosthetics, apart from pulmonary autografts (Ross procedure), is the inability to grow, repair and remodel, which is of particular importance in young patients with congenital defects who will require subsequent reoperation with increasing age [12, 21]. However, paediatric patients are not the only patients at risk of reoperation. Currently, 60% of all patients who receive heart valve prostheses will undergo subsequent operation due to artificial prostheses associated problems [12].

The Ross procedure has been shown to have low rates of reoperation and perioperative mortality. During this procedure, the patient's diseased aortic valve is replaced with their native modified pulmonary valve (autograft) while a cadaveric pulmonic valve allograft is used to replace their pulmonic valve [19]. In terms of advantages this procedure offers minimal thromboembolism, favourable hemodynamics, and valve growth potential. In terms of disadvantages, harvesting a healthy pulmonic valve leads to the development of pulmonary valve disease in addition to existing aortic valve disease [19].

1.1.3.2 Transcatheter heat valve replacements

All heart valve replacement options discussed to this point are surgical heart valve prostheses which are implanted through open heart surgery. Surgical aortic valve replacement (SAVR) has historically been the selected treatment for patients with severe symptomatic aortic stenosis and severe aortic regurgitation, and involves open heart surgery where the patient's heart is stopped, and they are attached to a bypass machine to oxygenate their blood. Since this procedure is invasive it is slowly being replaced by transcatheter aortic valve replacement (TAVR) in which valves are inserted through a transcatheter route [30]. Transcatheter valve technology has become a popular alternative in the last 20 years, especially in high risk surgical patients [27]. TAVR valves leaflets are made either of glutaraldehyde- treated bovine pericardium of porcine pericardium (today almost exclusively bovine pericardium) similar to surgical bioprosthetic heart valve replacement [30].

TAVR can have three different sites of vascular access: subclavian, transfemoral or the carotid artery with the transfemoral approach as the preferred choice [26, 31]. The majority of transcatheter devices are designed on either a self-expanding concept or a balloon-expandable concept with examples of each shown in Figure 4. Both valve types are crimped, inserted through a transcatheter route and correctly positioned. Once the valves are in the correct position, self-expanding valves are released, and the inherent material properties of their nitinol stents allow the valves to return to their uncrimped state. Balloon-expandable devices on the other hand are expanded using a balloon which is inflated inside of the stent [31]. The procedure is performed in cases where patients are at a high risk of death during surgery due to old age or comorbidities. However, in 2017 the FDA approved the use of TAVR in patients with intermediate risk after the success of two trials: PARTNER 2 and SURTAVI [26]. In addition to this research indicates that TAVR is becoming more popular as a surgical option among groups of patients at lower risk for surgery [31].

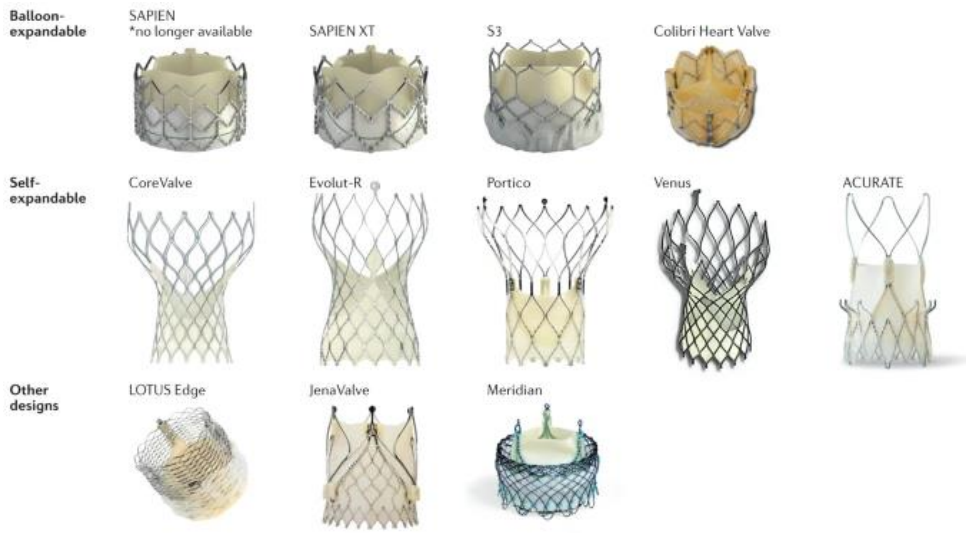

Figure 4 - TAVR heart valves [5]

Design principles for transcatheter heart valves are relatively complex in nature as valves must be implanted inside the native anatomy of the cardiac system without distorting the numerous components in this system [31]. To achieve this goal many design factors must be considered. An ideal transcatheter valve should have minimal to negligible residual gradients, no paravalvular or central leak, great coaptation of the leaflets, with a minimal rate of coronary obstruction, root rupture or need for a permanent pacemaker [31]. Additionally, these factors must be combined with a design that allows for repositioning as well as a low delivery profile to minimise vascular complication.

With regards to complication associated with TAVR, TAVR leaflets are thinner than SAVR leaflets (~0.25 mm and ~0.4 mm respectively) to allow for transcatheter delivery [30]. Thus, TAVR leaflets also experience higher stresses and strains than SAVR leaflets especially in the presence of native aortic annular calcification or an oval shaped annulus [30]. Additionally potential structural damage related to crimping, compression and expansion may impact valve durability; however the topic has not received adequate attention to date with the long-term durability of these valves still unknown [30]. Despite all of the aforementioned, the main challenge posed by TAVR is the correct positioning of the prosthesis. It is estimated that approximately 25% of TAVR can be attributed to abnormal device implantation, such as low or high implantation within the aortic root, requiring rectification with an additional procedure [31].

1.1.3.3 Alternative solutions

Polymeric valves have recently emerged as another potential heart valve prosthetic option. These valves are made using non-degradable polymers such as silicone, polytetrafluoroethylene and polyurethanes [32]. These valves are a promising and affordable alternative as raw polymer materials can be designed to more closely match the material properties of native tissue while polymer films can easily be formed into geometries which permit physiological flow [24]. Polymeric valves were initially designed to combine the physiological-like hemodynamic profile of the tri-leaflet bioprosthetic valve with the immune-compatibility of mechanical prosthesis. However, despite this polymeric valves have initially been associated with poor durability, variation between batches, pannus overgrowth, thrombogenicity, calcification and diminishing functionality over time [32].

With this in mind material researchers have attempted to optimise polymers to produce biocompatible, durable materials which can be used in the production of artificial heart valves. In comparison with conventional polyurethanes, siloxane poly(urethane-urea)-based heart valves have shown improved creep resistance, tear strength, an absence of permanent deformation and a durability of 600 million cycles, equivalent to 15 years, with the absence of in vivo thrombus and calcific degradation [33-35].

Regarding prominent figures in the polymeric heart valve research field, Straight Access Technologies from Cape Town, South Africa are focused on the development of cost effective and enabling technologies to treat heart valve diseases. Over the last couple of years, the company has been working on the development of a heparinised polyurethane heart valve which has recently passed over 600 million cycles during in vitro accelerated durability testing [36, 37]. Another group leading in the development of polymer heart valves is Foldax Inc. in Salt Lake City, Utah. The company has received FDA approval to initiate a clinical study of one of their valves [49, 52]. Lastly the TRISKELE TAVR valve has leaflets made of a novel synthetic functional nanocomposite polymer, developed at UCL, which is suitable for heart valve applications. The TRISKELE valve is fully repositionable/retrievable and provides improved anchoring and sealing. It is expected that further future developments in this field will combine minimally invasive transcatheter procedures with polymeric valves to provide a cost-effective solution for treatment of rheumatic heart disease in developing countries [32].

1.1.3.4 Polymeric valve fabrication techniques

A valve's design is ultimately governed by finding a balance between design considerations and constraints. The physical geometry, the aspects of the valve assembly and the surgical implantation technique to be used all share significant importance in the actual design of the heart valve. Furthermore, the choice of production method should also take into account the complexity of the design and the accuracy and reproducibility of the design within given tolerances as well as practical time and cost constrains [38].

Polymer valve manufacturing methods can be grouped into three broad categories: dip moulding, film fabrication, and injection moulding. Each method has distinct advantages and disadvantage and the choice of method selected is often dictated by the properties of the selected material.

Dip moulding generally produces valves with good durability with several prototypes, produced using this method, showing promising in vitro and in vivo results [24]. The dip moulding process is relatively simple and consists of a mould or mandrel with the desired geometry being dipped into a polymer solution. When the mould is removed from the solution the first layer of solution is adhered to the mould which is then heated to remove solvent, leaving a thin film of the polymer. These steps can be repeated until a desired polymer thickness is achieved [24]. Additionally, valve frames or stents can also be dipped which can allow a durable bond between the leaflet and the frame or even a skirt and the frame, even if the frame is constructed from a dissimilar material such as nitinol or PEEK [24].

In practice achieving repeatability with dip moulding required precise control of many factors including polymer concentration, solution viscosity, mould shape and surface roughness, mould orientation during dipping and drying, dipping speed and atmospheric conditions [24]. Mackay *et al*. and Rahmani *et al*. showed that even under well-controlled conditions, leaflet thickness can vary in the range of ± 50% within the same leaflet [39, 40]. To mitigate this some research groups have introduced robotic mechanism to improve control over the dipping process as well as the drying process by tumbling the mould during drying to improve polymer distribution uniformity [41, 42].

Injection moulding compared to dip moulding greatly increases reproducibility [24]. Injection moulding has been extensively used of the manufacturing of complex polymeric components. This method solidifies a polymeric solution (melt) inside a mould with the desired geometry, after which the construct is released. Moulding produced constructs with isotropic properties, in contrast with the native anisotropic properties of heart valves. Furthermore creating multicomponent valves which mimic the native heart valve would require opening and closing the mould several times which could lead to potential complications and discrepancy in manufacturing [43].

Film fabrication comprises manually manipulating flat polymer films into the desired valve geometry. Thus, a flat film is first obtained by a variety of methods such as solution casting, compression moulding, extrusion, or electrospinning. The film is then trimmed to the desired leaflet dimensions and attached to the valve frame by solvent bonding or suturing [24].

One disadvantage of this method is the resulting weakness at critical leaflet-frame interfaces. This includes sutures which introduce stress concentrations which can severely limit valve durability [24]. Leet and Fisher performed a study which compared film fabricated valves to valves produced through dip moulding [44]. They illustrated that PU valves manufactured trough film fabrication and solvent bonding to a PEEK frame tended to suffer subsequent debonding which resulted in low durability and valve failure prior to 100 million cycles. On the other hand, valves manufactured by dip moulding had reached 160 million cycles by the time of publication and exhibited no signs of debonding.

In conclusion, dip moulding and injection moulding appear to be the most promising techniques for fabricating polymer valves. This is since injection moulding offers the most reproducibility of leaflet thicknesses while dip moulding has produced extremely durable valves [24]. In terms of resources injection moulding required the most specialised equipment, while dip moulding equipment can become specialised at later stages when reproducibility becomes vital. Film fabrication techniques are however the simplest but result in weak leaflet-frame interface which limits durability. This method requires the least investment in equipment, but can be the most labour intensive if manual suturing is required [24]. Thus, film fabrication and dip moulding are appropriate for prototyping while advanced dip moulding and injection moulding are suitable for scalable production.

1.1.4 Tissue engineered heart valves

In another attempt to overcome the issues presented by existing heart valve prosthetics, tissue engineered heart valves (TEHVs) are also emerging as a promising new substitute. An ideal heart valve replacement is one where the replacement valve consists of the patient's own living tissue since these valves will be able to regenerate and grow with the patient, adapting to environmental changes as required. Currently this concept is still in its infancy with various routes being explored in order to achieve this ideal. Lots of hope currently lies in heart valve tissue engineering (HVTE) to potentially overcome the multifaceted challenges presented by this issue.

1.1.4.1 The tissue engineering concept

During a 1987 panel meeting held at the National Science Foundation (NSF), the term tissue engineering was first introduced [12]. Later in 1988 it was defined as "the application of principles and methods of engineering and life sciences toward the fundamental understanding of structure-function relationships in normal and pathological mammalian tissues and the development of biological substitutes to restore, maintain, or improve tissue functions" [45]. However, it was not until 1995 that the integration of tissue engineering into heart valve substitution came to life [12].

Tissue engineering is a science which applies engineering principles to the field of biology in an attempt to create viable structures which are able to replace deficient or diseased natural structures of the body [12, 46]. Tissue engineered heart valves could potentially overcome the majority of current shortcomings in the field by providing a viable valve capable of growth, remodelling and repair [12, 21]. This method's superiority also stems from the absence of thrombogenesis and infection possibilities, mechanical stability, lifetime durability and the resistance to calcification [12].

The goal of heart valve tissue engineering is to produce a heart valve prosthesis which mimics the physiological and structural traits of the native valve [21]. To achieve this goal a three-dimensional (3D) scaffold resembling the valve structure is required, along with appropriate cells to seed on the scaffold and a physiological condition in which the cells can proliferate [21]. This process can be summarised into four main steps which describe the formation of a complete prosthetic heart valve from a populated scaffold for tissue engineering purposes [21]. Firstly, seeded cells should proliferate and differentiate. Secondly, an ECM is produced and organized. Thirdly, degradation of the polymer scaffold must take place and lastly the remaining tissue should remodel and grow to adapt to the patient's physiology [12, 21].

Great advances have been made in the design, development, and optimization of scaffolds for tissue engineering with prominent figures in the polymeric heart valve research field highlighted in Table 1. This progress has been facilitated by the discovery of a variety of scaffold polymers and an enormous amount of processing techniques which have been iteratively improved to produce scaffolds which meet their required needs [23]. Cardiac tissue engineering has seen a particularly high level of innovation in recent years due to the high prevalence of cardiac disease [23].

Table 1 - Representative table of prominent figures in the polymeric heart valve research field

	Focus	Materials Used	Animal Studies	Findings	Ref
A Newly Developed Tri-Leaflet Polymeric Heart Valve Prosthesis					
1 (2015)	*Novel tri-leaflet heart valve prosthetic made from styrenic block copolymers.*	*poly(styrene-isoprene/ butadiene-styrene), with 19% polystyrene weight fraction.*	*Only finite element modelling and in vitro testing took place.*	*Performance of these valves is comparable with that of some bi-leaflet mechanical prostheses currently used in clinical settings, having a comparable tissue annulus diameter. Design improvements were deemed necessary to further minimize regurgitation and maximize EOA and long-term durability remains unknown.*	*[47]*
Bioinspired Heart Valve Prosthesis Made by Silicone Additive Manufacturing					
2 (2019)	*Aortic heart valves with customizable geometry and leaflet architecture.*	*A soft biocompatible silicone (Shore 43 A) and a harder silicone (Shore 73 A) were used.*	*Both finite element modelling and in vitro testing were utilised.*	*Significantly reduced maximum stress developed on the leaflet during diastole. In vitro cyclic testing demonstrated outstanding hemodynamic performance under physiological pressure conditions.*	*[48]*
Straight Access Technologies (SAT)					
3 (2017)	*Polymeric TAVI valve*	*Heparinised polyurethane valve.*	*In vitro accelerated durability testing.*	*Valves recently passed over 600 million cycles during in vitro accelerated durability testing.*	*[36, 37]*
PolyNova Cardiovascular Inc					
4 (2019)	*PolyNova xSIBS TAVR*	*xSIBS pellets with cured valves were sutured to laser-cut nitinol stents.*	*In vitro and fatigue testing.*	*Valves passed 400M cycles in AWT without failure. EOA kept stable at 1.8 cm2 with a desired gradual decrease in transvalvular pressure gradient and regurgitation. No tears or surface damage present after extensive crimping testing.*	*[49, 50]*
TRISKELE UCL TAV™, University College London, London, UK					
5 (2016)	*TAVR valve*	*TRISKELE urethane (POSS-PCU)*	*In vitro testing with valve currently under preclinical investigation.*	*Valves demonstrated a hydrodynamic performance comparable or superior to the controls (Edwards SAPIEN XT and Medtronic CoreValve) with significant reduction in paravalvular leakage. Valve exhibited enhanced anchoring and improved sealing.*	*[49, 51]*
Foldax Inc., Salt Lake City, UT, USA					
6 (2019)	*Foldax SAVR valve*	*Fabricated using vacuum compression with raw xSIBS pellets in inside the mould. Cured valves are sutured to laser-cut nitinol stents.*	*FDA approval received to initiate a clinical study of valve.*	*Baseline hydrodynamics showed superior EOA for the polymer valve. Regurgitation fraction was higher in the polymeric valve, but within the ISO minimum requirements. Polymeric valve was less thrombogenic than tissue vale control. Hemodynamic-wise, the results strongly indicate that the polymeric TAVR valve can outperform tissue valves.*	*[49, 52]*

1.1.4.2 Tissue engineering approaches

The approaches being considered to generate living, functional and durable tissue engineered heart valves, for simplicity, can be categorised into three distinct paradigms which have variants and some overlapping features. The first approach involves seeding cells in vitro onto a biodegradable polymeric scaffold and placing this into a bioreactor to mature and produce a construct which consists of a tissue/polymer composite which is then implanted in vivo [20]. Advantages of this approach include the flexibility and variability allowed for by the process [12]. Disadvantages include mechanical instability due to unpredictable structure and density [12]. Additionally, the process is also complex and time consuming.

The second approach utilises either in vivo or in situ endogenous tissue restoration. For this approach a biodegradable porous polymer is implanted without cells or biological adjuncts and induces in vivo polymer absorption leading to partial or complete replacement of the polymer with tissue, mediated entirely by endogenous cells [20]. Synthetic scaffolds can be viewed as the current mainstream approach to producing matrices for tissue engineering purposes. Advantages of this approach include controllable mechanical properties and degradation rates as well as biocompatibility [12, 21]. Disadvantages include possibly inducing inflammation due to incomplete scaffold degeneration, the risk of failure due to weakening of the scaffolds before sufficient tissue ingrowth is achieved, issues related to leaflet shrinkage, as well as potential poor cell interaction [12, 21].

The third approach involves the direct implantation of decellularized valvular or other tissue material. Scaffolds produced using this method are referred to as natural scaffolds and are mostly from xenograft pericardia or allograft-derived scaffolds which are prepared from human cadaver valves [12, 18]. Advantages of this approach include preservation of the natural ECM structure as well as good mechanical properties of the scaffold [12, 18, 21]. Disadvantages include potential side effects such as inflammation which can lead to fibrosis[12, 18, 21]. Additionally, these scaffolds are limited by the finite supply of cadaver tissue while variability will also exist between available valves. Lastly, during “purification” of these scaffolds, damage is caused to the ECM which could make effective seeding of new cells in the scaffold problematic. A study of aortic valve decellularization using various enzymatic and detergent-based methods, showed that decellularized leaflets displayed an 80% reduction in stiffness with a 100% increase in extensibility in comparison to native valves, where the principle problem with decellularized tissue, for tissue engineering, is that the pores are too small and therefor cells do not grow into the scaffolds fully [12, 18, 21].

Thus, what we see is that all approaches to tissue engineering utilise some combination of a scaffold and cells. Additional approaches exist which utilise combinations of the three basic approaches to tissue engineering. One of these approaches is a combination of the first and third approach and utilises decellularization of either the natural starting material or the tissue formed in vitro in order to avoid adverse leaflet changes [20]. These adverse changes include immunological rejection and/or calcification. This hybrid approach promotes recellularization with cells entirely from the recipient, intended to assume properties similar to those located in a native valve leaflet [20].

1.1.4.3 Tissue engineering scaffolds

The scaffold is one of the most important entities to consider for efficient tissue engineering since its surface properties, external geometry, pore size, porosity, biocompatibility, degradation rate, and mechanical properties will not only affect tissue generation but also implantation viability and functionality [19]. Scaffolds for heart valve tissue engineering can be produced from either synthetic or natural polymers and sources.

Natural scaffolds consists of acellular native heart valve scaffolds from xenogeneic/allogeneic sources [19]. Xenogeneic heart valves from cows, sheep and pigs are the main source of acellular heart valves since human valves (allogeneic valves) are in short supply especially for paediatric patients [19]. This is especially unfortunate since allogeneic valves are potentially less antigenic in comparison to their xenogeneic counterparts [19]. A potential advantage over synthetic scaffolds is the fact that decellularized scaffolds retain their original valve structure and many of the ECM molecules. During this approach, one of many existing decellularization techniques is applied to ensure that cells are removed from the scaffold while minimising damage to the original structure. Any damage to the ECM during decellularization can lead to problems during subsequent recellularization or implantation [19].

Synthetic polymer scaffold characteristics are generally preferred since their mechanical and physical properties can be controlled. These scaffolds also have varying degradation rates, are biocompatible and pose a low risk of causing an inflammatory response when implanted into the body [12, 23]. Synthetic scaffolds, which have been used in tissue engineering applications include hydrogels and porous scaffolds [12].

Porous scaffolds are characterised by interconnected homogeneous pore networks and large pore sizes which provide a continuous flow of nutrients and metabolic waste that enables growth and vascularisation of engineered tissue [19]. These scaffolds can be produced using either natural or synthetic polymers using a variety of techniques such as solvent casting, particulate leaching, gas foaming, vacuum drying, microfabrication, melt moulding, high internal phase emulsion and thermally induced phase separation [12, 53]. There are however some limitations to these classical techniques related to mimicking the elasticity and shape of native valves as well as creating scaffolds with non-uniform pores which are not interconnected [12].

The current gold standard in developing scaffolds for tissue engineered heart valves is fibrous scaffolds. This option is attractive due to the similarity between the scaffolds produced and the natural ECM, with fibre diameters mimicking the matrix proteins and proteoglycans [12, 21]. This similarity plays a significant role in improving cell proliferation, adhesion and differentiation while also providing high porosity with controlled pore sizes. These scaffolds can be produced using three methods: electrospinning, phase separation and self-assembly with electrospinning gaining popularity as the preferred method [12, 53]. This is since electrospinning is a versatile process applicable to most polymers offering both easy handling and cost-effectiveness [19].

Hydrogels are also an attractive scaffold type as they resemble the natural ECM consisting of polymers chains which are hydrophilic with high water content along with their ability to allow oxygen and nutrient penetration [12]. However, hydrogels are limited by their weak mechanical properties.

1.1.4.4 Design parameters for tissue engineered scaffolds

All scaffolds designed for tissue engineering applications should meet basic requirements including biocompatibility, sterilizability, and mechanical integrity. Since scaffolds for heart valve tissue engineering are in direct contact with blood, they face additional distinct challenges. Specifically, they should be resistant to calcification and thrombosis [19]. Additionally, these scaffolds must also withstand unique hemodynamic pressures and flow conditions of the cardiac environment from the instant of implantation [19]. These unique challenges underline the importance of diligently considering both the design and material when fabrication scaffolds for heart valve tissue engineering.

Overall, scaffolds which are to be used for tissue engineered heart valves must possesses certain characteristics which include providing the necessary mechanical support similar to that of the native valve. Scaffolds must also be biocompatible to limit the inflammatory response induced while also possessing a degradation rate that matches the neo-tissue deposition rate to ensure that necessary cell support remains as well as adequate valve function [12, 18]. Scaffolds should also be highly porous with pore seizes that allow for cell infiltration along with the diffusion of nutrients. Lastly, scaffolds should encourage cell attachment, proliferation, and migration [12, 18]. Thus, once the principle of using a scaffold has been decided on it is crucial to focus on a number of key parameters to ensure that the scaffold is adequate for heart valve tissue engineering. These parameters include material composition, surface characteristics, mechanical properties, biocompatibility and degradation rate [10, 54]. Managing these parameters correctly should lead to cardiac tissue engineered scaffolds which comply with required anisotropic mechanical properties as well as fibre alignment characteristics of the native tissue [54].

1.1.4.4.1 Scaffold composition

A scaffold with a fibrous structure with high porosity is crucial for cell organisation, function, and survival [10]. Additionally, a high surface-to-volume ratio is crucial for cell migration and vascularization and therefore indispensable in a tissue engineered scaffold [54].

1.1.4.4.2 Mechanical properties

Mechanical properties need to be considered in order to design a scaffold which is able to withstand the same mechanical forces as the native valve [10]. The stiffness of a cardiac scaffold is critical to its performance in vivo with regards to cardiac tissue repair and regeneration. This is since scaffolds with a stiffness that exceeds that of the surrounding native tissue may impede the function by increasing stiffness in the treated region [23]. If the goal is to achieve healthy and optimal heart function it is necessary to ensure that the selected material interacts with the host tissue and degrades such that the final tissue and construct complex will have the same stiffness properties as healthy native tissue [23].

Interestingly, similar to chemical or cell-cell interaction stimuli, material-related mechanical stimuli such as stiffness, has been shown to have an effect on cell behaviour. This includes the potential to direct cell differentiation. Thus, creating a scaffold with a stiffness similar to the native tissue will lead to tissue constructs with elasticity and contractility more similar to the native tissue, with both of these characteristics playing an important role in heart valve function [23]. Lastly, tensile strength must be considered since a well-designed cardiac scaffold will take into account the expected pressures in the surrounding cardiac regions in order to maintain structural integrity under these environmental pressures [23].

1.1.4.4.3 Biocompatibility

Biocompatibility has historically been the primary determining factor for materials used in medical or surgical implants and can be generalised as the interaction between the body and a material [23]. Biocompatibility is the first characteristic which should be considered in the design of any in vivo tissue engineering scaffold as it is necessary to ensure that the biomaterials selected for the polymeric tissue engineering scaffold are compatible with the native tissue and cells to induce a low inflammatory response after implantation [10, 23]. Furthermore, the biomaterials should also support cell adhesion, differentiation and proliferation [10].

Non-biocompatible materials may release toxic compounds resulting in destructive immune responsive which could do more harm than good in the long term. Ideally scaffold materials should produce either a neutral or beneficial response after introduction to the environment of its intended purpose [23]. In cardiac tissue engineering biocompatibility should include compatibility of the scaffold with all surrounding tissues and blood as well as compatibility of any degradation or metabolic by-products of the scaffold with the entirety of the body [23]. Lastly, the scaffold must function sufficiently in vivo up to the point of complete scaffold degradation to allow for correct repair and regeneration of infiltrating tissue [23].

Immune response is associated with biocompatibility since it is triggered by some implanted scaffold material. Upon implantation of a foreign material into the body, the body might react with a response which is either associated with negative healing such as fibrosis, scar formation or encapsulation or with positive healing such as tissue remodelling, angiogenesis or restoration of functionality [23]. In cardiac tissue engineering it is critical to elicit a positive immune response which encourages tissue regeneration in order to restore the complex mechanical characteristics of native tissues. Exactly how to ensure this response is not well understood however, evidence suggest that materials with similar degradation rates and chemical structures to native tissues, elicit the most advantageous responses [23].

1.1.4.4.4 Degradation rate

Degradation rate is crucial in ensuring support of both the appropriate cellular activity and the generation of new tissues [10]. Degradation rate also influences immune response and plays a very important role in vivo in ensuring scaffold functionality [23]. Ideally a scaffold must exist long enough to ensure infiltration and complete replacement by native ECM. Degradation prior to this point will result in cell death within the construct which will lead to reduced therapeutic benefit [23]. In the case of a heart valve, premature scaffold degradation will lead to a valve with incorrect mechanical properties and therefor improper functionality. On the opposite end of the spectrum scaffolds which persist in the body for too long may inhibit cell infiltration and thus cellular remodelling which can lead to scar formation and encapsulation leading to incorrect mechanical properties in that region [23].

In conclusion, an ideal scaffold for heart valve tissue engineering will combine mechanical properties, including anisotropy, elasticity, contractility etc., which match that of the native tissue with an extracellular matrix structure which mimics that of the native microenvironment as well as surface biochemistry to promote cell attachment, proliferation, and viability similar to that of the native tissue [10].

1.1.4.5 Challenges related to tissue engineered heart valves

In order for tissue engineered heart valves to become a clinical reality the balance between polymer scaffold degradation (and a resultant loss in mechanical strength) and the formation of an extracellular matrix (providing strength) must become both predictable and controlled. It is also of critical importance to determine if calcification, which is a major pathological process in bioprosthetic valve degeneration, will also be problematic in tissue engineered heart valves (TEHVs) [20, 24]. Issues regarding immunocompatibility must also be addressed since valves may elicit an immune response leading to calcific degradation [32]. Lastly, challenges associated with hemocompatibility should be researched since, when in contact with blood, the material surface of any heart valve replacement will absorb plasma proteins which promote platelet and leukocyte adhesion and activation, resulting in increased thrombotic and thromboembolic risk [32].

One of the major challenges currently hindering the development of this technology in preclinical studies is the absence of concurrent clinically approved controls for TEHV. All preclinical studies should contain clinical controls of a similar design and construction which are approved and so have a clinical history. Since this is not possible in the case of TEHV some researchers have suggested that approved bioprosthetic valves serve as these controls in the absence of prior clinical history of TEHV [20]. This will however produce the need for extensive iterative studies, redesigns and data analysis between bench and animal phases (potentially even more than those required for conventional mechanical and bioprosthetic valves) [20].

Another fundamental research need to address is the development of science-based approaches to the characterisation of TEHV, including the measurement of relative and absolute mechanical properties of the scaffold and tissue-scaffold complex as this structure evolves after implantation [20]. Additionally, the highly dynamic cell phenotypes and ECM components should also be characterised along with the evolution of the final manufactured product, including stability, shelf-life, and potential shipping/transportation considerations.

Further research is required to understand four key sources of variability in response to TEHV. These include: (1) the effects of genetic variation which will affect healing mechanisms (presumed to be non-modifiable), (2) the effects of co-morbidities and age-related changes in patients, (3) the effects of medications and environmental factors such as diet and smoking, and (4) the potential patient variability in the kinetics and completeness of scaffold degradation. In an attempt to understand and predict these variations some researchers have even gone as far as to suggest applying principles similar to those of the pharmacogenetics-pharmacokinetics field, which aims to understand the mechanism of individually determined variation in drug metabolism and to understanding the range of variability. Additional key areas of uncertainty include (1) quality assurance and characterisation of substrates and tissue constructs, (2) defining animal models for testing of these products, (3) understanding differences both in kinetic and mechanistic modalities of tissue remodelling between animal model species and humans (4) developing assays to monitor surrogate and true endpoints both before and during function, (5) accommodating both potential patient-to-patient and location-to-location heterogeneity of tissue remodelling processes within the implant, and (6) developing quantifiable, validated biomarkers and surrogates which predict early and extended outcomes [20]. In conclusion, before this technology can progress to clinical study stages it is of paramount importance to determine, understand and control the following through preclinical tests: polymer resorption and new tissue formation, inflammation, and immunological responses, ensuring mechanical stability, minimizing degradation mechanisms like calcification and ensuring predictable functionality and overall durability [20].

1.1.5 Electrospinning

1.1.5.1 Brief history of electrospinning

The principle of electrospinning is derived from the phenomenon of electrostatic attraction which was discovered more than 400 years ago. This involves the concept that like charges repel while dislike charges attract. In 1600, Englishman William Gilbert discovered that when a piece of rubber amber was held close to a water drop, the droplet was drawn to the rubber and could form a cone shape [55, 56]. This phenomenon occurred due to the electrostatic attraction between dislike charges in the water and rubber, and the force/charges which caused the droplet deformation to follows Coulomb's law [55].

Following Gillbert's observations Jean-Antoine Nollet, a French physicist, studied the behaviour of water through an electrified capillary. He found that once water was electrified intermittent dripping from the capillary turned into a continuous spraying [55, 57]. Nollet found that although the flow of droplets under the force of gravity could be accelerated with a narrower capillary and electricity, the same was not true when water flowed out of the capillary in a steady stream [55]. This finding led to the work of John Zeleny who conducted studies on this spraying phenomenon [10, 53, 55, 58]. Zeleny was the first person in history to provide time-lapsed images of liquid meniscus. These images proved that changing the applied voltage and hydrostatic pressure in the capillary would lead to different spray behaviours [55, 56]. The most notable advance in the electrospinning field was the work of Geoffrey Taylor in documenting and explaining the mathematical model behind the Taylor cone and theoretically understanding droplet deformation under an electric field [55, 59]. From this Taylor concluded that a semi-angle conical angle of 49.3° should be obtained at a stable air-fluid interface and that this cone forms during both electrospray and electrospinning [55, 60].

An application filed by John F. Cooley in the United Kingdom in 1900 is considered as the first patent on electrospinning [12, 55, 56]. Herein Cooley proposed several different designs of tubes as the spinneret. Anton Formhals is also considered as a great contributor to the electrospinning field and filed a series of patents on electrospinning setups between 1931 and 1944 [12, 53, 55, 58, 61]. In the 1990's, Dr Darrell H. Reneker from the University of Arkon took a second look at the effect of electrostatic force on fibre formation of a polymeric solution [55]. Reneker's work was focused on characterising the electrospinning process and identifying the parameters which govern it [62]. Due to the emergence of nanotechnology Reneker's work drew interest from both industry and academia and the terms "electrospinning" and "nanofibers" were immediately popularised [55, 63].

1.1.5.2 Overview of electrospinning process

Electrospinning has become a popular method of creating extracellular matrices for application in tissue engineering as it is a relatively simple and robust technique which can be effectively up-scaled and thus used in industrial settings [10, 53-55, 58]. It has been found that electrospun nanofiber matrices display morphological similarities to the native ECM, characterised by continuous fibres, high surface-to-volume ratio, high porosity, and variable pore size distribution [10, 64]. Furthermore, electrospinning offers simplicity, cost effectiveness, scalability, high-yield, controlled porosity, and the ability to consistently produce fibres in the submicron range using a wide variety of synthetic or natural polymers [12, 53, 54, 58].

Nearly any polymer with an adequately high molecular weight can be electrospun. This has been successfully demonstrated through nanofibers made of either synthetic or natural polymers, polymer blends and drug- or nanoparticle-impregnated polymers [63]. Currently there are two main electrospinning setups, vertical and horizontal, with more sophisticated configurations being developed by groups to allow fabrication of more complex nanofibrous structures [53].

A traditional electrospinning setup consist of three main components, illustrated in Figure 5; a spinneret, a high voltage power source and a collector which can be a metal screen, rotating mandrel or plate [10, 12, 53, 58]. The process is directly related to surface tension in the conductive polymer solution which can be overcome by strong electrical potential [12, 53]. The process is initiated by applying a high voltage, 10-20 kV, to the polymer solution which is held in the spinneret needle by its surface tension [54]. This stimulates electrical charges in the polymeric solution which in turn creates instability due to the repulsive electrostatic charges within the solution which oppose the surface tension [12, 62]. Once a threshold, Rayleigh's limit [55], is reached where electrostatic forces exceed the surface tension of the solution, the charged solution is ejected from the tip of the Taylor cone as a jet which is deposited on the oppositely charged grounded collector, as the jet trajectory can be controlled by an electric field [58, 62]. Interestingly, Taylor cones tend to have different angles due to the high viscosity associated with electrospinning solutions. Yarin et al developed a mathematical equation to calculate a Taylor cone and suggested that a Taylor cone can only be produced by self-similar solutions and that nonself-similar solutions will likely produce a smaller cone angle [60].

After initial ejection the stable jet undergoes a whipping movement, which stretches the, now unstable, jet into fine fibres [55, 58, 63]. Whipping is attributed by columbic repulsion which is caused by the interaction between the applied external electrostatic field of attraction and the repulsive forces of the surface charge within the jet [58]. During ejection the solvent evaporates in the space between the spinneret and the collector allowing the solution to be deposited as dried nanofibers on the collector, generally with a random orientation [10, 12, 55, 58, 62].

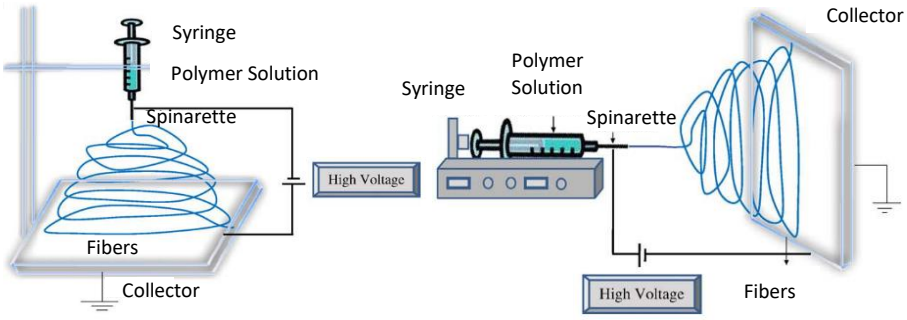

Figure 5 - Vertical and horizontal electrospinning setups. Images obtained from [53]

1.1.5.3 Electrospinning parameters

A variety of parameters govern the electrospinning process; these can be broadly categorized into solution properties, process parameters and ambient parameters [10, 12, 53-55]. Under each of these broad categories, parameters exist which affect fibre morphology [53]. These parameters are outlined in Table 2 and discussed in detail in this section.

Table 2 - Parameters which govern the electrospinning process

Parameter	Effect on fibre morphology	References
Solution Parameters		
Viscosity	*-High viscosity results in uniform fibres with larger diameter.*	*[12, 53, 55]*
Conductivity	*-Higher conductivity leads to more fibre whipping result in smaller diameter fibres.*	*[12, 53]*
Surface tension	*-High surface tension results in sprayed droplets.* *-Lower surface tension allows electrospinning to take place at lower voltages.*	*[12, 53, 55]*
Molecular weight	*-Polymers with high molecular weights result in larger diameter fibres.* *-Polymers with a molecular weight which is too low, result in bead formation.*	*[12, 53]*
Concentration	*-High solution concentration results in large diameter fibres.* *-Low solution concentration leads to bead formation.*	*[12, 53, 55]*
Solvent selection	*-Solvents with a low boiling point ensure rapid drying of the electrospun fibre.* *-Solvents with a high boiling point could result in flattened fibres.*	*[12]*
Process parameters		
Voltage intensity	*-Higher voltage difference between the spinneret and mandrel leads to increased fibre stretching resulting in smaller diameter fibres.* *-Increasing voltage difference between the mandrel and spinneret will decrease fibre diameter up to a point after which it will begin to increase.*	*[12, 53, 55]*
Flow rate	*-High flow rates lead to bead formation due to incomplete solvent evaporation as well as the formation of flat fibres.* *-Low flow rates lead to complete solvent evaporation resulting in cylindrical fibres with smaller diameters.*	*[12, 53, 55]*
Needle to collector distance	*-The distance must be sufficient to allow complete solvent evaporation.* *-Larger distance leads to smaller diameter fibres* *-Smaller distances lead to flat fibres.*	*[12, 53, 55]*
Collector type	*-Smaller surface areas have smaller conductive areas and therefor can result in bead formation.*	*[12, 53]*
Ambient parameters		
Temperature	*-There is an inverse relationship between solution viscosity and temperature.*	*[53]*
Humidity	*-Low humidity can lead to rapid evaporation of a volatile solvent.* *-High humidity can lead to nanofiber discharge.*	*[12, 53, 55]*

1.1.5.3.1 Concentration

In order for fibre formation to occur during the electrospinning process, a minimum solution concentration is required [53]. When the solution concentration is too low a mixture of beads and fibres are produced.

When increasing the solution concentration, the beads and fibre mixture produced will change from spherical to spindle-like beads and eventually to uniform fibres with an increasing diameter as the solution concentration is increased [53, 55]. This is due to the increased viscosity resistance produced by the increase in solution concentration. The solution concentration can however reach a point where it is too high, where the formation of continuous fibres will no longer be possible due to the inability to maintain the solution flowrate at the needle tip [53, 58].

It is important to understand that both surface tension and viscosity play important roles in determining the range of solution concentration from which continuous fibres can be electrospun [53, 58]. This is since process parameters are all interconnect and dependent on one another; thus, ensuring the correct electrospinning environment is created is a balancing act between parameters. Some argue that polymer concentration is the most important factor which affects the electrospinning process since it affects so many other solution properties including viscosity, conductivity and surface tension [55].

1.1.5.3.2 Molecular weight

Molecular weight is another very important factor which affects the electrospinning process. In general high molecular weight polymers are used for electrospinning as they produce the desired viscosity which is required to produce uniform fibres [53]. The molecular weight of a polymer also has a significant effect on properties such as surface tension, dielectric strength and conductivity [53].

It is understood that high molecular weights produce uniform fibres with larger average diameters, while low molecular weight polymers tend to produce beads instead of continuous fibres. The molecular weight of a polymer determines the number of entanglements of polymer chains in that solution and thus solution viscosity [53, 55]. It has been observed that if sufficient intermolecular interaction can provide a substitute for the interchain connectivity achieved trough chain entanglements, high molecular weight polymers are not always necessary to successfully electrospin [53].

1.1.5.3.3 Solution viscosity

Solution viscosity plays an important role in fibre morphology and size during the electrospinning process. As discussed above, solution viscosity is highly determined by intermolecular interaction within a polymer solution, and viscous solutions are formed due to chain entanglement. In order to successfully electrospin an optimal viscosity is required. This is since low viscosity solutions cannot produce continuous fibres while ejection of the polymer solution becomes a concern when solution viscosities are too high [53, 58]. Increasing solution viscosity leads to continuous fibres since the viscoelastic force in the polymer is increased, which allows the polymer to resist rapid change in jet shape. This results in a continuous and homogeneous fibre structure since it allows stretching of the solution jet [55].

Viscosity, molecular weight and polymer concentration are all related to one another as outlined. In solutions with a low viscosity, surface tension is the governing factor while above a critical viscosity point concentration governs morphology. Thus there is generally a polymer-specific, optimal viscosity value for electrospinning which, for specific polymers, greatly influences fibre morphologies [53].

1.1.5.3.4 Surface tension

Surface tension plays a critical role in the electrospinning process. It can be considered that, if all other variables are held constant, surface tension determines the upper and lower bounds of successful electrospinning parameter combinations [53]. This is since a reduction in surface tension will lead to continuous fibres without beads being produced. While higher surface tension leads to sprayed droplets due to the instability of the solution jet. At the same time a lower surface tension of a solvent will not always be more suitable for electrospinning [53].

1.1.5.3.5 Solution conductivity

The conductivity of a solution is mainly determined by the solvent used, the polymer type and the availability of ionisable salts, the combination of which could affect the fiber size by one to two orders of magnitude [53, 58]. An increase in solution conductivity generally results in electrospun fibres with a decreased diameter. On the other hand, a solution with low conductivity produce either fibres with a large diameter or beads due to insufficient elongation of the solution jet [58]. Generally, electrospun fibres with the smallest diameters are obtained with the highest electrical conductivity solutions and this is due to jet stretching during the whipping phase of electrospinning, since solutions with a higher electrical conductivity will whip more rapidly [53]. It has been observed that jet radius varies inversely with the cube root of the electrical conductivity of the solution [53, 58].

1.1.5.3.6 Applied voltage

The applied voltage is a crucial factor in electrospinning since it affects factors such as fibre diameter, flow rate, jet travelling speed and current density [53, 55]. Generally electrospinning uses direct-current (DC) voltage, since alternating-current (AC) voltage is not as safe as DC voltage, especially when working with the high voltage sources required by the electrospinning process [55]. Fibre formation during electrospinning can only be initiated once a polymer specific threshold voltage is reached [53, 58]. Applied voltage is the source of stretching force in electrospinning and it is through this process that it controls fibre diameter. This is since bending instability and jet stretching become more intensive under a higher applied voltage which leads to the production of finer fibres [55]. However, since the applied voltage does not only affect jet stretching, the impact thereof can become very complex. This is evident in the fact that higher voltages can also lead to bead formation and at a voltage of more than 30 kV, “corona discharge” occurs and impedes the electrospinning process [55].

There is a slight dispute regarding the behaviour of applied voltage in the electrospinning process. According to research by Reneker and Chun [65], electric fields do not have much of an effect on fibre diameter when spinning with polyethylene oxide. Researchers have also proposed that higher voltages lead to more polymer being ejected which results in larger diameter fibres [66, 67]. Contradictory to this a variety of researchers have reported that an increase in applied voltage favours narrowing of fibre diameter as reported on previously [53]. In general, it is accepted that a higher voltage causes more stretching of the solution due to greater Columbic forces in the solution jet along with a stronger electric field, all of which lead to a reduction in fibre diameter [53, 58].

1.1.5.3.7 Flow rate

Polymer flow rate from the spinneret is an important process parameter as it influences jet velocity and therefor the material transfer rate [53]. Flow rate also affects fiber diameter, porosity and the geometry of the elctrospun fibres [58].

It Is generally accepted that higher flow rates lead to beaded fibres due to incomplete solvent evaporation, while lower flow rates are associated with uniform fibre production due to complete solvent evaporation [53, 55]. High flow rates also cause an accumulation of solution at the needle tip which interrupts the Taylor cone and causes dripping from the needle. Fibres produced by higher flow rates also tend to bond together at intersecting areas upon deposition as well as potential flattened ribbon-like fibres due to incomplete drying before reaching the collector [55, 58]. With this in mind it is also important to understand that higher flow rates will produce fibres with larger average diameters than lower flow rates, within the bounds of acceptable flow rates to produce uniform fibres [55, 58]. This is since the delivery rate of the spinning solution increases which allows for an increased consumption of the solution. Furthermore, in electrospinning a minimum flow rate is also required to ensure that the consumption rate of solution is satisfied in order to maintain the generation of a continuous jet [58].

1.1.5.3.8 Collector type

In electrospinning the collector serves as a conductive surface where dry fibres are deposited. The alignment of electrospun fibres will be determined by the collector type as well as it's rotation speed. In general the generated fibres are randomly deposited on the collector due to the whipping instability of the solution jet [53].

1.1.5.3.9 Tip to collector distance

The tip to collector distance is another important parameter in determining fibre morphology and diameter however the effect hereof are less profound than that of other processing variables [58]. Since the tip to collector distance is directly related to the electrical field intensity and solution jet travel time, a shorter distance leads to a stronger electrostatic force which can either lead to more effective stretching of the solution jet or instability which increases the possibility of producing defected fibres [55]. This is also true in the case of a longer distance which will lead to less electrostatic force and therefor, a longer stretching and drying time for fibres [55]. The distance must be sufficiently large to allow the solution solvent to evaporate sufficiently before fibre deposition in order to assure cylindrical, uniform, and dry fibres are deposited [53, 55]. Fibres deposited over an insufficient tip to collector distance will have a flattened morphology due to insufficient solvent evaporation [53, 55]. It can be concluded that an optimum distance exists between the capillary and collector and on either side of this range electrospraying or bead formation can occur instead of fibre formation [58].

1.1.5.3.10 Ambient parameters

Ambient parameters also play an important role in the electrospinning process as they affect other electrospinning parameters. There is an inverse relationship between viscosity and temperature which will affect the spinnability of a solution [53, 55]. Humidity also affects the electrospinning process considerably. It has been found that very low humidity during electrospinning leads to rapid solvent evaporation which can cause the needle tip to clog inhibiting a continuous fibre formation [53].

An increase in humidity during the electrospinning process will result in an increase in pore size, pore size distribution and the number of pores present on fibres [55]. This is due to rapid solvent evaporation which removes heat energy from the surface of fibres leaving frozen moisture behind. Once fibres are deposited on the collector their surfaces are warmed up and the frozen moisture evaporates to produce pores [55].

1.1.5.4 Electrospinning solvents

The selection of solvent used during the preparation of a polymer solution has a significant impact on the spinnability thereof. This is since solution viscosity is determined by polymer concentration, but the value of surface tension depends on both the solvent and the polymer [55]. Thus the properties of the solvent have a great effect on fibre diameter [53]. In essence a solvent performs two critical roles in electrospinning: firstly, to dissolve the polymer molecules to allow the formation of an electrified jet within the spinneret and secondly to carry this electrified solution to the collector.

In summary it is important to understand that solvent properties such as boiling point, conductivity, polarity, dielectric constant and vapour pressure can influence solution properties such as conductivity, surface tension and viscosity [55]. With this is mind two important considerations in solvent selection are the solubility of the polymer in the solvent along with the boiling point of the solvent as an indication of its volatility [58]. Table 3 provides a summary of solvent properties and their effect on fibre morphology.

Table 3 - Electrospinning solvents

Solvent	***Boiling point (C)***	***Surface tension (mN m-1)***	***Dielectric constant***	***Fibre morphology***	***Polymer utilised during fibre morphology characterisation***	***Ref***
DCM	*39.8*	*28.1*	*9.1*	*Beaded, large diameter.*	*Poly(vinyl pyrrolidone)(PVP) and Poly(DTE-co-20%DT carbonate)*	*[58, 68]*
Chloroform	*61.2*	*27.2*	*4.8*	*Smooth at high polymer concentration, beaded at very low concentrations.*	*Poly(ethylene oxide) (PEO)*	*[58, 68]*
Methanol	*64.7*	*22.6*	*32.6*	*Small fibre diameter with high solvent concentration up until 50% concentration where after fibre diameter increases.*	*Poly(DTE-co-20%DT carbonate)*	*[58, 69]*
THF	*66*	*26.4*	*7.58*	*High pore density with smooth and beaded, ribbon-like fibres.*	*Poly(D,L-lactic acid) (PDLLA) and Polystyrene*	*[58, 70]*
Ethyl acetate	*77.1*	*24*	*6.02*	*Smooth and beaded, ribbon-like.*	*Polystyrene*	*[58, 69]*
Ethanol	*78.3*	*22.3*	*22.4*	*Smooth, large diameter.*	*PEO and PVP*	*[58, 69]*
MEK	*79.6*	*24.6*	*18.5*	*Very few beads, flat, ribbon-like.*	*Polystyrene*	*[58, 69]*
Water	*100*	*72.8*	*80.1*	*Beaded, small diameter.*	*PEO*	*[58, 70]*
DMF	*153*	*33.92*	*36.71*	*Smooth and beaded, round.*	*Polystyrene & PEO*	*[58, 70]*

1.1.5.5 Dual electrospinning

Dual-spinneret, co-spinneret or side-by-side electrospinning setups were initially designed to combine the attractive properties of two different materials into the same scaffold. This method was later popularised when Baker *et al.* [64] utilised this approach to improve scaffold porosity by electrospinning with water soluble, sacrificial fibres [6].

Fundamentally the electric field design of a dual electrospinning setup can only have three variations; spinnerets charged with like charges, opposing charges or using alternating current (AC) electrospinning. Li *et al.* designed a dual electrospinning system with two spinnerets and a rotating drum as a collector as shown in Figure 6. The spinnerets were located next to each other on the same end of the mandrel and were charged with opposite polarities with respect to one another. The configuration resulted in a highly intertwined and three-dimensional isotropic network structure [7].

Later a study by J. Voorenveld investigated the effectiveness of both like and opposing polarity configurations as well as modifications of each to further improve control of electrospinning jets [6]. The study found that charging both spinnerets with a like, positive, charge while providing the collector with a negative charge delivered the best results, as shown in Figure 7. Spinnerets were positioned on opposing sides of the collector mandrel with fibre deposition further improved by erecting two positively charged aluminium shields parallel to the jet trajectory to guide fibre deposition [6].

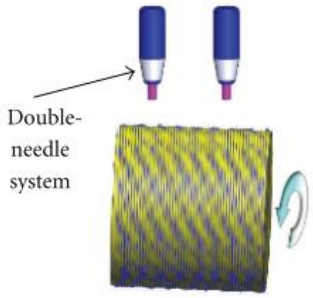

Figure 6 - Li et al. dual electrospinning setup. Image obtained from [7]

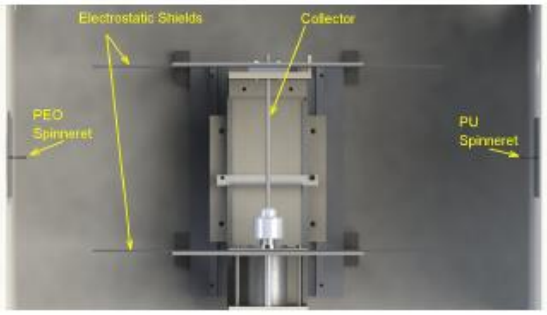

Figure 7 - J. Voorenveld dual electrospinning setup. Image derived from [6]

1.1.6 Synthetic biomaterials

Typically, polymers selected for heart valve applications are elastomers with low stiffness, high elasticity, and low glass transition temperatures so that the materials are pliable and rubbery at physiological temperatures. Polyurethanes (PU) have found the most success in this field with several PU-based devices reaching several hundred million cycles during in vitro durability testing [71].

1.1.6.1 Pellethane®

Polyurethane elastomers stand alongside the highest performing medical-grade polymers. They have mechanical and biological properties which make them suitable for use in a wide variety of medical applications due to their unique combination of durability, toughness, flexibility, biocompatibility and biostability [72, 73].

Pellethane® is a segmented polyurethane which holds a good balance between its biological and physiochemical properties along with ease of processing. As shown in Figure 8, Pellethane®'s segments consist of poly (tetramethylene oxide) (PTMO) as the soft-segment and a hard-segment made up of an aromatic junction unit 4,4'methylene-di-phenyldiisocyanate (MDI) and chain extender 1,4-butanediol (BDO) [72]. It has been found that this polymer may undergo oxidative degradation, however it is still generally considered to be hydrolytically stable [72]. Over many years polyurethanes have become widely used in the medical field as wound dressings, artificial heart valves, vascular grafts and an artificial heart [73].

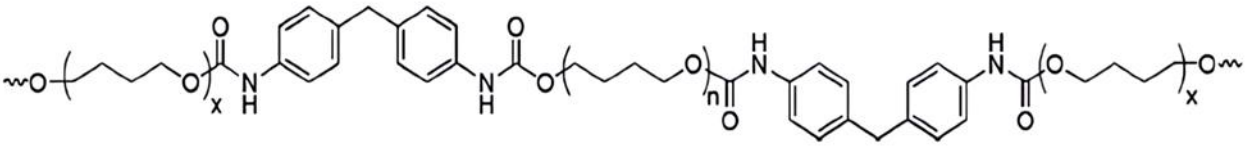

Figure 8 - Chemical structure of Pellethane®. Image obtained from [3]

1.1.6.2 DegraPol®

DegraPol® is a biodegradable polyester-urethane block copolymer that consists of poly(ε-caprolactone-co-glycolide)-diol soft segments and poly(3-(R-hydroxybutirrate)-co(ε-caprolactone))-diol hard segments. Both polymer segments are biodegradable, and their degradation products are considered non-toxic [73, 74].

Interestingly adjusting the hard and soft segment ratio, shown in Figure 9, alters the mechanical properties of the polymer allowing it to meet specific tissue engineering applications [75, 76]. Additionally, the hydrolytic degradation of the copolymer is both independent of mechanical properties and can be controlled by varying the glycolide content of the soft segment side of the copolymer, generally 0, 15 or 30% [3].

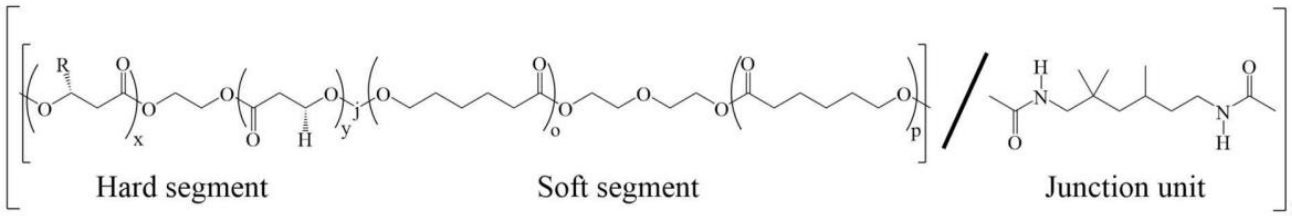

Figure 9 - Chemical structure of DegraPol®. Image obtained from[3].

1.1.7 Hybrid tissue engineered heart valves

1.1.7.1 Existing tissue engineered heart valves

Initial success has been widely reported in generating functional tissues in vivo through the combination of an appropriate cell type and a biodegradable scaffold, which is a commonly applied method in tissue engineering. However, a recent review by Yang *et al.* highlighted the increasing need and demand for methods which will accommodate the formation of more complex, composite tissues possessing coordinated function [77]. These hybrid methods remain largely unseen in the field of HVTE with very few studies of this nature being performed in other tissue engineering fields. In this section Table 4 and 5 aim to provide the reader with an overview of existing biodegradable and polymer heart valves to create an understanding of current research successes and shortfalls. To this end Table 5 provides a brief insight to hybrid tissue engineering approaches which have been researched in order to address some additional issues.

Prominent research groups in the field of biodegradable tissue engineered heart valves include the department of Biomedical Engineering at Eindhoven University of Technology. This group focuses on the mechanobiology of heart valves, cell and tissue homeostasis, micro-tissue platforms for high-throughput analysis, computational modelling of heart valve mechanics and remodelling, molecular signalling, manufacturing and molecular imaging of tissue differentiation and scaffold design [78, 79]. Another prominent group in this field is the Institute for Regenerative Medicine which focuses on combining advances in tissue engineering with new research in stem cell biology to improve existing and create novel regenerative medical treatments [80-84]. Lastly, Xeltis, a European medical device company, have produced extremely promising results in the last couple of years. The group develops fully bioabsorbable, implantable, heart valve replacements which are intended to spontaneously grow and remodel into functional heart valves in vivo. Their initial focus is on the treatment of children with complex congenital heart diseases with two clinical feasibility studies recently performed, as touched on in Table 3 [85, 86].

Hybrid approaches vary significantly depending on the intended application of the scaffold. All hybrid approaches mentioned in Table 5 have made use of co-spinning to create either distinct varying scaffold regions or scaffolds containing multiple polymers homogenously electrospun throughout the scaffolds.

It is well known in the tissue engineering field that porosity of a scaffold is an important parameter in controlling homogenous cell distribution, cell motility, nutrient supply, and waste removal. Insufficient porosity will lead to cell death and therefor delayed tissue ingrowth [87]. To overcome this limitation Baker *et al.* proposed the production of scaffolds with two simultaneously co-spun polymers with varying solubilities. The fibres produced by one of the polymeric solutions are treated as sacrificial fibres which are dissolved out of the scaffold, through extensive rinsing after electrospinning, to increase scaffold porosity [87]. A study conducted on the co-spinning of PCL and PEO concluded that a linear relationship exists between sacrificial fibre removal and overall scaffold properties. These findings are consistent with the work of Ding and co-workers [88]. Additionally, a notable improvement in cellular infiltration was seen in scaffolds after the removal of PEO fibres, particularly in meshes which started with a greater than 40% sacrificial component [64]. Voorneveld achieved significant improvement in in vivo tissue ingrowth using PU scaffolds enhanced in porosity through sacrificial fibre extraction [6].

Finally, another generally proposed failure mechanism of tissue engineered heart valves is leaflet shrinkage. This is the result of cell-mediated tissue contraction resulting in leaflet shortening in the radial direction. This shrinkage leads to insufficient coaptation and thus valvular incompetence. Interestingly it has been reported that this process already occurs during in vitro tissue conditioning, thus mild to moderate valve regurgitation is already present in these valves at the time of implantation [89]. Various solutions have been proposed by researchers over the years. One of these propositions was a constraining bioreactor insert proposed by Sanders *et al.* [90]. The study designed an insert which was used during culture in a bioreactor to maintain leaflet shape during cell culture, decellularization, and during the removal of the insert. The study resulted in a fully competent off-the-shelf available decellularized TEHV with a large coaptation area. Additionally long term functionality of the valve up to 16 weeks in vivo was maintained, slowing adequate time for host cell repopulation [90]

Table 4 - Representative table of prominent research groups in the biodegradable tissue engineered heart valve field

	Focus	Materials used	Animal studies	Findings	Ref
Department of Biomedical Engineering, Eindhoven University of Technology, Netherlands					
1 (2014)	*Evaluation of in vivo functionality, host cell repopulation, and matrix remodelling of transcatheter TEHVs.*	*PGA/P4HB.*	*TEHV implanted in the pulmonary position of sheep, evaluated up to 24 weeks post implantation.*	*Significant matrix remodelling was observed in the entire valve and corresponded with the rate of host cell repopulation. Moderate to severe insufficiency in all TEHV after 24 weeks of implantation.*	*[78]*
2 (2017) ***conducted with IREM***	*Proof-of-concept of in situ TEHV using a cell-free synthetic scaffold, to be populated by endogenous cells.*	*Custom-developed bioresorbable supramolecular elastomer, based on bis-urea-modified polycarbonate (PC-BU).*	*TEHV were implanted into the pulmonary position of sheep and were evaluated up to 12 months post implantation.*	*The valves demonstrated sustained functionality over the 12 months follow-up period and were extensively colonized by host cells, throughout the entire leaflet, although scaffold degradation was not yet complete within 12 months follow-up. Lastly, pathological calcification was absent throughout the 12 months implantation period. Together, these results present the initial proof-of-concept of in situ HVTE.*	*[79]*
Institute for Regenerative Medicine (IREM)					
1 (2011 – 2014)	*Investigation of the combination of TAVI and a novel concept of stem cell-based, tissue-engineered heart valves (TEHV).*	*Biodegradable synthetic scaffolds, self-expanding nitinol stents, seeded with autologous bone marrow mononuclear cells.*	*TEHV were implanted into adult sheep using the TAVI procedure and follow up procedures were scheduled for up to 2 weeks after surgery.*	*TEHV showed intact leaflet structures with well-defined cusps without signs of thrombus formation or structural damage with adequate leaflet motion and coaptation . Indication of early cellular remodelling and in-growth after 2 weeks with long term functionality of TEHV not confirmed. Importantly, these studies demonstrated the principal feasibility of a transcatheter, stem cell based TEHV implantation into the aortic valve position.*	*[80-82]*
2 (2018)	*Development of a Novel Human Cell-Derived TEHV for TAVR.*	*Polyglycolic acid meshes (Cellon) coated with 1% P4HB in tetrahydrofuran.*	*Valves were implanted transapically in the orthotopic aortic position of sheep.*	*Valves successfully withstood the aortic hemodynamic and demonstrated good in vitro and in vivo functionality with free coronary flow, normal leaflet motion, and the absence of stenosis or paravalvular leakage. Furthermore, fast host cell infiltration was observed.*	*[83]*
3 (2018)	*Computational modelling to guide tissue remodelling towards long term functionality.*	*Polyglycolic acid meshes (Cellon), sewn nitinol stents , and coated with 1.75% P4HB.*	*TEHV were implanted in the pulmonary position of sheep and evaluated 1 day, 1 week and 1 year after implantation.*	*Computational modelling improved long-term in vivo performance and remodelling and is recommended for safe and efficient clinical translation of TEHV.*	*[84]*
Xeltis					
1 (2017)	*Evaluation of acute valve performance in a preclinical setting.*	*polyester-urethanes which contain the (UPy) binding motif, mounted on a nitinol frame.*	*XELTIS aortic valve were transapically implanted in sheep.*	*In a transapical ovine model, the valve demonstrated good hemodynamic performances, comparable to commercially available devices. The valve leaflets demonstrated good competence immediately after implantation with no cases having more than mild transvalvular aortic regurgitation.*	*[85]*
1(2021)	*First use of a biorestorative valved conduit in children (pulmonary position).*	*The conduit wall and leaflets consist of poly-carbonate-based UPy.*	*Twelve children (six male) median age 5 (2 to 12) years.*	*valved conduit, demonstrated promising early clinical outcomes in humans with 17 of 18 patients being free of reintervention at 1 year. Early onset PI seen in the XPV-1 version seems to have been corrected in the XPV-2, which has led to the approval of an FDA clinical trial.*	*[86]*

1.1.7.2 Hybrid approach to tissue engineering

Table 5 – Representative table of previous hybrid approached to tissue engineering.

	Hybrid scaffold application	***Biomaterials used***	***Findings***	***Ref***
1 (2014)	*Scaffolds for bladder tissue regeneration.*	*8 wt% PLGA co-spun with 30 wt% PEG, both in chloroform.*	*Composite scaffolds were produced by co-spinning polymer onto the external side of a wet bladder acellular matrix. Composite scaffolds spun with more than 25% PEG were not stable enough for surgical handling and were not used for analysis. In vitro evaluation showed no statistical significance between single-spun and co-spun scaffold cell numbers from day 2 to 4. However, significantly deeper cell migration into co-spun scaffolds were found with more even cell distribution. In vivo evaluation revealed significant shrinkage of single-spun scaffolds (spun with PLGA as the control) while co-spun scaffolds maintained their original size.* *Rat implant studies revealed that revascularization of the regenerated bladder wall increased with the duration of implantation for co-spun scaffolds with blood vessels tending to be more numerous, denser and differentiated for these scaffolds when compared with single-spun scaffolds.*	*[87]*
2 (2007)	*Small to medium sized vascular grafts.*	*20wt% (Pellethane) (solvent: DMF), co-spun with PEO varying between 15 to 35wt%.*	*Lower concentrations of PEO tended to show beads. The porosity of the scaffolds after extraction of PEO was highly increased with porosity increasing with increased concentrations of PEO. In vitro studies revealed higher proliferation rates of smooth muscle cells at higher concentration of PEO than at the lower concentration and without PEO. In conclusion, the dual electrospinning technique was expected to overcome the current barrier of cell penetration by providing higher porosity for cellular proliferation.*	*[91]*
3 (2011)	*Scaffolds for muscle-tendon junction site tissue engineering.*	*(1) 5% (w/v) PLLA/collagen (1:1) wt% (2) 10% (w/v) PCL/collagen (1:1) wt%. Solvent for both solutions – HFP.*	*Co-electrospinning was used to create three distinct scaffold regions: a PCL/collagen region (PCL side), a PLLA/collagen region (PLLA side), and an overlap region (centre). Mechanical testing revealed that the centre (composite) region of the scaffold exhibited mechanical property values in between those of the two side regions where only single spun fibres resided. Thus, it can be concluded that co-spinning with two polymers will result in a scaffold with unique mechanical properties.*	*[77]*
4 (2011)	*3D fibre fleeces electrospun for soft tissue engineering applications.*	*8wt% PLGA and 24wt% DegraPol® (DP) were co-spun with PEG, respectively. Chloroform was used as the solvent.*	*DP- and PLGA were co-spun with different ratios of PEG (0, 25, 50, 75, 100%). Scaffolds electrospun with more than 50% PEG were not stable and therefor were not used for cross sectional analysis or for cell experiments. An inverse relationship between scaffold porosity and Young's Modulus was found.* *In vitro studies revealed cells proliferated on all scaffolds however proliferation was faster on PLGA-scaffolds in comparison to DP-scaffolds, while varying porosities of DP- and PLGA-scaffolds had no notable effect on cell proliferation. Regardless of the scaffold polymer it was found that cells were most homogeneously distributed within scaffolds with highest porosity, while cells cultivated in scaffolds without water-soluble polymer were mostly present at the surfaces of the scaffolds.*	*[92]*

1.2 Aim and Objectives

The aim of this study was to produce hybrid electrospun scaffolds, consisting of both degradable and non-degradable fibres, for an application in tissue engineering and to characterise the behaviour of these scaffolds in comparison with scaffolds spun purely from degradable and non-degradable polymers. The non-degradable thermoplastic polyurethane, Pellethane®, and degradable polyester urethane block copolymer, DegraPol15® were used in this study.

The rationale of the study was to provide scaffolds with mechanical strength and the ability to partially degrade driving tissue ingrowth into the scaffolds, while retaining non-degradable reinforcement. Thus, providing scaffolds that are initially a hybrid of degradable and non-degradable fibres which could result in hybrids of tissue and non-degradable fibres if they were to be implanted.

The aim of the study was achieved through the following objectives:

- Electrospinning DegraPol® and Pellethane®, modifying parameters to determine suitable conditions to produce hybrid scaffolds.
- Producing novel hybrid scaffolds containing both polymers using dual spinning.
- Characterising polymer bulk properties through solution cast films to investigate the effect of processing/electrospinning on polymer and scaffold strength.
- Characterising the mass loss and mechanical behaviour of single-spun and dual-spun scaffolds before and after periods of exposure to hydrolytic degradation.
- Characterising scaffold morphology, permeability, and wettability.
- Producing TAVR heart valves from single-spun and dual-spun scaffolds to be evaluated in vitro to compare hydrodynamic performance and durability variations between scaffold types.

The results of this study will contribute to the knowledge of DegraPol® characteristics such as thermal and mechanical properties as well as degradation characteristics as this polymer's properties are not widely documented. The development of hybrid scaffolds using degradable and non-degradable fibres is novel and could form a basis for future work in the field of tissue engineering scaffolds, especially the field of heart valve tissue engineering.

2 Materials and Methods

This chapter provides information on selected materials and methods used during the development of all electrospun scaffolds and TAVR valves. Among others scaffold morphology, degradation and mechanical properties were analysed using a series of in vitro tests. Furthermore, this section describes the methods used to manufacture valves, and to characterise scaffold permeability and hydrophilicity as well as valve hydrodynamics and durability.

2.1 Materials

Two biomaterials were selected for scaffold development. The first, a biodegradable polyester urethane block copolymer called DegraPol15® (90 000 – 110 000Da, 1.15 g/cm^3) obtained from ab medica, S.p.A, Lainate Italy. Secondly, a thermoplastic elastomer, Pellethane® (2363-80AE, 1.12 g/cm^3), obtained from Dow Chemicals, Midlands Michigan, USA.

Solvents Tetrahydrofuran (THF), Dimethylformamide (DMF), Hexafluoro Isopropanol (HFIP), Chloroform (CHCl3) and Dimethylacetamide (DMAC) were all purchased from Sigma-Aldrich (Pty) Ltd, Johannesburg, South Africa.

2.2 Scaffolds

Both films and three-dimensional scaffolds were used during this study to allow for an improved understanding of the effect of processing methods on polymer bulk properties. Films were produced using a casting method, while three-dimensional scaffolds were produced by electrospinning.

2.2.1 Casting

Cast Pellethane® films were produced using a solution which consisted of 5 wt% Pellethane® in Dimethylformamide (DMF) solvent and DegraPol® castings were produced using a solution of 3 wt% DepraPol15® in a 1:1 v/v ratio of Hexafluoro Isopropanol (HFIP) and Chloroform ($CHCl_3$) solvent. The solutions were left on a magnetic stirrer for 24 hours after which they were poured (10 ml) into a Ø6 cm glass dish. Filter paper was placed over each dish to minimise exposure to contamination and slow down initial solvent evaporation. Pellethane® scaffolds were subsequently placed into an oven at 50℃ and left to dry for 48 hours, while DegraPol® scaffolds were placed in a fume hood and left for 48 hours. Hereafter Pellethane® scaffolds were removed from the dish by cutting around the edge of the dish and pulling the scaffold free from it. DegraPol® scaffolds were removed from the dish by cutting around the edge of the dish and placing it in distilled water for 30 seconds to lift the scaffolds from the dish. All scaffolds were then placed in the vacuum oven at room temperature for an additional hour to remove any remaining solvent. Hereafter scaffolds were stored in a desiccator to avoid exposure to moisture before and after further processing.

2.2.2 Electrospinning

2.2.2.1 Solution preparation

Solution concentrations were expressed as weight-to-weight (wt%) for polymer to solvent and were prepared in glass bottles (Pyrex®). Solutions were prepared through magnetic stirring for at least 12 hours at room temperature. After mixing, solutions were allowed to rest for one hour to remove any heat or bubbles generated by stirring, before transferring it to a syringe for electrospinning.

2.2.2.2 Electrospinning equipment and design

The electrospinning setup used to produce scaffolds consisted of a custom built rotating and translating mechanism with both variable rotation speeds (0-400 rpm) and translation distances (0-90 mm). A custom-built gear box (1:4 ratio) was also attached to the rotating axis to allow rotation at higher speeds. Both the translational and rotational speeds were controlled with an Arduino Mega 2560 micro-controller.

Three high-voltage power supplies were available, with the first positive power supply used for single electrospinning (ES30P-5W, Gamma High Voltage Research, USA) and the addition of the second for dual spinning (ES60P-20W, Gamma High Voltage Research, USA) to charge the spinnerets (hypodermic needles). The negative power supply (ES30P-5W, Gamma High Voltage Research, USA) was used to charge the rotating collector (75 mm diameter, 80 mm length, stainless steel). Two separate syringe pumps were used to feed polymer solutions from 20 ml syringes (B Braun, Germany) through tubing into blunted hypodermic needles (40 mm length) for either single spinning (SE400B, Fresenius, Bad Homburg, Germany) or dual spinning (SE200, Fresenius, Bad Homburg, Germany), where a second hypodermic needle was added on the opposite end of the collector. The hypodermic needles were fed though 6 cm x 6 cm stainless steel base plates.

As part of controlling the ambient conditions of electrospinning, a custom-built environmental control unit was attached to the electrospinning chamber. The unit contained an activated carbon filter (Advanced Air Carbon Filter, 4”x12”, 200 CFM flow rate, Futurama, RSA) to remove solvent vapour, a filter fitted with desiccant silica gel to remove moisture from the air, a nebulizer (NB-80E-01-H, TDK Corporation, Digi-Key, USA) to increase relative humidity as and when required and a humidity sensor (Adafruit SHT31-D, Communica, RSA) controlled by an Arduino Uno micro-controller. Air flow in the unit was directed by three high-speed fans (10 cm × 10 cm, 12 VDC, 0.35 A, Communica RSA) all controlled by the Arduino Uno. Figure 10 indicates the various flow configurations, where white arrows indicate the inlet flow though the activated carbon filter, blue arrows indicate the wetting loop (nebuliser), and red arrows indicate the drying loop (desiccant). When the desired set point was reached flow redirected to follow the white and blue arrows and the nebuliser was switched off by the micro-controller. Lastly, a non-contact thermo-hygrometer (testo 175H1) was fitted inside the electrospinning box to record current temperature and humidity while spinning. The voltage of each power supply, tip to collector distance, polymer flowrate and humidity were set to the optimum conditions required for each polymer, as determined by initial pilot experiments. Figure 11 depicts the overall electrospinning rig setup.

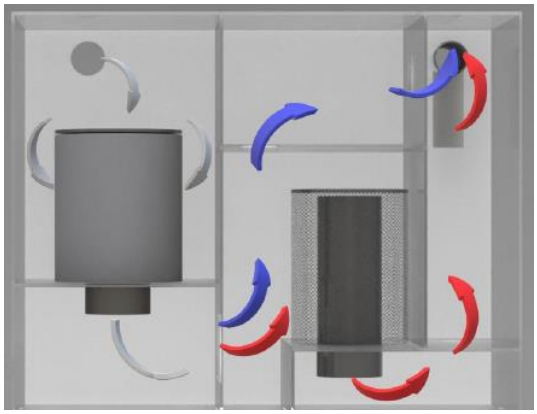

Figure 10 - Illustration of flow through the humidity control unit. White arrows indicate flow at set point conditions, blue arrows indicate the wetting loop and red arrows indicate the drying loop. Image from [2]

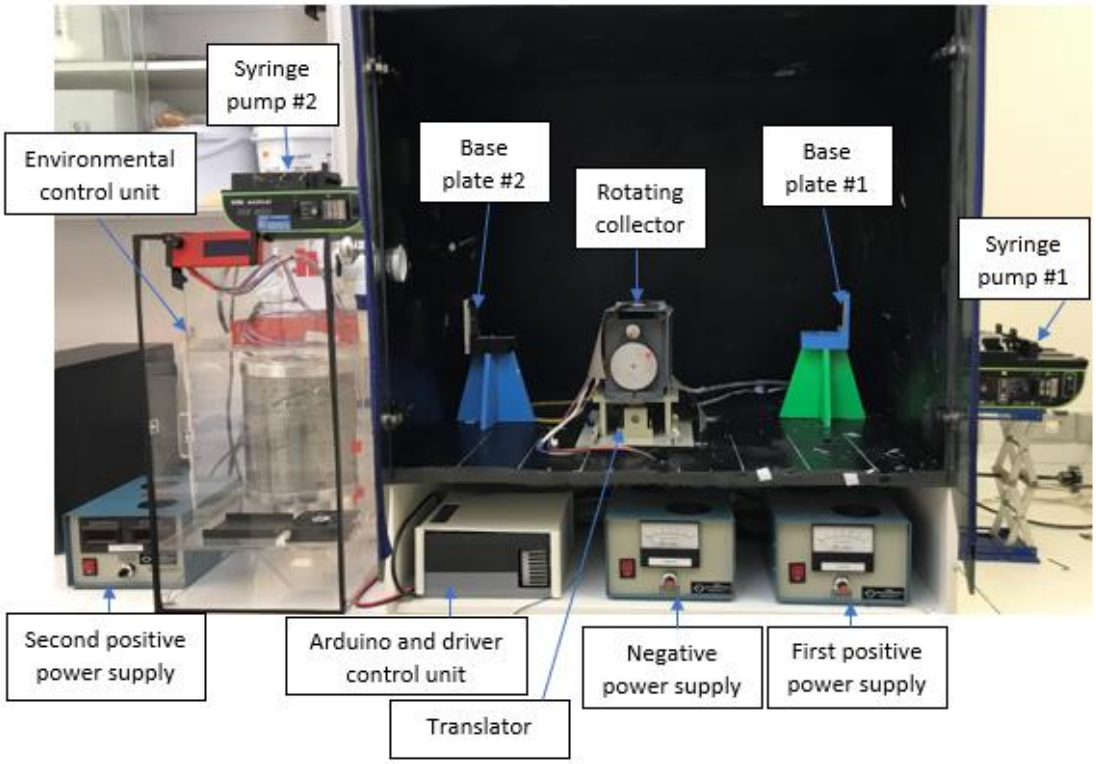

Figure 11 - Electrospinning rig setup

2.2.2.3 Composite scaffold fabrication

As previously touched on, dual scaffolds were spun through the addition of a second positive power supply and spinneret on the opposite end of the collector. To effectively produce hybrid scaffolds with a 50%-50% ratio of each polymer it was decided to electrospin solutions with similar polymer weight percentages at the same flowrate. This method was chosen to ensure that both solutions are spinning simultaneously throughout the entire scaffold spinning time, in order to create a homogonous hybrid scaffold. The electrospinning conditions used for the dual scaffold fabrication are listed in Table 7 along with all parameters which were kept constant throughout the study in Table 6.

Table 6 - Electrospinning parameters which were kept constant throughout the study

Parameter	Value
DegraPol® polymer concentration	*15 wt%*
DegraPol® solvent	*95%$CHCl_3$:5%HFIP*
Pellethane® polymer concentration	*18 wt%*
Pellethane® solvent	*DMF:THF*
Mandrel rotation speed	*180 rpm*
Translating distance	*80 mm*
DegraPol® needle size	*19 G*
Pellethane® needle size	*18 G*
Relative Humidity	*31.82 ± 2.39%*
Temperature	*23.02 ± 0.75℃*

Table 7 - Conditions for dual scaffold fabrication

Solution ratio	Flowrate	Tip to collector distance
100% DegraPol®	*3 ml/h*	*38 cm*
50% DegraPol® – 50% Pellethane®	*3 ml/h*	*38 cm*
	3 ml/h	*22 cm*
100% Pellethane®	*3 ml/h*	*22 cm*

2.3 Scaffold characterisation

2.3.1 Scanning electron microscopy

Degradation samples, single spun and dual spun samples were gold sputter coated (Polaron SC7640, 120s at 1.4kV and 33 mA) prior to SEM imaging (JEOL, JSM – IT200). SEM images were captured of the luminal and abluminal surfaces as well as at sites of interest on scaffolds. Three sample sections were taken from each scaffold and three images were captured per sample section for each of the samples. Luminal and abluminal images were used for morphological analysis while site-of-interest images were used for illustrative purposes. Images of electrospun fibres were captured at suitable magnifications for their respective image analyses.

2.3.2 Fibre diameter, orientation, and pore size measurement

2.3.2.1 Fibre diameter

ImageJ (Version 1.53e) software was used to measure fibre diameter, fibre orientation and pore size of electrospun scaffolds. Fibre diameter was measured manually as outlined in Figure 12. Firstly, a line was drawn over the scale bar of the SEM image and the scale for measurements was calibrated (µm/pixels). A diagonal line was drawn from the bottom left corner of the image to the top right corner and the diameter of all fibres, in the foreground, intersecting the diagonal line were measured. To measure fibres a line was drawn perpendicular to the fibre length across its width, and the length of the line was recorded and later exported to excel. The average fibre diameter was then calculated using all the fibre width measurements from the image.

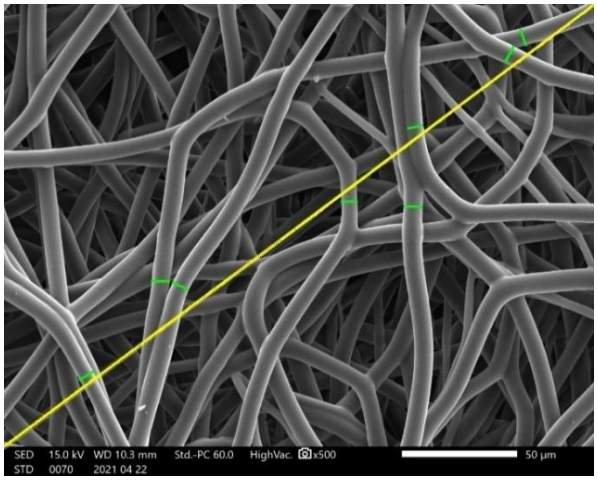

Figure 12 - Measuring fibre diameter using ImageJ

2.3.2.2 Fibre orientation

Fibre orientation was calculated using the ImageJ plugin, OrientationJ, which produces a coherency value for an image. The entire SEM image, excluding the bottom scale bar, was used as the area of interest for measuring alignment. An orientation index, 0<x<1, was used to quantify fibre alignment, with a value approaching zero representing randomly distributed fibres and a value approaching one representing perfectly aligned fibres, as shown in Figure 13.

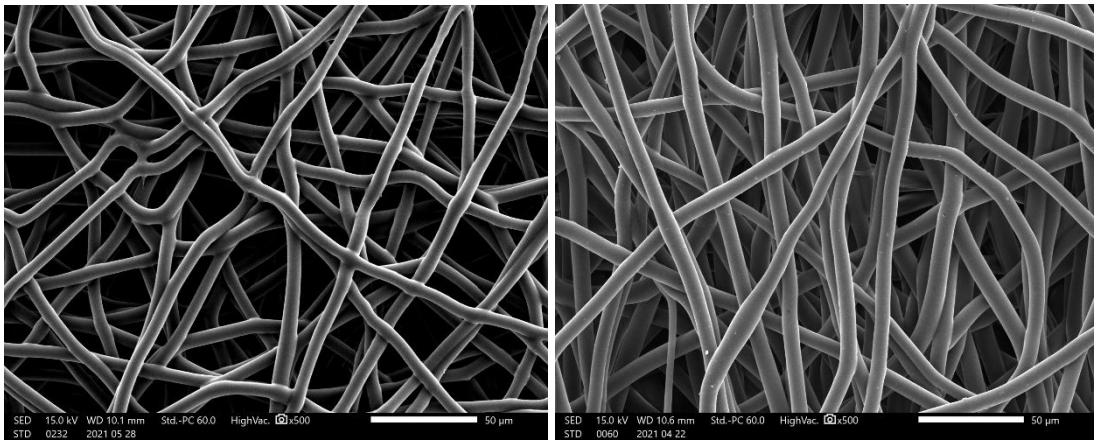

Figure 13 - (Left) Very randomly distributed fibres with an OrientationJ coherency value of 0.085%. (Right) Slightly more aligned fibres with an OrientationJ coherency value of 0.286%.

2.3.2.3 Pore size

Sample pore size was calculated using an ImageJ macro which was developed in our laboratory. The macro was used to adjust the selected micrograph (auto threshold filter -> 3.5 pixels median filter -> find edges function -> fill holes function) to detect available pores in the selected region and to measure the area of each pore, as shown in Figure 14.

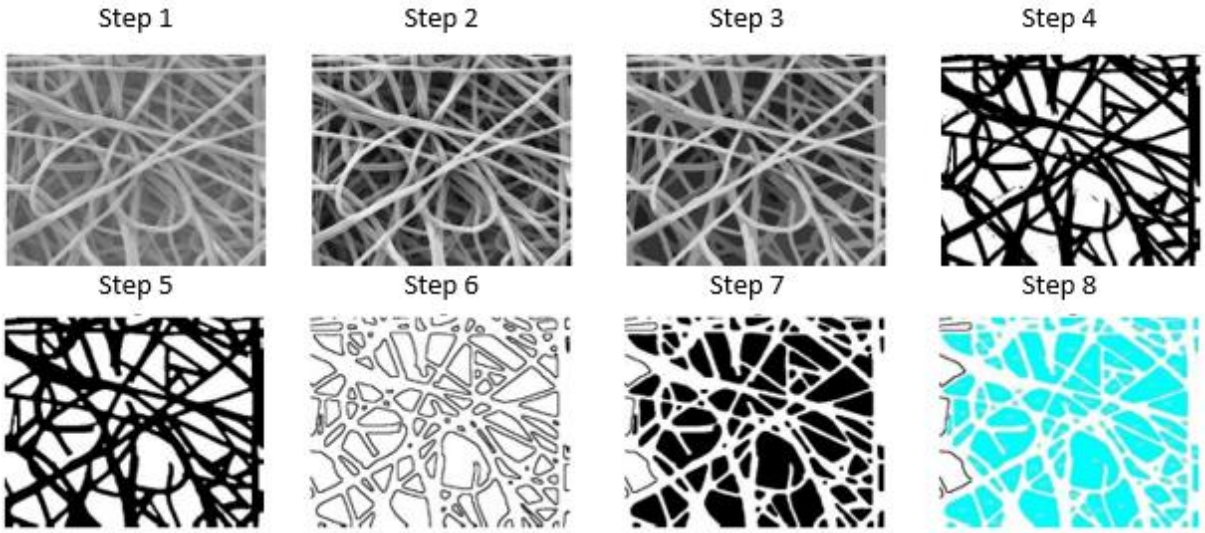

Figure 14 - Intermediate steps of scaffolds pore size determination macro. Developed by [3].

Equation (1) was used to find the equivalent circular pore size of each pore from the pore area;

$$P_S(\mu m) = 2 \times \sqrt{\frac{P_A}{\pi}} \qquad (1)$$

with P_S the pore size and P_A the pore area.

2.3.3 Porosity measurement

Sample porosity was calculated using the ratio of the volume of the sample fibres (V_f) to the bulk volume (V_{bulk}) of the scaffold, as in Equation 2. From this ratio Equation 3 was derived. Scaffold samples for porosity determination were discs with diameters of 5 mm and porosity was determined through hydrostatic weighing using a five-decimal lab balance (Mettler Toledo, Switzerland) fitted with a densitometric kit. Samples were weighed in air as well as in hexane (ρ = 0.15 g/cm^3) to remove all air from the scaffold, as shown in Figure 15.

$$P_{scaffold} = 1 - \frac{V_{fibres}}{V_{bulk}} \qquad (2)$$

$$P_{scaffold} = 1 - \frac{m_{x,air} - m_{x,hexane}}{\rho_{hexane} \times V_{bulk}} \qquad (3)$$

With $m_{x,air}$ the mass of the sample in air, $m_{x,hexane}$ the mass of the sample submerged in hexane, and V_{bulk} the total volume of the scaffold sample.

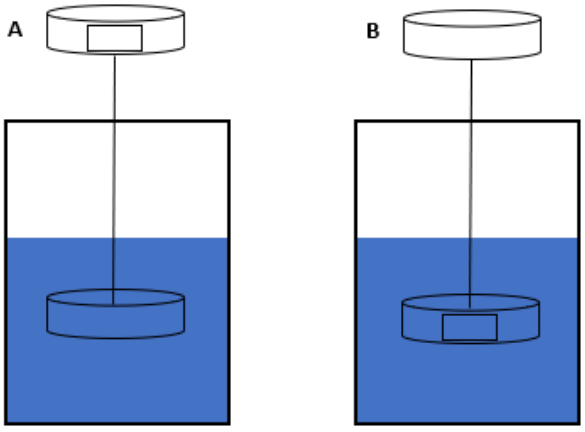

Figure 15 - Hydrostatic weighing A) in air, B) in hexane

2.3.4 Contact angle measurement

The surface hydrophilicity of microfibre scaffolds was investigated by observing water contact angles. A drop of DI water was dispensed onto a scaffold sample and contact angles were evaluated by analysing the drop shape. Images of the drop for analysis were captured using a CCD camera (Techgear Eaglescope, China), and were analysed using an ImageJ plugin, named the LBADSA (Low-Bond Axisymmetric Drop Shape Analysis) method [93].

The plugin is based on the fitting of the Young-Laplace equation to the image, as indicated in Figure 16. Measurements were repeated three times for each scaffold type on both the luminal and abluminal surfaces.

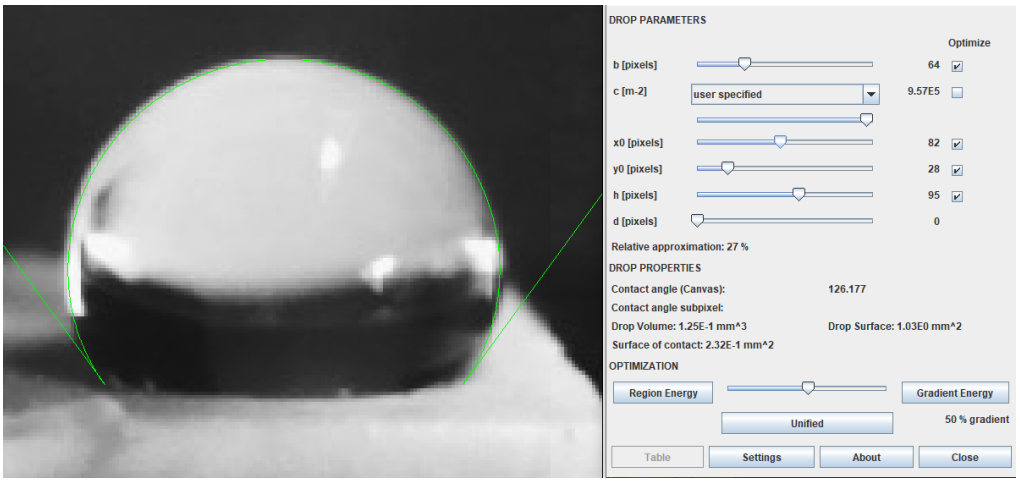

Figure 16 - Water contact angle measurement analysis using ImageJ

2.4 Mechanical testing

The mechanical properties of both electrospun and cast scaffolds were determined using a tensile tester (Instron 5544) using a 500 N load cell for DegraPol® and 2000 N load cell for both Pellethane® and hybrid scaffolds. Samples were punched from electrospun scaffolds into samples compliant with ASTM size requirements (test area: L = 22.24 mm, W = 4.75 mm) and had thicknesses of 0.38 ± 0.057 mm, 0.29 ± 0.050 mm and 0.31 ± 0.057mm for electrospun Pellethane®, DegraPol® and hybrid samples respectively and 0.24 ± 0.042 mm and 0.18 ± 0.016 mm for cast Pellethane® and DegraPol® films, respectively. The number of samples tested in each group was three (n = 3) and all tests were conducted at room temperature. In the case of electrospun scaffolds three specimens radial to - and three specimens longitudinal to the direction of spinning, were mechanically tested.

Initially, “air-wet” Pellethane® samples, which were soaked in phosphate-buffered saline (PBS) for 20 minutes prior to testing in air, along with dry samples were tested at the same strain rate until failure. Data produced during these tests showed no significant difference between air-wet and dry sample values and therefor all samples here after were tested at air-wet conditions. This was beneficial for all degradation study samples, which had been degraded in PBS, as no additional potential anomalies during drying needed to be introduced, and the wet state also better approximated in vivo conditions.

2.4.1 Tensile testing

Specimens of known thicknesses, for all polymer sample groups, were subject to tensile testing until failure at a strain rate of 50 mm/min. The strain rate was calculated based on the recommended ASTM D638-10 speed of testing rates. The recommended strain rate for non-rigid specimens of the size selected for this study is 50 ± 10% mm/min [94].

A pretension of 0.02 N was applied to each sample after which the machine load was reset to 0 N before starting each test. Raw data captured by the Instron system was processed as stress strain plots from which mechanical properties could be determined.

The maximum recorded stress along with its corresponding strain value were defined as the ultimate tensile strength (UTS) and maximum elongation (ε_{max}) respectively. Young's modulus (E_Y) was approximated as the slope of the line fitted to the stress/strain curve between strain of 0% to 10%.

2.4.2 Cyclic Tensile testing

Specimens of known thicknesses, for all polymer groups, were subject to cyclic testing which consisted of 120 cycles at a strain rate of 160 mm/min with an extension value of 6.67 mm (30 % of the sample test length). A pretension of 0.02 N was applied to each sample after which the machine load was set to 0 N before starting each test. After the 120 cycles were complete each sample was extended by 7.5 mm at a strain rate of 160 mm/min to end off the test. Raw data captured by the system was processed into stress strain curves to produce data on cyclic fatigue of electrospun scaffolds. During this study hysteresis was calculated from cyclic testing data using the trapezoid rule to calculate area under curves.

2.4.3 Suture retention analysis

Suture retention strength determination was conducted using the straight-across method as per ISO 7198 using the tensile tester previously mentioned. Rectangular specimens were clamped at the edge located opposite to the suture. A coated, braided, polyester 5-0 suture was inserted 2 mm from the end of the 4.75 x 11.12 mm sample and passed through the sample to form a loop, fasted with two surgeon's knots. The crosshead speed was set to 50 mm/min and tests were conducted at room temperature in a dry environment, for all test groups. Once the suture was taut, the test was initiated, and the force required to pull the suture through the sample or to cause the sample to fail was recorded. Three specimens parallel and perpendicular to the direction of spinning were analysed for each of the sample groups.

2.4.4 Resistance to tear analysis

Resistance to tear tests were conducted inline with ISO 6383-1 guidelines, which is relevant to plastic films or sheets less than 1 mm thick, in the form of standard trouser-shaped test specimens. The standard ISO 6383-1 test procedure requires specimens with a length of 150 mm where the first 20 mm and final 5 mm portions of the force/distance graph produced are ignored. As specimens of 150 mm could not be produced from the electrospun scaffolds, test specimens of adequate length were produced and the first 27% and last 7% of the force/distance graph were ignored, to keep in line with testing procedures.

Specimens were separated by a slit of half the length of the sample resulting in two "legs" which could be torn apart at a constant speed while tensile force was measured. The thickness of all samples was measured across the length of the specimen and an average value was recorded. The test was set in motion at a fixed crosshead speed of 200 mm/min and tear resistance was calculated as the mean load (Ft, N) divided by the sample thickness (d, mm).

2.5 Valve fabrication

Valve fabrication consisted of three distinct processes, described below. The first process consisted of coating all TAVR stents to allow for the second process which was the bonding of electrospun skirts to the stents. Lastly valve leaflets were punched from electrospun scaffold sheets and sutured onto the stents.

2.5.1 Stent coating

Stents used during this study were provided by Straight Access Technologies (SAT, Cape Town), and were tri-leaflet TAVR stents. The stents consisted of three commissure posts, three scallop lines and various struts, all indicated in Figure 17.

A rack style coating method was implemented to coat all stents during this study, as the process is relatively simple and cost effective to implement. It was found that stents could be coated with a range of solution concentrations varying from 3 wt% to 5 wt% Pellethane® in DMAC. Although more viscous solutions (higher concentration) required less coats to reach the desired coating thickness, these solutions were prone to spanning across the stent struts. Therefore, stents were coated with 4 wt% Pellethane® DMAC solution which required more coats but delivered a more uniform stent coating.

In terms of the coating process, stents were dipped into a glass bottle containing the coating solution, ensuring that the entire stent area was at some point emerged in the solution. The stent was then removed from the container and a rod was placed through two of the struts, suspending it above a drip tray to dry. After the stent was initially submerged into the solution for coating, each consecutive dip thereafter only lasted for a maximum of 10 seconds. This was to ensure that previous layers coated onto the stent would not be removed while the stent was submerged in the solution during a subsequent coating. Between each coating the stents were placed in an oven (Scientific, Series 9000) at 60℃ for 20 mins to dry. It was determined that for 4 wt% Pellethane DMAC, a total of 8 coats was sufficient for bonding of electrospun skirts. Lastly, between each coating the stents were hung onto the rack in varying configuration, to ensure that the stent was coated evenly, as shown in Figure 18.

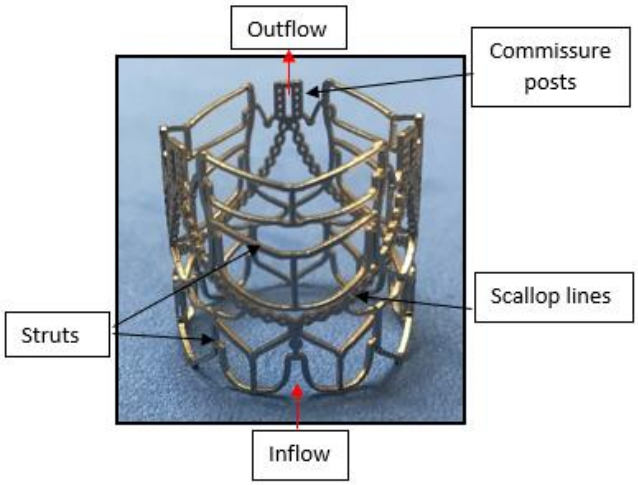

Figure 17 - Straight Access Technologies stent components

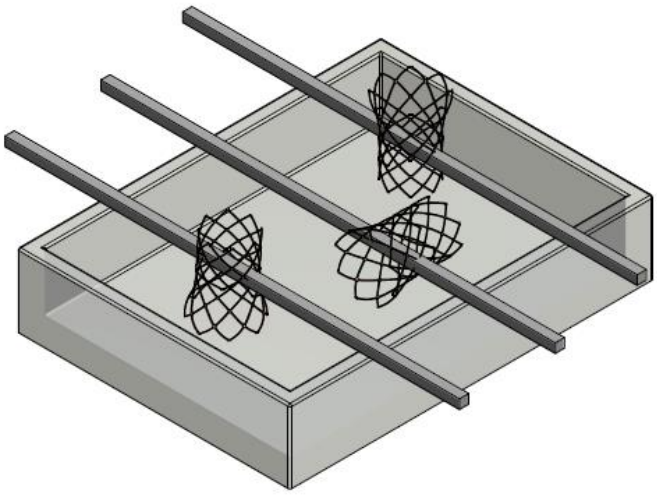

Figure 18 - Stent coating procedure using a rack style coating method

2.5.2 Skirt bonding

Heart valve skirts were produced to mitigate paravalvular leakage and were produced from electrospun scaffolds to allow transmural tissue ingrowth. All skirts were electrospun using parameters for Pellethane® as set out in Table 8, to obtain the desired scaffold thickness of 150 microns. Skirts were electrospun onto a 25 mm diameter mandrel using the single spinning electrospinning setup described in section 2.2.2.2.

Table 8 - Pellethane® skirt electrospinning parameters

Parameter	
Solution concentration	*16 wt%*
Needle gauge	*18G*
Tip to collector distance	*23 cm*
Mandrel size	*25 mm*
Mandrel rotation speed	*200 rpm*
Humidity	*30.00 ± 1.56%*
Temperature	*22.89 ± 0.62℃*
Solution flow rate	*4.5 ml/h*

All stents also had two skirts individually bonded to it by means of a soldering iron (Magnum 2005, 24V, 80W) equipped with a flat edge on its tip to avoid puncturing the skirts during bonding. The first electrospun skirt was stretched over the stent so that it stretched from halfway through the commissure posts, down over the struts with some excess still protruding past the bottom end of the stent. Once the skirt was placed in the correct position the stent was positioned over a light box so that the stent frame could be visualised through the skirt scaffold. The soldering iron temperature was initially set to 165℃, with soldering iron temperatures being varied between 165℃ and 180℃ depending on a variety of factors such as scaffold thickness and stent coating thickness.

All three scallop lines of the stent were bonded before moving down to the struts, to ensure that no residual stresses or scaffold bulging was induced along the circumference of the stent. Again, for strut bonding, proceeding from the top struts moving around the stent until all struts were bonded. Hereafter the excess skirt material was trimmed away. A second skirt was also bonded over the first, using the same method, however the second skirt bonding was extended up past the scallop lines. This entire process is outlined in Figure 19.

Figure 19 - Skirt bonding procedure

2.5.3 Leaflet fabrication and suturing

Valve leaflets were punched out of electrospun scaffolds with circumferential fibres running parallel to the leaflet edge, using a leaflet punch and mechanical press as shown in Figure 20. Hereafter leaflets were attached to the stent using double armed sutures (Ti-Cron 5-0, coated braided polyester, CV-337 taper). Leaflets were positioned within the stent frame with their rough side (abluminal) facing the outflow and their smooth side (luminal) the inflow.

The leaflet lugs were pulled through the commissure posts of the stent and the leaflets were placed flush with the stent, with their overlapping edges organised into a repeating pattern (ex. the leaflet's left edge goes under its neighbouring leaflet and the right edge over). The suturing process was then initiated along the scallop lines after which the commissure posts were secured. Similar to the skirt bonding process, a lightbox was used to visualise suturing holes on the stent. A running saddle stitch was used to secure the distal edge of the leaflets to the stent scallop lines, taking care to ensure that the leaflets do not shift during the process. Tension was applied to the sutures between each stitch to ensure that leaflets were secured flush to the stent with equal force at each suture point, so as to not create weak spots on the leaflet. Once all three scallop lines were continuously sutured, the suture was tied off using a square knot.

To secure the commissure posts, a single armed suture was inserted into the topmost suturing hole of a scallop line and pushed back out of the top suturing hole of the neighbouring scallop line, leaving both halves of the suturing string on the outside of the valve. Using a continuous suture, the single suturing needle was then passed through the suturing holes in the commissure posts from the bottom to the top and back down again (Steps 1 and 2 in Figure 21), taking care not to suture through the leaflet inside the stent. Once the suture was at the bottom of the commissure post it was passed over to the other half of the commissure post and again passed through the leaflet lug from bottom to top and back down again (Steps 3 to 5 in Figure 21). Once both halves of the commissure post were secured, the suture was tied off with a square knot (Step 6 in Figure 21). This process was repeated for all three commissure posts.

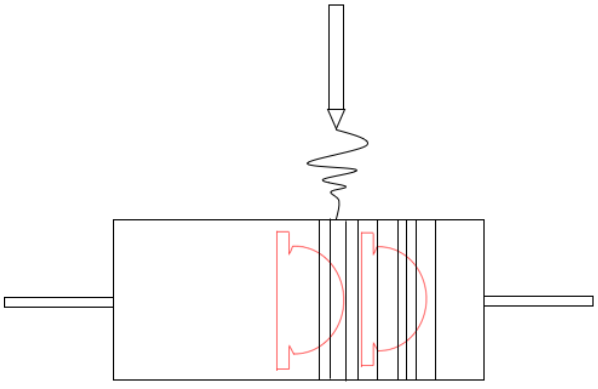

Figure 20 - Depiction of leaflets punched with circumferential fibres running parallel to the leaflet edges

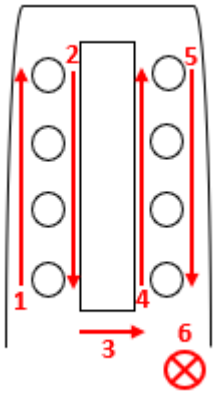

Figure 21 - Commissure post suturing procedure

2.6 Valve function and hydrodynamic testing

A pulse duplicator system (ViVitro Pulse Duplicator) was used to assess the hydrodynamic performance of produced TAVRs under simulated cardiac conditions. Two prototypes of the Pellethane® and DegraPol® valve groups along with three hybrid valve prototypes were made for testing. Valves were placed inside a silicon tube to secure them during individual testing.

Valves were allowed an appropriate seating time after being fitted into the system, which was dependant on the stiffness and permeability of the leaflet material but was generally around 15 minutes. This ensured that all valve leaflets were fully saturated to produce stable regurgitation and leakage fraction results throughout all tests conducted. All valves were initially tested at 3.5 l/min with data recorded for 10 cycles and if valves survived initial testing, they were tested at 5 l/min with data again recorded for 10 cycles. All tests were conducted at left heart pressures (100 mmHg) using saline at 37℃ at a cycle rate of 70 bpm with a minimum systolic duration of 35%, to comply with test conditions specified by ISO 5840.

Simultaneous flow and pressure readings both upstream and downstream from the aortic valve were recorded. A camera was used to capture footage of valve performance in vitro to allow for additional analyses such as complete leaflet opening and closure, simultaneous leaflet motion etc. This footage in combination with recorded data allowed for a holistic understanding of valve performance.

The main focus of the hydrodynamic testing was to assess physiological flow and pressure data such as the effective orifice area (EOA), pressure gradient (dP) and regurgitant fraction (RF). The EOA and the RF were calculated according to and compared with current ISO 5840 standards. Effective orifice area (Equation (5)) was determined as the root mean square of the forward flow (q_v, Equation (4)) divided by a constant value times the square root of the mean pressure difference (Δp (mmHg)), measured across the forward flow, divided by the density of the test fluid (ρ (cm^3)). Lastly, RF (Equation (6)) was calculated as the ratio of the regurgitant volume (RV) to the stroke volume (SV).

$$q_{vRMS} = \sqrt{\frac{\int_{t1}^{t2} q_v(t)^2 dt}{t_2 - t_1}} \tag{4}$$

$$A_{EO} = \frac{q_{vRMS}}{51.6 \times \sqrt{\frac{\Delta p}{\rho}}} \tag{5}$$

$$RF = \frac{RV}{SV} \times 100 \tag{6}$$

2.7 Valve durability testing

Valve durability was evaluated in an accelerated durability tester (vivitro labs, Hicycle AR series). Tests were conducted at 10 Hz with DI water at 37℃ as the working fluid. All tests were conducted under ISO 5840 specified conditions, which requires 100 mmHg pressure difference across the closed aortic valves which must be maintained for 95% or more of all test cycles. Furthermore, each test valve should experience a difference pressure equal or greater than the defined differential pressure for 5% or more of the duration of each test cycle.

Test valves were placed inside silicon rings which were mounted in diametrically opposite individual chambers in order to balance the loading on the module, as shown in Figure 22. Samples were tested in the recommended sterile DI water.

Figure 22 - Valve mounting configuration for 2 (A), 4 (B), 6 (C), 8 (D) valves [1]

Hereafter the system frequency was set to the desired 10 Hz and the amplitude setting was slowly increased to create some movement of the valves to allow de-bubbling of the system. Once all air bubbles were removed from the system, the amplitude setting was gradually increased until an adequate opening and closing leaflet motion was observed. By referring to live pressure readings in the HiTest software program, the flow restrictor for each valve was adjusted until a mean pressure differential of 100 mmHg was achieved for the 5% and 95% rule. Valve failure was identified by abnormal pressure readings and visual inspections.

2.8 Permeability

Permeability of electrospun scaffolds was measured by flowing DI water through samples, with known dimensions, at a set pressure difference (100 mmHg) and measuring the flow rate produced. It was decided to use fixed time intervals (10 minutes) and measure the fluid flow through the scaffolds over this time. Equation (7) (adapted from [95]) was used to calculate sample permeability. Figure 23 shows the experimental setup used, where a large reservoir tank was used to ensure that during fluid flow through the specimen, the fluid level in the reservoir did not significantly decrease. Once three consecutive time-intervals produced similar volume readings, it was assumed that the test specimen was saturated, and permeability stabilised, and these final readings were used to determine the permeability of the specimen.

$$k = 1000\frac{L}{A}\mu Q\frac{1}{P_o - P_i} = 1000\frac{L}{A}\mu\frac{\Delta V}{\Delta \mathrm{T}}\frac{1}{P_o - P_i} \qquad (7)$$

With:
ΔV = the volume of liquid flowed in the set time ΔT(cm^3)
ΔT = the time period over which flow is measured (s)
P_o = outlet fluid pressure (atmosphere absolute, atma)
P_i = inlet fluid pressure (atmosphere absolute, atma)
μ = dynamic viscosity of fluid (centipoise, cP)
L = length (thickness) of the sample (cm)
A = area of sample cm^2
k = sample permeability (millidarcy, mD)

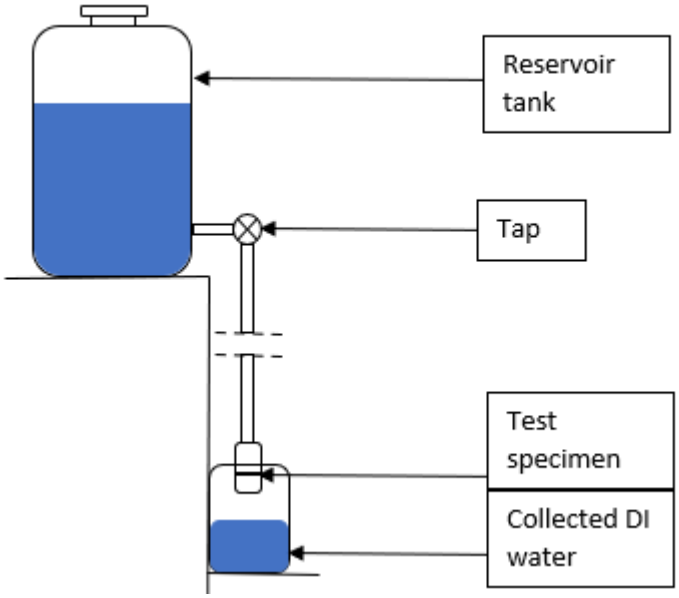

Figure 23 - Permeability experimental setup

2.9 Degradation analysis

An initial degradation study was conducted to determine the sensitivity of each of the polymer groups to a variety of pH levels. The study lasted for 7 days, and the data gathered was used to justify an appropriate solution for samples to degrade in during the six-week degradation study. Scaffolds for each of the polymer groups were incubated under physiological (pH = 7.4), acidic (pH = 0.8) and basic (pH = 13.0) conditions at 37 ℃. DegraPol® scaffolds under basic conditions at a pH of 13.0 degraded completely in less than 24 hours. Due to this an additional basic condition of pH = 11.9 was added to the study.

2.9.1 In vitro degradation of scaffolds

For the degradation study, scaffolds of each sample group were electrospun at conditions previously described. These electrospun scaffolds were punched into different shapes, depending on their analysis application in the study, as shown in Table 9, so as to easily distinguish between groups for analysis. It was decided to include three samples for measurement at each time point, with mechanical properties measurements having three samples for measurement in the radial direction and three samples for measurement in the longitudinal direction.

Mass loss and mechanical properties samples were weighed using a five-decimal balance, and their mass documented, while the thickness of only the mechanical testing samples was measured using a clip gauge. Hereafter, all samples were placed into individual glass vials which contained 20 ml standard PBS (physiological at pH = 7.4) and incubated at 37℃. At each time point the PBS was pipetted out of the vial, and the samples were rinsed in DI water to remove PBS salts that could influence mass measurements. Depending on the application of the samples they were either dried (mass loss) or tested directly after removal from the PBS (mechanical testing). Samples which were dried were placed in the vacuum oven overnight.

Table 9- Sample preparation and time points for degradation study

Shape & Dimensions	Analysis application	Time points (weeks)	Polymer group
	Mass loss	0, 1, 2, 3, 4, 6	DP15, Pell, Hybrid
	Mechanical properties	0, 1, 2, 3, 4, 6	DP15, Pell, Hybrid

Mechanical properties of degradation samples were tested as previously described in section 2.4. Mass loss was determined by percentage mass loss over time using equation (4), shown below, with m_t the sample weight at that timepoint after degradation and m_0 the sample weight before degradation.

$$Mass\ loss\ (\%) = (1 - \frac{m_t}{m_0}) \times 100 \qquad (4)$$

2.10 Statistical analysis

References of results as well as graph error bars were expressed as mean ± standard deviation, unless otherwise stated. Data were tested for normalcy using the Shapiro-Wilk test for normality followed by a Q-Q plot. Statistical analysis of variance for normally distributed data was conducted using the one-way ANOVA and student t-test models. For non-parametric models the Kruskal-Wallis one-way analysis of variance and the Wilcoxon sign-rank tests were used to determine the P-values between data sets. A value of $P \leq 0.05$ was considered to be significant and all computations and data plotting was performed using Microsoft Office Excel (2020).

3 Results & Discussion

The results of this study are presented under three main topics, i.e., scaffold development, hydrolytic degradation of DegraPol®, Pellethane® and hybrid scaffolds, and valve hydrodynamics and durability testing.

3.1 Scaffold development

Dual spinning was utilised to produce hybrid (composite) scaffolds which contained both DP15 and Pellethane® fibres. This section starts by describing the initial dual spun scaffolds produced and then discusses the optimisation that was carried out to produce dual scaffolds containing both DegraPol® and Pellethane® with similar fibre sizes. Hereafter, the final scaffolds which were used for valve development and in vitro testing are discussed.

3.1.1 Development of dual electrospun scaffolds

As the goal of this study was to produce dual spun composite scaffolds, these scaffolds were produced and optimised before the electrospinning conditions for single-spun Pellethane® and DegraPol® were determined.

During initial dual spinning, on a 25 mm diameter rotating collector, Toluidine blue was added to Pellethane® solutions to visualise fibre deposition on the mandrel. These initial dual electrospinning attempts resulted in uneven fibre distribution, with one half of the mandrel dominated by blue, Pellethane®, fibres and the other by white, DegraPol®, fibres.

During a dual spinning study to produce scaffolds with enhanced porosity, Voorneveld *et al.* researched various dual spinning configurations, as shown in Figure 24, to identify the most functionally successful experimental setup [6]. They found that a configuration consisting of positively charged spinnerets, with electrostatic shields (also positively charged) to guide fibre deposition, along with a negatively charged collector to be most successful [6].

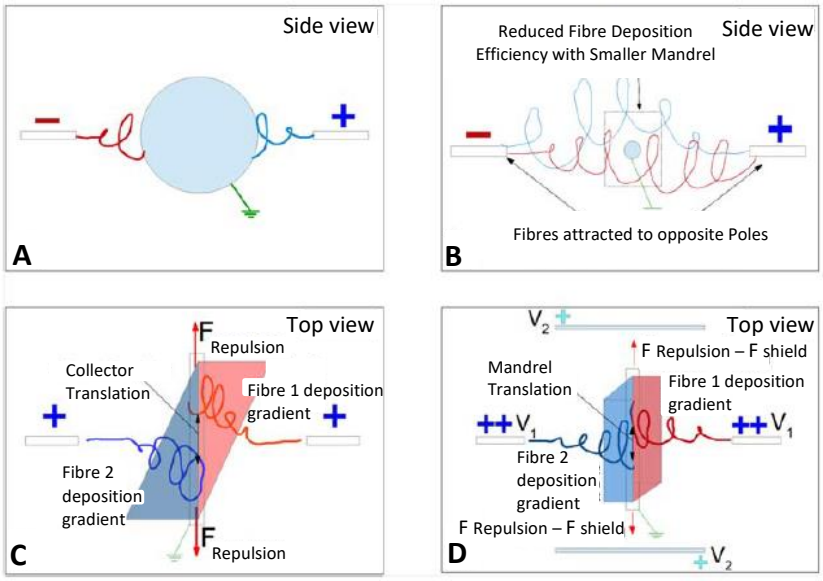

Figure 24 – Schematic of different electrospinning configurations investigated for dual spinning. Oppositely charged spinnerets with (A) large diameter collectors and (B) small diameter collectors were investigated. Along with like polarity spinnerets (C) translating collectors and (D) translating collector with electrostatic shiels. Adapted from [6]

Building on the work of Voorneveld [6, 96], it was decided to improve fibre deposition distribution by increasing the collector size drastically to reduce fibre repulsion from the like charged spinnerets, as this eradicated the need for additional electrostatic shields. It was found that using a 75 mm diameter mandrel rendered improved fibre deposition with homogeneous distribution of both solutions across the mandrel. Thus, from this point forward all hybrid scaffolds were electrospun onto a 75 mm mandrel.

3.1.2 Process optimization

Initial dual spun scaffolds contained large DP15 fibres (7.62 ± 0.49 µm) along with much smaller Pellethane® (1.36 ± 0.1 µm) fibres, as shown in Figure 25. It was decided to produce scaffolds with similar fibre sizes to have comparable morphological proportions between scaffold groups and to allow pore size distribution control to enhance theoretical cell infiltration. This section outlines the methods and processes used to decrease DP15 fibre sizes and increase that of Pellethane®.

Factors such as humidity and mandrel rotation speed could not be altered to vary the fibre diameter of one polymer without affecting the fibre diameter of the other polymer. Additionally, the flowrate of solutions could not be greatly altered as solutions with similar weight percentages were electrospun at similar flowrates to achieve hybrid scaffolds with a 50% ratio of each polymer. Therefor factors which could be individually controlled for each polymer were varied in order to achieve the desired fibre diameter change.

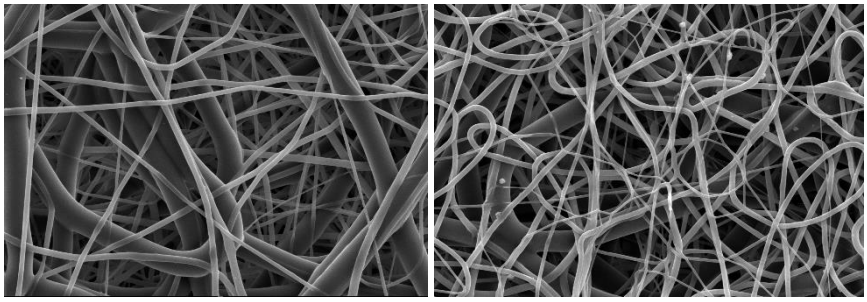

Figure 25 - Initial hybrid scaffold morphology; (left) abluminal and (right) luminal surfaces.

3.1.2.1 Decreasing DegraPol15® fibre size

In an attempt to decrease the DegraPol® fibre size DegraPol® solution concentrations were varied and HFIP was included in DegraPol® electrospinning solution. Decreasing the concentration of polymer in DegraPol® solutions from 15wt% to 13 wt% resulted in an increase in fibre diameter even at the same flowrate of 3.0 ml/h (7.61 ± 0.49 µm compared to 8.65 ± 0.18µm, $p < 0.05$) and no statistically significant difference in either pore size (14.21 ± 0.59 µm^2 compared to 10.56 ± 2.24 µm^2, $p > 0.05$) or fibre orientation (0.18 ± 0.09% to 0.14 ± 0.08%, $p > 0.05$), as shown in Figure 27. Further decreasing the concentration to 12wt% produced fibres which were non-uniform with varied diameters and a further reduction to 10wt% produced a scaffold which was too weak to remove from the electrospinning mandrel for further processing, indicated in Figure 26.

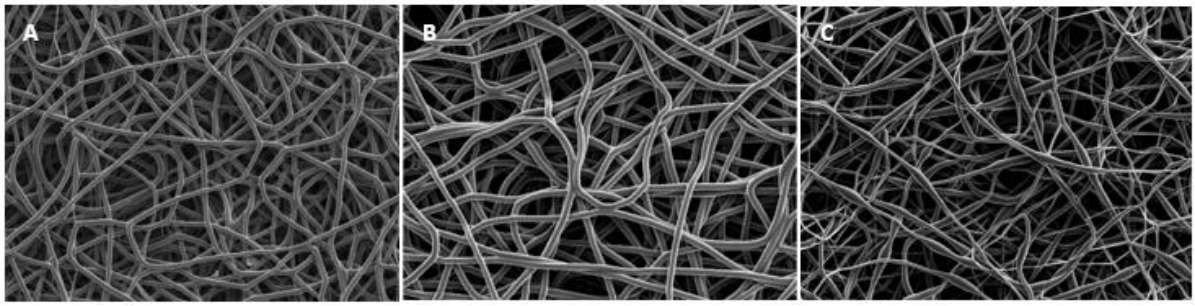

Figure 26 - SEM images of various DegraPol® solution fibres, with (A) 15wt% (B) 13wt% (C)12wt%

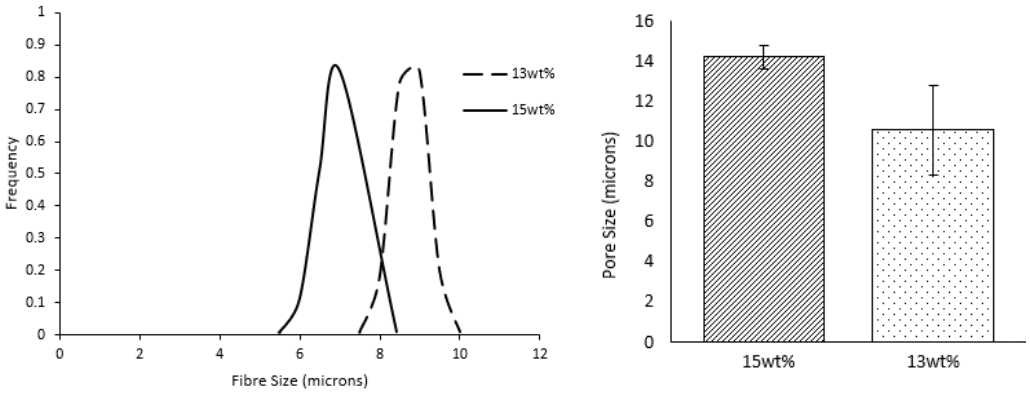

Figure 27 - Fibre size (left) and pore size (right) of electrospun scaffolds with varying DP15wt%.

Yalcinkaya *et al.* found that there is a non-linear relationship between polymer concentration and electrospun fibre size with surface tension most likely playing a dominant role in fibre morphology at low viscosities [97]. Thus, it is possible that the decrease in polymer concentration, from 15wt% to 13wt%, led to a decrease in solution viscosity and subsequently a decrease in surface tension, allowing more solution to be expelled from the spinneret, at the same flow rate, leading to the increase in fibre size seen for the 13wt% DP15 solution. Furthermore, it has been shown that beaded fibres form at low viscosities, due to insufficient viscosity to resist fibre deformation, which explains why fibres were non uniform for 12wt% DP15 [97, 98].

As shown in Figure 28, the inclusion of HFIP reduced fibre size significantly (7.62 ± 0.49 µm compared to 5.99 ± 0.09 µm ($p < 0.05$) and 5.96 ± 0.14 µm ($p < 0.05$) for a 5wt% and 10wt% HFIP inclusion, respectively), while pore size (14.21 ± 0.59 μm^2 compared to 18.29 ± 3.79 μm^2 ($p > 0.05$) and 16.37 ± 2.98 μm^2 ($p > 0.05$) for a 5wt% and 10wt% HFIP inclusion, respectively), and fibre orientation (0.176 ± 0.09% compared to 0.13 ± 0.05% ($p > 0.05$) and 0.14 ± 0.09% ($p > 0.05$) for 5wt% and 10wt% HFIP inclusions respectively) did not see change after the inclusion of HFIP, as shown in Figure 29.

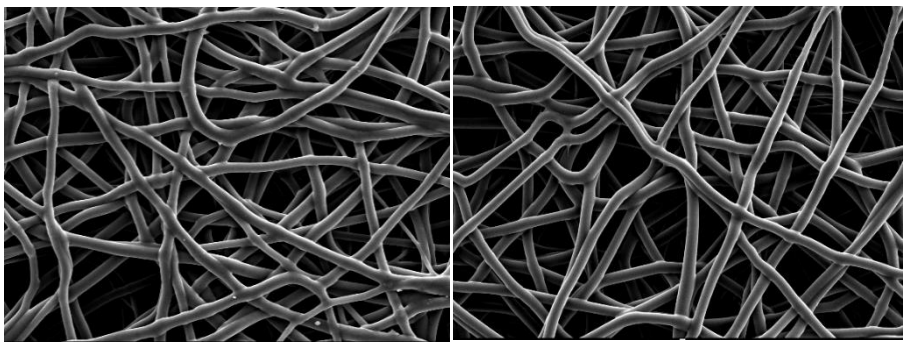

Figure 28 - (left) 10 wt% and (right) 5 wt% HFIP inclusion in DP15

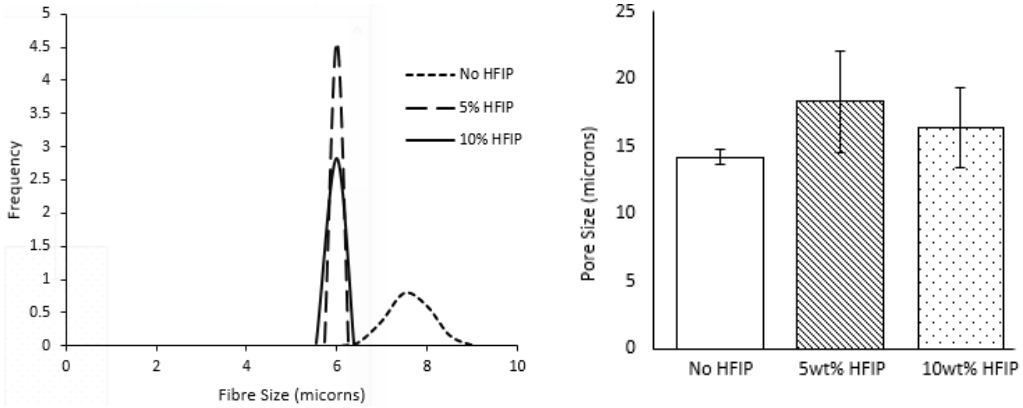

Figure 29 - Fibre size (left) and pore size (right) of electrospun scaffolds with varying HFIP wt% inclusions.

Increasing the amount of HFIP in the DP15 – chloroform solution most likely increased the dielectric constant of the solvent system which led to an expected decrease in fibre diameter as the solution carried more charge, leading to increased whipping and thinner solution jets being formed [99-101]. The high vapour pressure of HFIP leads to wet landing of fibres which results in potential fibre fusion and therefor smaller pores between fibres [99].

3.1.2.2 Increasing Pellethane® fibre size

As indicated in Figure 30 and summarised in Figure 31, increasing the polymer concentration of Pellethane® from 16wt% to 18wt% and 19wt%, in a DMF:THF solvent system, resulted in an increase in fibre diameter (1.36 ± 0.1 µm to 3.66 ± 0.33 µm ($p < 0.001$) and 3.3 ± 0.27 µm ($p < 0.001$), respectively) as well as pore size (4.26 ± 1.19 µm^2 compared to 9.24 ± 0.71 µm^2 ($p < 0.05$) and 8.07 ± 1.25 µm^2 ($p < 0.05$), respectively) with no significant change to fibre orientation (0.09 ± 0.03% compared to 0.18 ± 0.05% ($p > 0.05$) and 0.16 ± 0.1% ($p > 0.05$), respectively). Further increasing the polymer concentration to 20wt% led to non-uniform fibres with a wet landing.

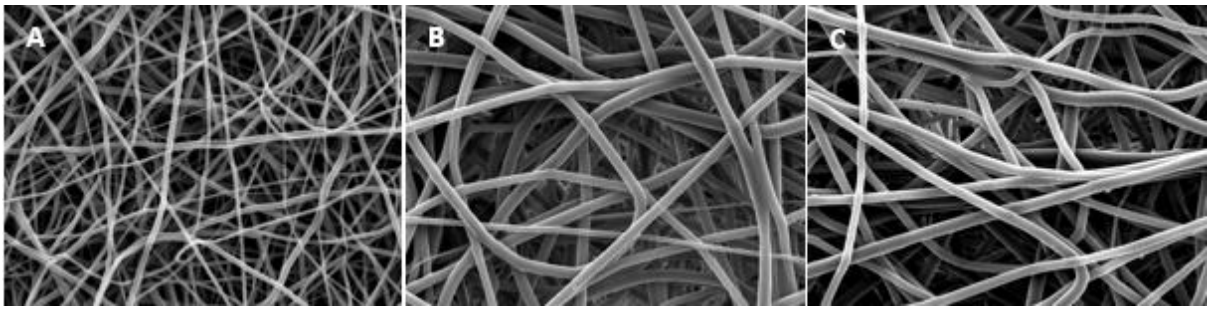

Figure 30 - Fibre size increase with Pellethane® wt% increase, with (a) 16wt%, (b) 18wt% and (c) 19wt%

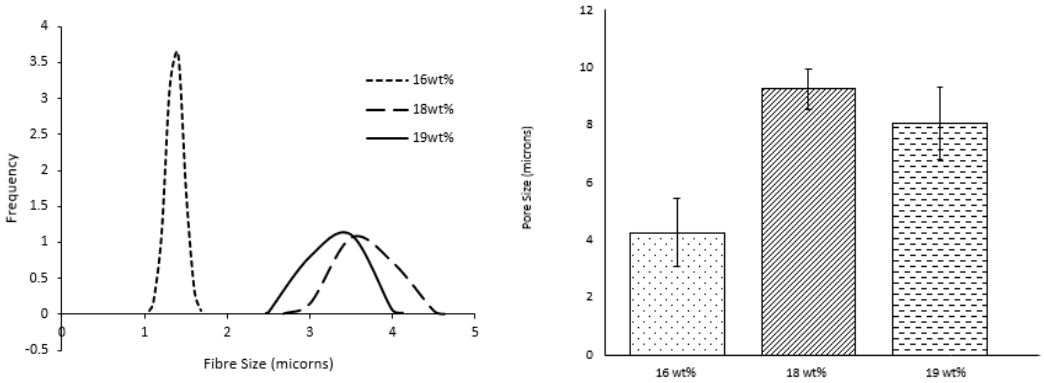

Figure 31 - Fibre size (left) and pore size (right) of electrospun scaffolds for varying Pellethane® wt% in DMF:THF solvent system.

As expected, increasing the polymer concentration within the optimal range for electrospinning did increase fibre diameter [102]. Further increasing the polymer concentration to 20wt% had likely resulted in a solution with a viscosity range outside of the optimum which makes it difficult to extrude polymer from the spinneret and leads to non-uniform fibre formation [103]. Additionally, pore size increased along with an increase in fibre diameter, as the two factors are closely related to one another [104].

Varying DMF:THF ratios was also employed as an additional measure to further increase the fibre size of 18wt% and 19wt% Pellethane® solutions. Solutions were electrospun with 3DMF:7THF solvent systems, different from the previous DMF:THF solvent system used, to reduce the dielectric constant of the solution in an attempt to cause less fibre whipping and consequent fibre thinning. This change led to non-uniform fibre formation, potentially due to solution jet splitting, as well as an increase in pore size (9.24 ± 0.71 μm^2 to 10.61 ± 1.47 μm^2 ($p > 0.05$) for 18wt% and 8.07 ± 1.25 μm^2 to 11.33 ± 1.83 μm^2 ($p > 0.05$)) and decrease in pore size uniformity, as can be seen in Figure 32.

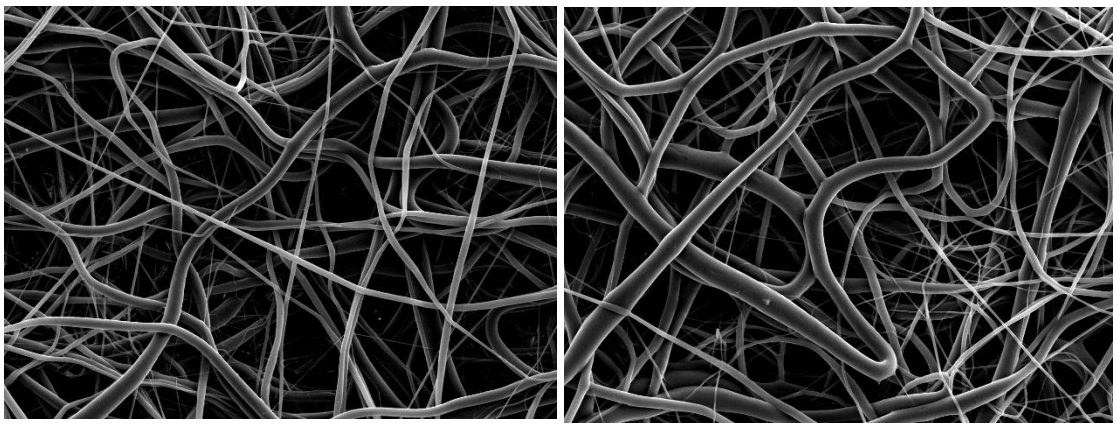

Figure 32 - Varying solvent ratios to 3DMF:7THF for (left) 18wt% and (right) 19wt% Pellethane® solutions

This is consistent with the work of Xiaohua *et al.* who found that morphology of electrospun PBC nanofibers was strongly dependent on the solvent's dielectric constant with a low dielectric constant causing a reluctant jet flow split, leading to a tendency to form a plait structure in the scaffold pattern [100]. This could explain the non-uniform fibre diameters produced due to the decrease in the systems' dielectric constant.

Using various polymers Megelski *et al.* also investigated the effect of varying THF/DMF ratios as the solvent system on electrospun scaffold properties, and found that at ratios of 75/25% THF/DMF, pores became larger and less uniform in comparison to scaffolds spun with 100% THF, and that this feature along with surface roughness disappear when the fibres are spun from 100% DMF [105].

3.1.2.3 Optimized dual electrospun scaffolds

The optimized conditions used for dual spinning of scaffolds are listed in Table 10.

Table 10 - Final dual spinning conditions

Polymer	Concentration (wt%)	Solvent	Flowrate (ml/h)	+ Voltage (kV)	-Voltage (kV)	Distance (cm)
DegraPol®	15	9.5:0.5 w/w $CHCl_3$:HFIP	3	19	-3	38
Pellethane®	18	DMF:THF	3	14	-3	22

SEM micrographs of the final dual spun scaffold morphology are shown in Figure 33A while Figure 33B depicts a dual spun scaffold after DegraPol® extraction. The white arrows indicate areas were DegraPol® fibres were prior to extraction with NaOH and proves the of fibres of both polymer groups.

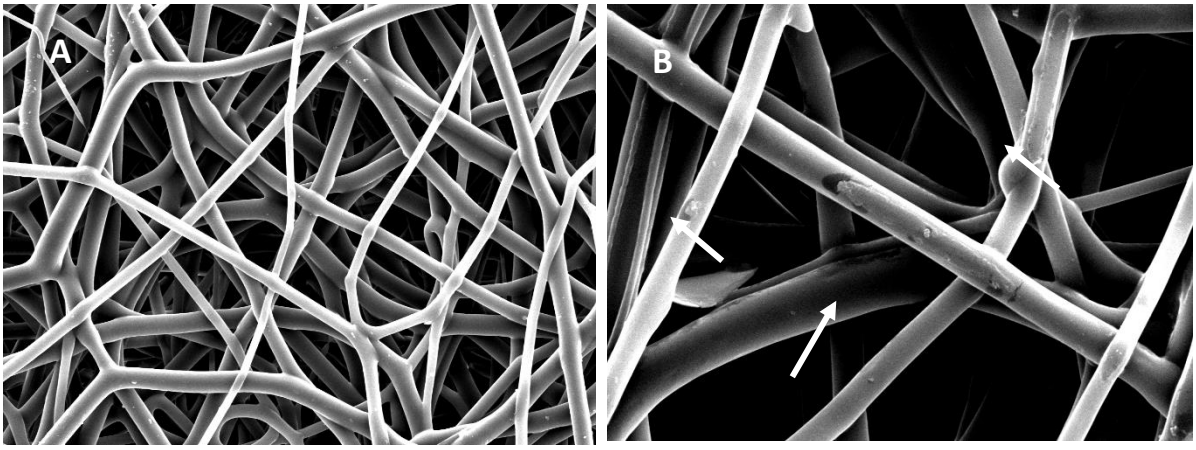

Figure 33 - SEM images of a (A) dual spun scaffold and (B) sites of DegraPol® fibre attachment post extraction.

DP15 and Pellethane® fibres were successfully optimised to reach similar average fibre sizes (Figure 34). DP15 fibres were significantly decreased from 7.62 ± 0.49 µm to 5.99 ± 0.09 µm ($p < 0.05$), while Pellethane® fibres were significantly increased from 1.36 ± 0.1 µm to 3.66 ± 0.33 µm ($p < 0.001$).

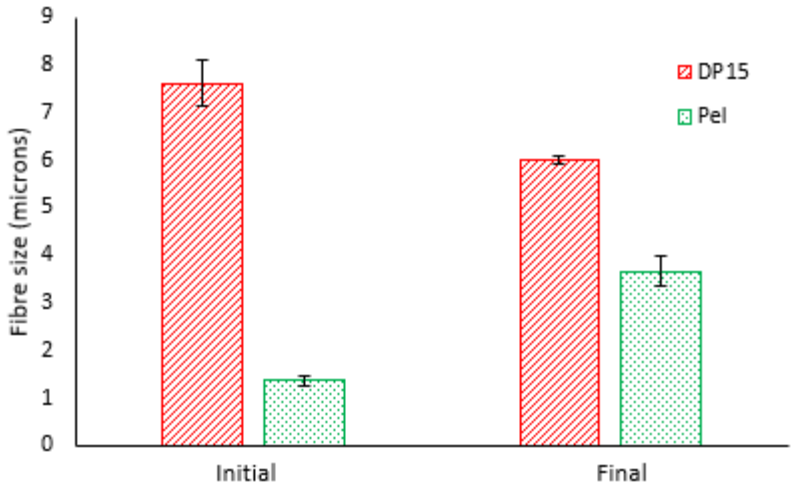

Figure 34 - Initial and final fibre diameter of DP15 and Pellethane®

3.2 Degradation study

During an initial pilot degradation study it was found that hybrid and DegraPol® samples degraded at a more rapid rate in basic solutions (pH = 11.9) in comparison to acidic solutions (pH = 0.8), which was expected from literature [106]. After 7 days of incubation many of the DegraPol® samples had completely degraded away or were too weak to survive drying for weighing. Similarly, DegraPol® samples in the acidic medium also did not survive drying. Ultimately PBS (pH = 7.4) was used as the final degradation medium to simulate physiological parameters and to allow a slow and controlled degradation of DegraPol® which was favourable for data collection with regards to reduction in mechanical strength and mass.

3.2.1 Scaffold morphology

Figure 35 depicts SEM micrographs of each sample group at Day 0. Their average fibre diameters were (DP15: 5.99 ± 0.49 µm, Pellethane®: 3.66 ± 0.33 µm and hybrid: 4.06 ± 0.69 µm) statistically significantly different ($p < 0.05$) between groups. While pore size (DP15: 18.29 ± 3.79 μm^2, Pellethane®: 9.24 ± 0.71 μm^2 and hybrid: 15.94 ± 5.08 μm^2), fibre orientation (DP15: 0.132 ± 0.05%, Pellethane®: 0.184 ± 0.05% and hybrid: 0.09 ± 0.03%) and porosity (DP15: 67.93 ± 2.74%, Pellethane®: 63.98 ± 5.85% and hybrid: 67.78 ± 4.48%) were similar across all groups ($p > 0.05$).

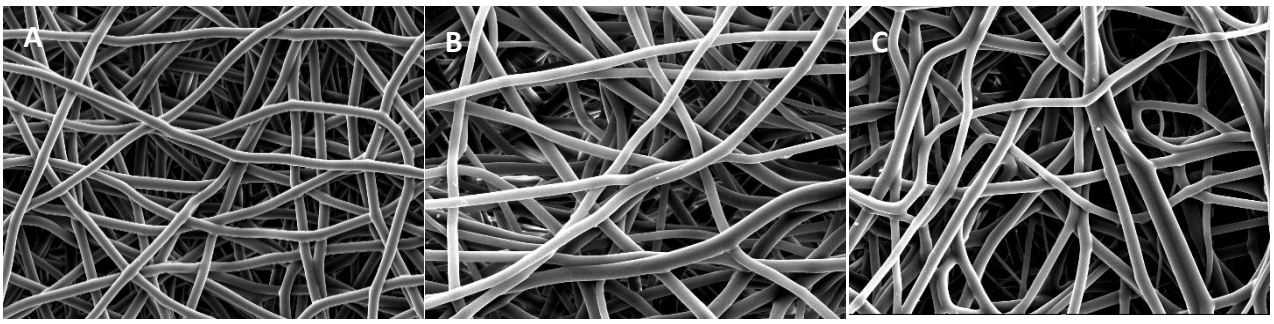

Figure 35 - SEM micrographs of (a) DP15, (b) Pellethane® and (c) hybrid electrospun scaffolds at appropriate magnifications of X500, X1000 and X700 respectively.

3.2.2 Mechanical properties

Initially tensile testing was conducted on dry and "air-wet" (AW) samples which had been soaked in PBS for 20 minutes. It was found that for all polymer groups in both the circumferential and longitudinal direction, there was no notable difference between the values obtained for UTS [MPa], ε_{max} [%] or E_Y [MPa], as can be seen for example in Figure 36. It was therefore decided to conduct all tests at air wet conditions for practicality reasons, as all degradation study samples had been soaked in PBS, and additionally air wet conditions more closely mimicked physiological conditions in comparison to dry testing condition.

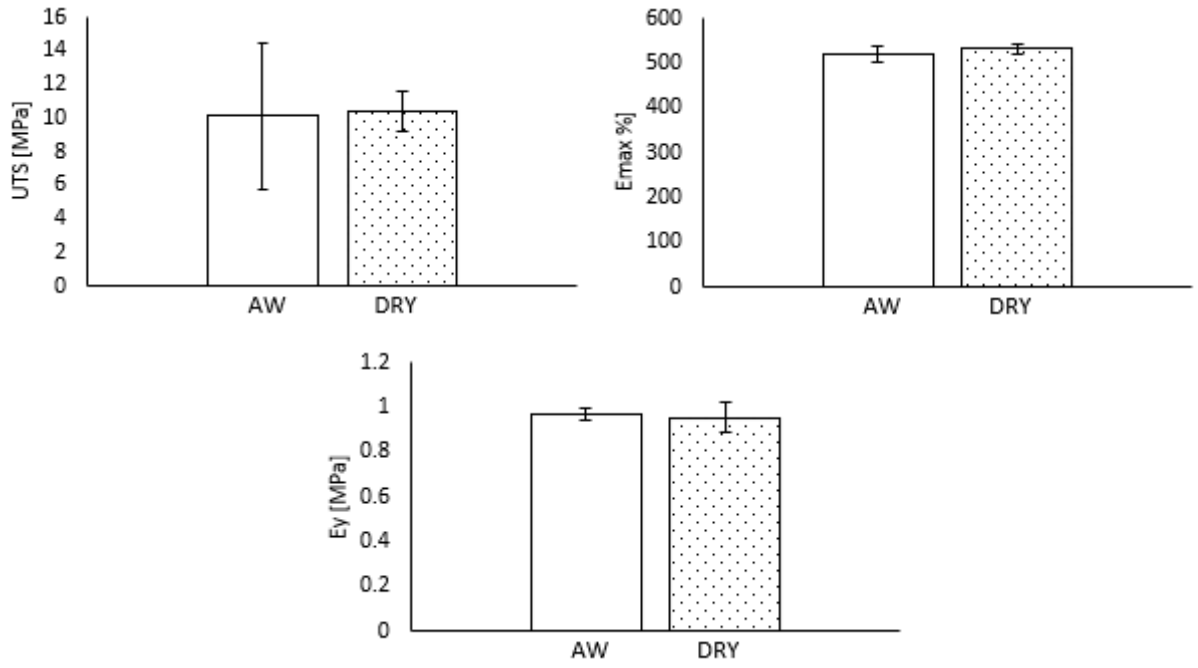

Figure 36 - Initial air-wet vs. dry tensile testing for Pellethane® in the longitudinal direction

3.2.2.1 Bulk mechanical properties

Polymer films were produced to characterise the inherent bulk mechanical properties of each polymer. This allowed for an improved understanding of the effect of processing/electrospinning on polymer and scaffold strength. Results from tensile tests for cast films made from Pellethane® and DP15 are illustrated in Figure 37. Mechanical properties were characterised in terms of ultimate tensile strength (UTS), maximum elongation ($Ɛ_{max}$), and Young's modulus (E_Y). Pellethane® films had an UTS (32.81 ± 6.19 MPa) approximately four times that of DegraPol® (7.81 ± 0.35 MPa, $p < 0.05$), while DegraPol® had a maximum elongation (1177.49 ± 34.46%) roughly double that of Pellethane® (504.13 ± 41.75%, $p < 0.001$). Lastly, the Young's modulus of Pellethane® (2.9 ± 0.04 MPa) films was nearly five times larger than that of DegraPol® (0.59 ± 0.02 MPa, $p < 0.001$).

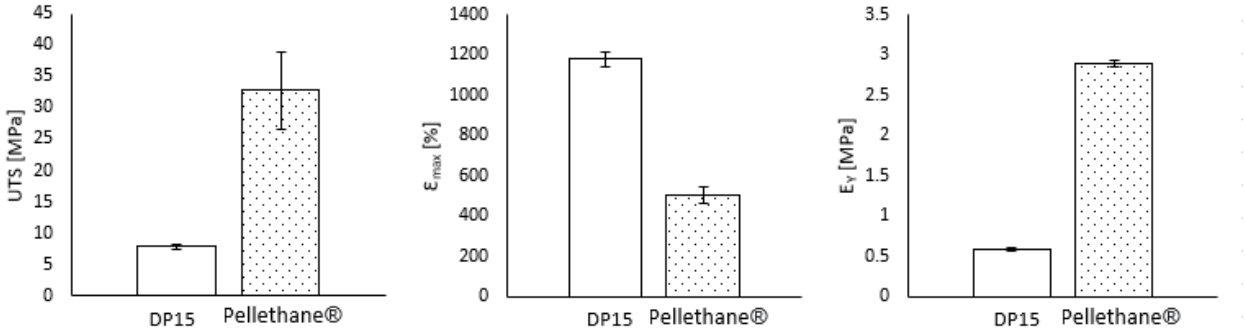

Figure 37 - Mechanical properties of 2D scaffolds. a) Ultimate tensile strength (UTS), b) maximum elongation ($Ɛ_{max}$) and c) Young's modulus (Ey)

The UTS results for Pellethane® films are similar to those of previous studies (UTS between 35-40 MPa) while the maximum elongation was slightly lower than expected (usually well over 700%) [107]. The UTS for DegraPol® correlates well with previous work, while the maximum elongation was much higher than predicted and Young's modulus lower than expected [108]. Mechanical properties of DegraPol® can be altered by varying the hard to soft segment ratio with a hard segment dominating DegraPol® being stronger [3].

3.2.2.2 Tensile testing

The ultimate tensile strength (UTS), Young's Modulus (E_Y) and maximum elongation ($Ɛ_{max}$) of all three electrospun groups before and after incubation in PBS for 3 and 6 weeks are depicted in Figure 38. Initially the UTS of the three groups varied significantly with hybrid scaffolds exhibiting an UTS situated almost halfway between that of DegraPol® and Pellethane® in both the longitudinal (5.23 ± 0.06 MPa, 3.39 ± 0.29 MPa, 10.09 ± 0.63 MPa, respectively, $p < 0.05$ for all pairings) and circumferential directions (7.09 ± 0.17 MPa, 3.86 ± 0.29 MPa, 14.93 ± 0.71 MPa, respectively, $p < 0.05$ for all pairings). The UTS strength of DP15 samples then decreased the most, after 6 weeks of incubation, losing 53.6 ± 5.82% longitudinally and 59.95 ± 4.55% circumferentially, while Pellethane® scaffolds lost 2.88 ± 11.34% longitudinally and 19.15 ± 5.52% circumferentially and hybrid scaffolds 19.27 ± 26.47% longitudinally and 6.59 ± 1.32% circumferentially, of their initial UTS.

The initial E_Y of DegraPol® was the lowest, with that of Pellethane® the highest while the E_Y of hybrid scaffolds was intermediate, for both the longitudinal (0.27 ± 0.02 MPa, 0.96 ± 0.03 MPa, 0.66 ± 0.02 MPa respectively, $p < 0.05$ for all pairings) and circumferential directions (0.26 ± 0.01 MPa, 0.79 ± 0.02 MPa, 0.58 ± 0.13 MPa respectively, $p > 0.05$ for hybrid and Pellethane® scaffolds, $p < 0.05$ for all remaining pairings). Six weeks of incubation did not affect the E_Y of most

groups ($p > 0.05$), except for Pellethane® in the longitudinal direction and hybrid scaffolds in the circumferential direction ($p < 0.05$).

Lastly, the ε_{max} decreased most significantly ($p < 0.05$) for DegraPol® with a 36.08 ± 5.04% and 34.04 ± 5.56% reduction in the longitudinal and circumferential directions respectively. Pellethane® had no significant reduction in ε_{max} ($p > 0.05$), while hybrid scaffolds showed a significant decrease ($p < 0.05$) in the circumferential direction of 17.77 ± 6.37% with a insignificant reduction ($p > 0.05$) of 17.82 ± 10.49% in the longitudinal direction.

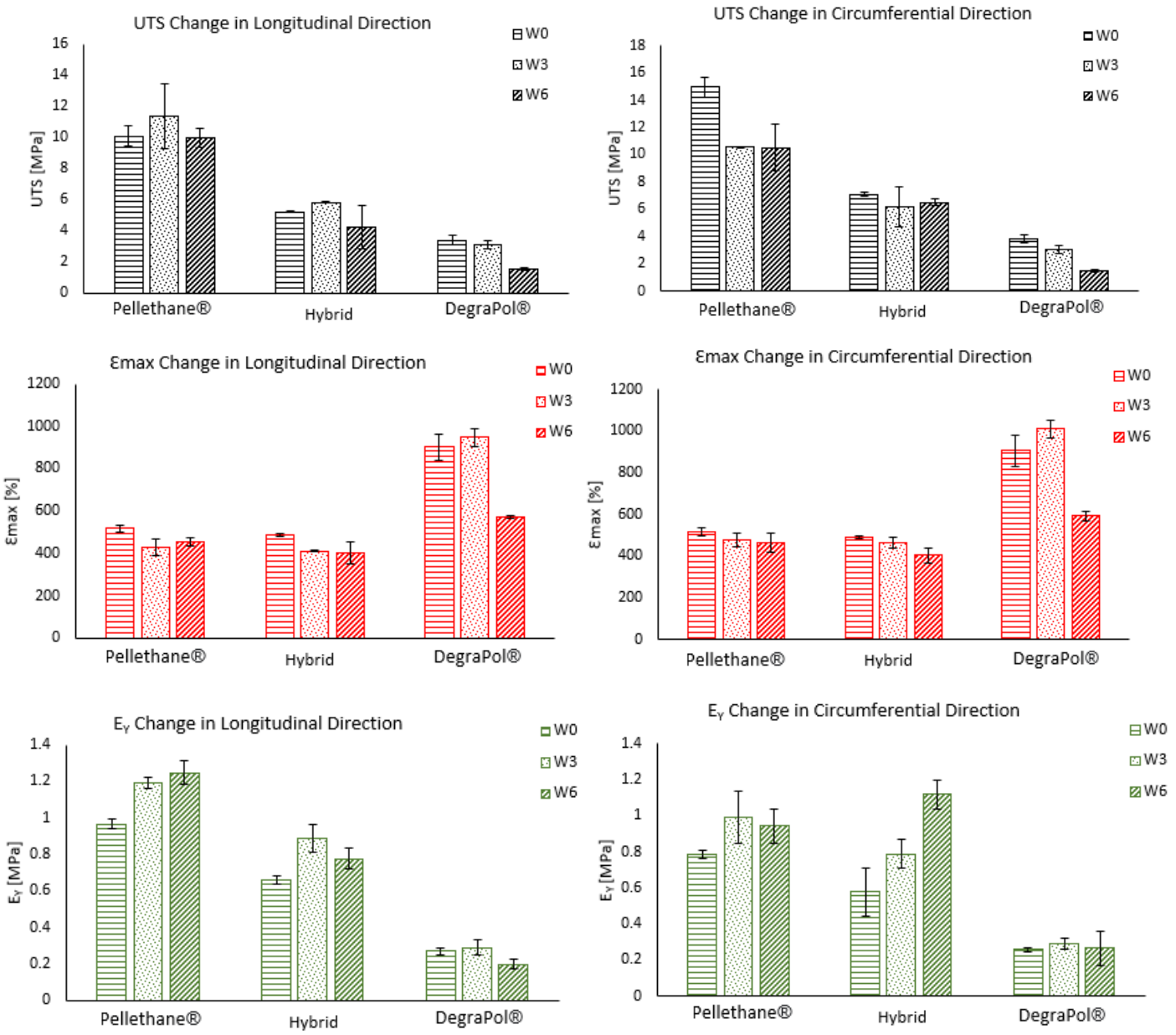

Figure 38 - UTS, ε_{max}, and E_y change over 6-week incubation period for Pellethane®, DegraPol® and hybrid scaffolds in both the longitudinal and circumferential direction

The decrease of UTS and ε_{max} after 6 weeks of incubation in PBS is expected [109-111]. Henry *et al*. found that after 346 days of incubation in PBS, DegraPol® polymer with a 47wt% hard segment content showed a 90% decrease in UTS. The rate of decrease of UTS found by Henry *et al.* is much slower than the rate of decrease observed in this study, which is likely due to the difference in the hard and soft segment ratios between the polymers. DP15 has a 25wt% hard segment content which

results in a less mechanically strong polymer than that investigated by Henry *et al*. which has a 47wt% hard segment content [110].

The mechanical properties of electrospun hybrid scaffolds being situated almost halfway between that of single-spun DegraPol® and Pellethane® was expected. What is interesting to note is that the decrease in UTS and ε_{max} of hybrid scaffolds more closely resembles the rate of UTS loss seen in Pellethane®, than that of DegraPol®. This is due to the fact that Pellethane® fibres are nearly three times stronger than DegraPol® fibres, thus even after the total degradation of DegraPol® fibres in hybrid scaffolds, Pellethane® fibres will provide the hybrid scaffolds with a strength that exceeds that of DegraPol® scaffolds and mimics the behaviour of Pellethane® scaffolds, as seen in Figure 38.

The retained stiffness of most groups after 6 weeks of incubation is also in line with the findings of Henry *et al.* and others, who suggested that the rate of change in stiffness is slow due to the crystalline segments which degrade at a slower rate than the amorphous segments [109, 110]. The behaviour exhibited by hybrid scaffolds in this study is consistent with the findings of De Hart *et al.* who found that in fibre reinforced scaffolds, reinforcing fibres can carry up to 60% of the stresses experienced by the scaffold [112]. This supports the notion that even after the degradation of DegraPol® fibres, hybrid scaffolds will still be stronger than pure DegraPol® scaffolds, due to the inclusion of Pellethane® fibres which have not degraded.

3.2.2.3 Cyclic testing

Cyclic testing showed that scaffolds were all able to withstand repeated cyclic loading up to 120 cycles. Figure 39 shows that scaffolds experienced hysteresis that decreased during subsequent cycles, with hysteresis defined as the difference in energy between loading and unloading which represents energy loss from the system.

Hybrid scaffolds experienced similar ($p > 0.05$) hysteresis to DegraPol® scaffolds during day-0 testing losing $1.82 \pm 0.12 \times 10^{-3}$ J compared to $1.75 \pm 0.1 \times 10^{-3}$ J for DegraPol® scaffolds, while Pellethane® scaffolds experienced the least hysteresis ($1.4 \pm 0.04 \times 10^{-3}$ J). During cyclic testing after six weeks of incubation DegraPol® exhibited a hysteresis of $2.44 \pm 0.11 \times 10^{-3}$ J and hybrid scaffolds a hysteresis of $1.98 \pm 0.45 \times 10^{-3}$ J. Pellethane® scaffolds still exhibited the lowest hysteresis of $1.46 \pm 0.07 \times 10^{-3}$ J. Importantly, there was no significant difference between the hysteresis experienced by Pellethane® and hybrid scaffolds after 6 weeks of incubation ($p > 0.05$), but there was a significant difference between that of Pellethane® and DegraPol® scaffolds ($p < 0.05$). Thus after 6 weeks of incubation Pellethane® and hybrid scaffolds exhibited similar hysteresis which was less than that of DegraPol® scaffolds. Interestingly, DegraPol® showed a 39.36% increase ($p < 0.05$) in hysteresis experienced in the first testing cycle after six weeks of incubation, while Pellethane® and hybrid scaffolds only showed a 4.83% and 8.9% difference, respectively ($p > 0.05$ for both groups). Therefore, the hysteresis experienced by hybrid and Pellethane® scaffolds did not increase after 6 weeks of incubation however the hysteresis experienced by DegraPol® scaffolds did. This nearly constant value for hysteresis, displayed by hybrid scaffolds, could be important in an application such as heart valves where repeated cyclic loading is experienced, and mechanical properties need to be maintained.

Stress relaxation provides a means to analyse the viscoelastic properties of a scaffold, whereby the cyclic or static strain imposed on the scaffold remains constant over a period of time. In the case of this project scaffolds underwent continuous loading and unloading and a rapid drop in force followed by levelling to a relatively constant value, as shown in the Stress vs. Cycle number graphs in Figures 40 to 42.

As can be seen from Table 11, DegraPol® showed the greatest average stress decrease over time, reducing roughly twice as much as both Pellethane® and hybrid groups during day-0 testing, and nearly three times as much as Pellethane® after 6 weeks of incubation. Interestingly, hybrid scaffolds displayed stress reduction behaviour nearly identical to that of Pellethane®, thus also displaying significantly less stress relaxation than DegraPol®.

The peak stress difference between the first and last cycle during day-0 testing was significantly different ($p < 0.05$) for both Pellethane® and hybrid scaffolds, however not for DegraPol® scaffolds ($p > 0.05$). This trend shifted during week 6 cyclic testing where only Pellethane® scaffolds showed a significant decrease in peak stress ($p < 0.05$). Additionally, only Pellethane® scaffolds showed a significant difference between the average peak stress decrease of day-0 and week 6 ($p < 0.05$). This finding indicates that there was no significant difference between the creep experienced by DegraPol® and hybrid scaffolds after 6 weeks of incubation ($p > 0.05$).

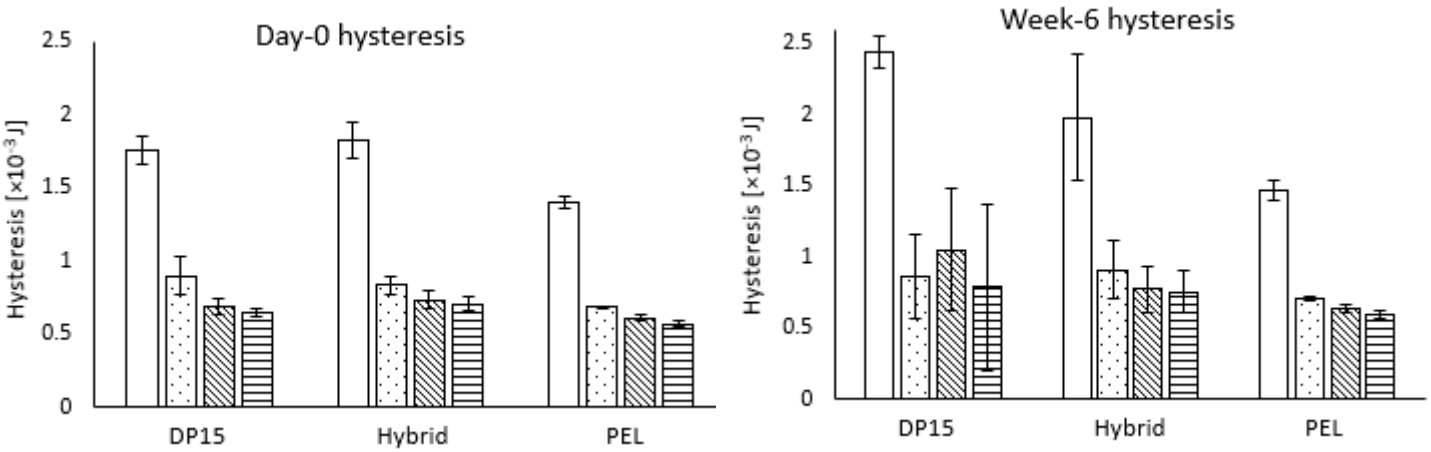

Figure 39 - Hysteresis experienced by scaffolds before and after six weeks of incubation

Table 11 - Peak stress at initial and final cycles of cyclic testing for all polymer groups

	Day 0 (W0)			Week 6 (W6)		
	Stress at first cycle [MPa]	**Stress at last cycle [MPa]**	**Average stress decrease [%]**	**Stress at first cycle [MPa]**	**Stress at last cycle [MPa]**	**Average stress decrease [%]**
DegraPol®	0.16 ± 0.1	0.08 ± 0.09	50	0.12 ± 0.09	0.05 ± 0.08	58.33
Pellethane®	0.26 ± 0.16	0.19 ± 0.15	26.92	0.28 ± 0.17	0.22 ± 0.17	21.43
Hybrid	0.23 ± 0.14	0.17 ± 0.14	26.1	0.27 ± 0.17	0.2 ± 0.16	25.93

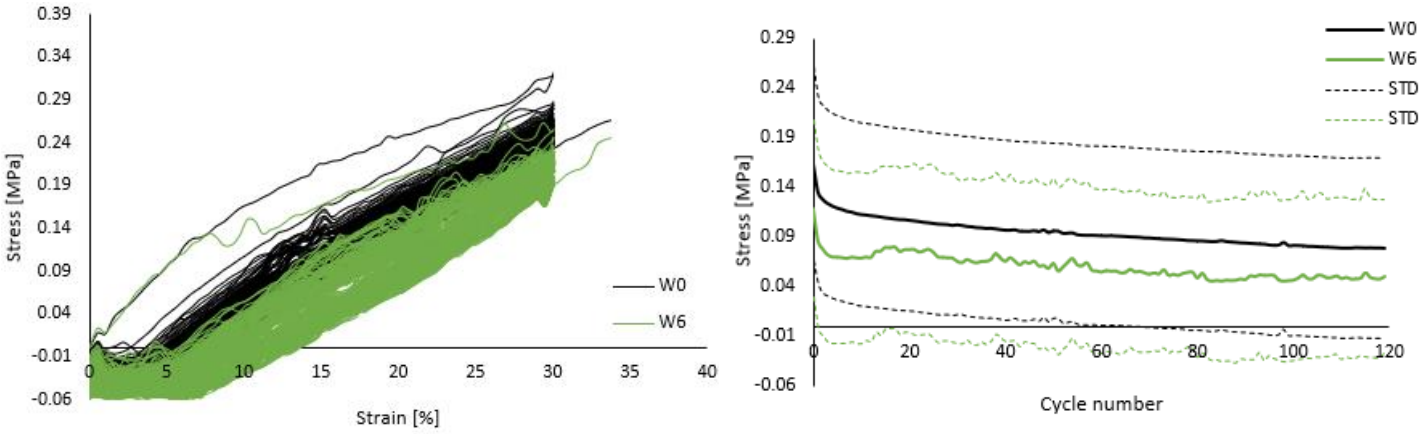

Figure 40 - Average curves for cyclic testing of DegraPol® scaffolds (n = 3). (left) Average stress-strain curve of 120 cycles. (right) Average peak stress vs. cycle number curve showing one standard deviation above and below

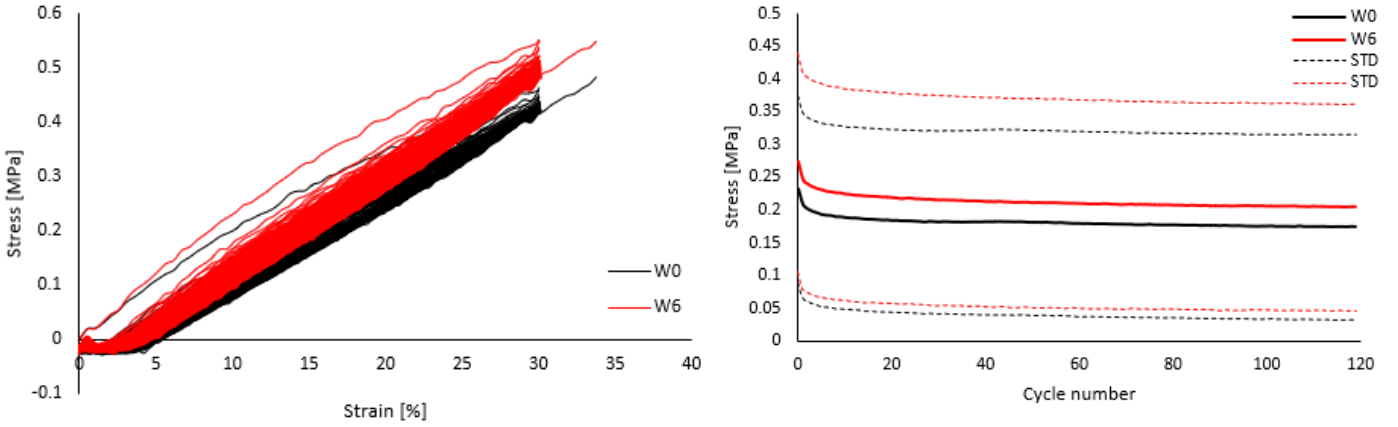

Figure 41 - Average curves for cyclic testing of hybrid scaffolds (n = 3). (left) Average stress-strain curve of 120 cycles. (right) Average peak stress vs. cycle number curve showing one standard deviation above and below

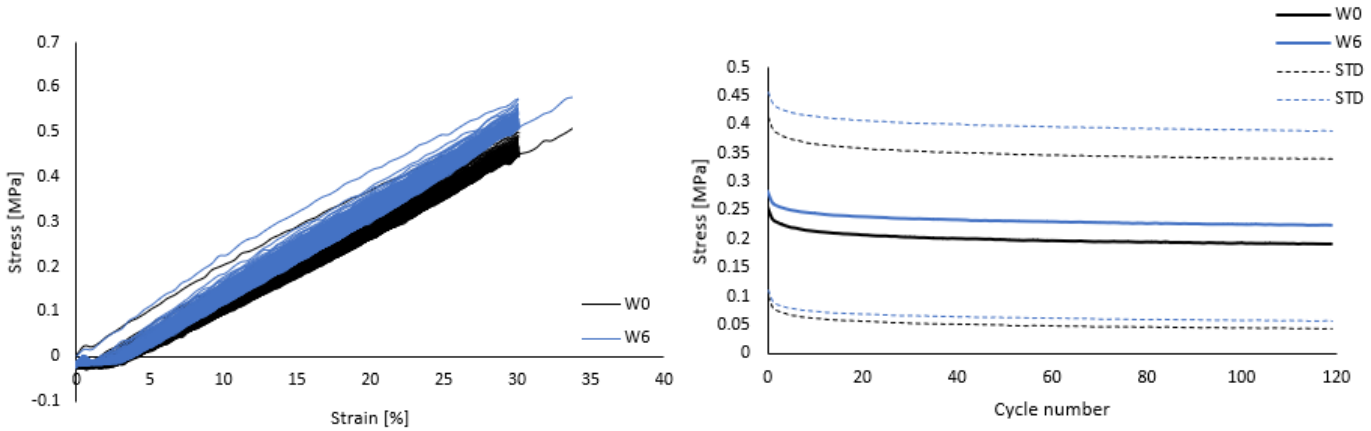

Figure 42 - Average curves for cyclic testing of Pellethane® scaffolds (n = 3). (left) Average stress-strain curve of 120 cycles. (right) Average peak stress vs. cycle number curve showing one standard deviation above and below.

A study by Stella *et al.* found that the mechanisms responsible for creep and relaxation in the aortic valve leaflet (AVL) are functionally independent and that a more appropriate description of valvular tissue would be qausi-elastic [113]. That is to say valvular tissues exhibited four unique mechanical properties of which properties of interest in this study include (a) no measurable creep under physiologically relevant loading conditions and (b) small viscous dissipative effects (hysteresis) [113,

114]. With this in mind, the small hysteresis exhibited by Pellethane® scaffolds would be more applicable to AVL behaviour than that of hybrid or DegraPol® scaffolds. However, the low percentage change in hysteresis after six weeks of incubation exhibited by hybrid and Pellethane® scaffolds is beneficial to AVL behaviour as valve leaflets will need to maintain mechanical integrity in vivo during recellularization to support adequate valve functioning once scaffolds degrade away.

The measurement of stress relaxation allows the prediction how a scaffold would behave in vivo under pulsate conditions [115]. Stress relaxation is associated with a reduction in stiffness and therefore the high stress relaxation exhibited by DegraPol® scaffolds (50% initially and 58.33% after six weeks of incubation) could indicate potential in vivo reduction in stiffness before cellular ingrowth, potentially resulting in improper valve functioning. The large difference in stress relaxion between DegraPol® and both hybrid and Pellethane® scaffolds, demonstrates a disparity in viscoelastic properties. There is however a similarity between all scaffolds, in which after 120 cycles scaffolds reach an almost constant stress. All scaffolds underwent an initial reduction in peak-stress, however hybrid and Pellethane® scaffolds then stabilised (gradient = -0.0002 for both groups) and show this same trend both during day-0 testing and after six weeks of incubation. DegraPol® scaffolds also showed some stabilisation, however the gradient of the curve indicates that these scaffolds experienced stress relaxation at a slightly increased rate (gradient = -0.0004 and -0.0003 for day-0 and week 6 testing respectively) in comparison to that of Pellethane® and hybrid scaffolds. This response represents how scaffolds would behave after initial implantation in situ [115].

3.2.3 Mass loss

Figure 43 depicts the percentage of mass loss from scaffolds as investigated over a period of 42 days. There was no significant difference ($p > 0.05$) between the mass loss at week 3 and week 6 for any of the groups. After 21 days of incubation all polymer groups showed similar mass loss with hybrid scaffolds depicting the highest average mass loss ($0.87 \pm 0.46\%$ for hybrid scaffolds and, $0.39 \pm 0.35\%$, and $0.41 \pm 0.27\%$, for Pellethane® and DegraPol® respectively with $p > 0.05$ for all pairings). However not significant ($p > 0.05$ for all pairings), after 42 days of incubation hybrid scaffolds still showed the highest average mass loss, with DegraPol® scaffolds now exceeding the average mass loss shown by Pellethane® ($1.78 \pm 0.85\%$, $1.20 \pm 0.61\%$, and $0.35 \pm 0.31\%$, respectively).

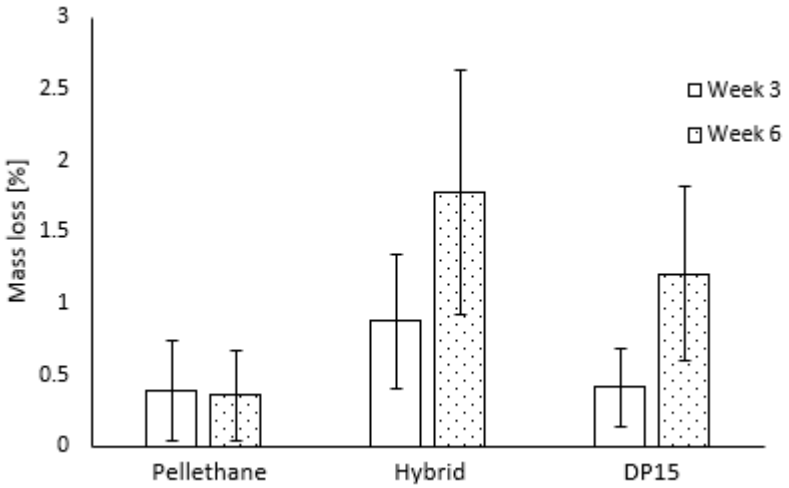

Figure 43 - Mass loss from Pellethane®, hybrid and DP15 scaffolds over 6 weeks

A previous 28-day degradation study on electrospun biodegradable polyester-urethanes, specifically DegraPol® DP30 with a 30% glycolide content at the soft segment side, showed a mere 0.2-2% mass loss over the period of a month [116]. The degradation of DegraPol® occurs through random chain scission of hydrolysable glycolyl-glycolate ester bonds of the soft segments, resulting in molecular weight reduction which is followed by the loss of mechanical properties and the loss of mass due to degradation products [75, 117].Thus, DegraPol® with a higher glycolide content will degrade faster and it is expected that the DegraPol® used in this study, with 15% glycolide content, will depict less mass loss than the 0.2-2% shown by DP30 [116]. Therefore, the 1.2 ± 0.61% degradation of DP15 found in this study is in-line with what was expected. Other studies have also shown that mass loss from polyester urethanes ranges from 8-50% after 70 to 90 days of incubation at 37℃ in PBS, which is higher than the 0.35 ± 0.31% mass loss experienced by Pellethane® in this study [118-121]. However, it is possible that if the study were to have run for longer than 42 days (ex. 70-90 days) Pellethane® scaffolds would have lost slightly more mass correlating with previous work.

The high mass loss exhibited by hybrid scaffolds is not well understood as hybrid scaffolds were more robust after degradation in comparison to DegraPol® scaffolds. Additionally, the high standard deviation seen in the data is the cause of no statistical significance being displayed between groups. This could be caused by the rinsing method used or could be attributed to the degradation being so low that the signal:noise ratio is too low to show significant differences in mass.

3.3 Valve hydrodynamics & durability study

3.3.1 Water contact angle

The wettability of electrospun scaffolds plays an important role in their in vivo performance, affecting cell attachment, adhesion and proliferation and was characterised using water contact angle measurements, as displayed in Figure 44 [122]. There was no significant difference ($p > 0.05$) between the luminal and abluminal surface water contact angle measurements of DegraPol® (126.62 ± 2.67° and 127.34 ± 1.52°, respectively) and hybrid (121.62 ± 5.53° and 118.97 ± 1.74°, respectively) scaffolds. The same was not true for Pellethane® scaffolds ($p < 0.05$) with average contact angle measurements of 132.42 ± 2.7° for abluminal- and 117.63 ± 2.27° for luminal surfaces. In Figure 44 “DP” refers to DegraPol®, “PEL” to Pellethane®, and “H” to hybrid scaffolds while “C” refers to cast scaffolds and “AL” and “L” to the abluminal and luminal side of electrospun scaffolds respectively.

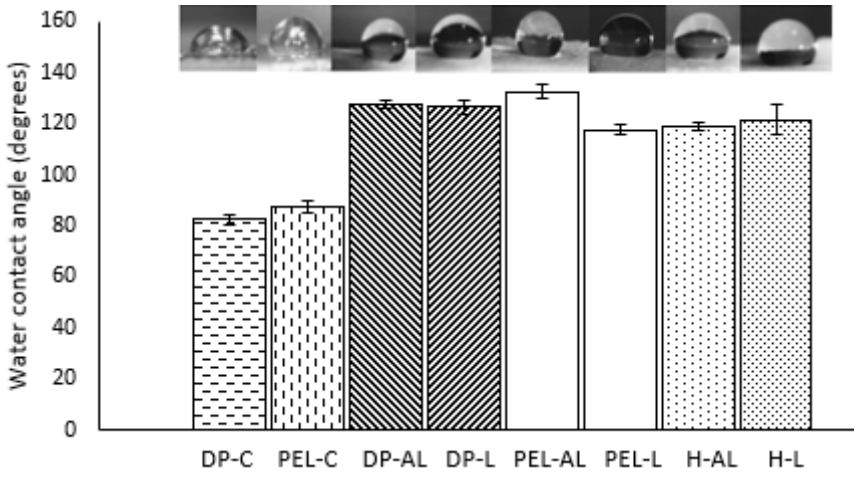

Figure 44 - Water contact angle measurements for cast and electrospun scaffolds

Electrospun DegraPol® and Pellethane® scaffolds exhibited a much higher ($p < 0.001$) water contact angle than their cast film counterparts, however this was expected as it has been previously reported [122]. This is since a surface mechanism of hydrophobic and hydrophilic behaviour exists, where smooth surfaces, such as cast films, are generally more hydrophilic (water contact angle < 90°), while rough surfaces, such as electrospun scaffolds, are hydrophobic (water contact angle > 90°) [123].

The water contact angle of electrospun DegraPol® with a 25wt% crystalline hard segment and 75wt% soft amorphous segment has been reported as 104.61 ± 1.49° when purely electrospun and 124.86 ± 2.87° when emulsion electrospun with biomolecules[124]. Although the contact angle reported for pure electrospun DegraPol® is slightly lower than that found in this study, both are hydrophobic and when taking the contact angle of the emulsion spun DegraPol® into account the data correlates well with the values recorded. Additionally, the water contact angle of electrospun Pellethane® has been reported as 115.3 ± 0.2° which correlates well with the values recorded for the luminal surfaces of Pellethane® scaffolds [125]. The notable difference in contact angle measurements for abluminal and luminal surfaces of Pellethane® can be attributed to surface roughness, where the luminal surface of all electrospun Pellethane® scaffolds were noticeably smoother than the abluminal surfaces, and therefore less hydrophobic. The hydrophobic water contact angle of hybrid scaffolds was expected as both Pellethane® and DegraPol® are hydrophobic and therefor a scaffold containing both polymers would also be expected to be hydrophobic [123]. Previous research suggests that hydrophobic polymer matrices greatly support cell attachment in comparison with highly hydrophilic natural and synthetic materials (contact angle ~18°), thus the hydrophobic behaviour of scaffolds produced could be applicable for tissue engineering applications [126]. Other researchers suggest that hydrophobic electrospun surfaces are unfavourable for tissue engineering, for example scaffolds with contact angles between 116° – 135°, suggesting contact angles below 100° to be more suitable for tissue engineering [127]. Webb *et al.* studied the highest level of cell attachment and found that at hydrophilic surfaces the best results were observed at contact angles in the range of 20° – 60° [127]. With this in mind appropriate hydrophilic functionalisation to improve contact angle for tissue engineering might be necessary.

3.3.2 Permeability

Permeability tests were conducted as electrospun scaffolds are generally highly porous and therefore a large portion of the leakage fraction and regurgitation volume seen during the pulse duplicator analysis (described in section 2.6) could potentially be attributed to fluid flow through the leaflet material. Quantifying material permeability assists in creating an understanding of what amount of leakage can be attributed to leakage through the material. The permeability of Pellethane® was significantly lower ($p < 0.001$, for all groups) than that of either DegraPol® or hybrid scaffolds, which also significantly different from one another ($p < 0.05$). Pellethane® scaffolds had a permeability of 53.04 ± 14.09 mD compared to 2469.94 ± 297.03 mD for DegraPol® scaffolds and 1743.46 ± 95.57 mD for hybrid scaffolds. Figure 45 outlines the instantaneous change in scaffold permeability with time, for all three scaffolds.

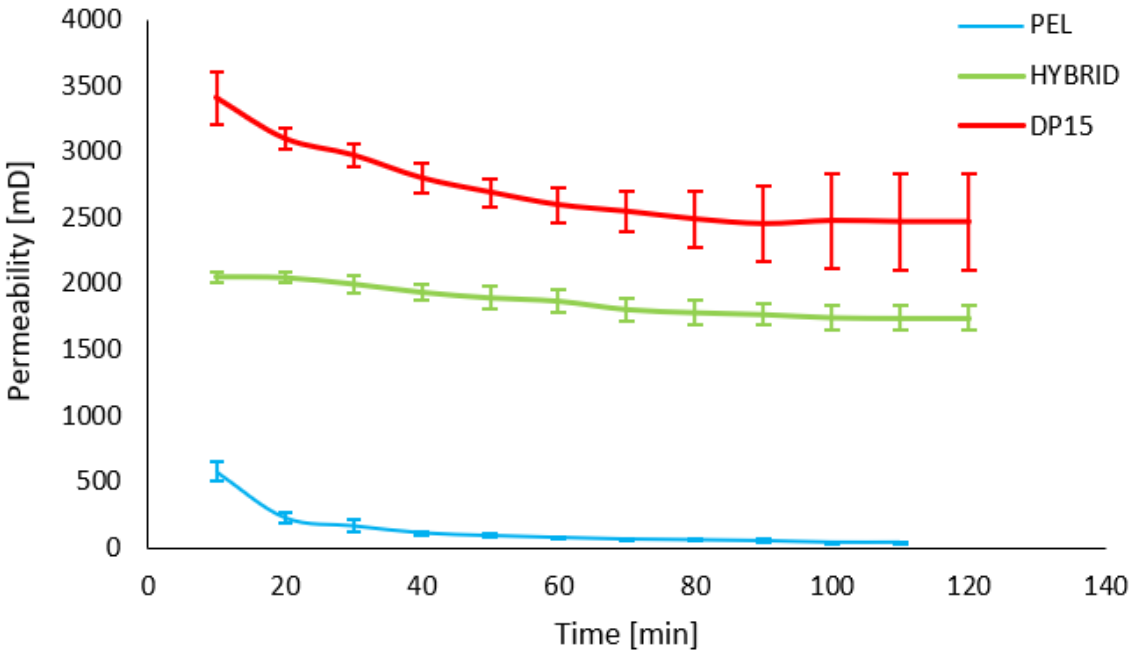

Figure 45 – Instantaneous change in scaffold permeability with time

The terms porosity and permeability are often incorrectly used interchangeably in the field of tissue engineering and in consideration of scaffolds which mimic the ECM. By definition, porosity represents the amount of void space within a structure, while permeability is a measure of the ease with which a fluid or gas can flow through a structure [128]. Generically speaking, an increase in scaffolds porosity will result in increased permeability, however this ultimately depends on a combination of scaffold porosity, pore size and distribution, pore orientation and interconnectivity, and scaffold tortuosity [128].

However not significant in comparison to DegraPol® and hybrid scaffolds ($p > 0.05$), Pellethane® scaffolds do have the lowest porosity (DP15: 67.93 ± 2.74% ,Pellethane®: 63.98 ± 5.85% and hybrid: 67.78 ± 4.48%) and smallest pore size (DP15: 18.29 ± 3.79 μm^2, Pellethane®: 9.24 ± 0.71 μm^2 and hybrid: 15.94 ± 5.08 μm^2) of all groups, which is consistent with the low permeability of the group. Pore size in particular is of interest as Pellethane® pore size is roughly half that of DegraPol® and hybrid scaffolds. The small pore size of Pellethane® scaffolds could be associated with a reduction in the interconnectivity of pores as well as tortuosity, ultimately leading to lower scaffold permeability. Additionally, wettability strongly affects relative permeability as it is an influential factor in the control of the location, flow and distribution of fluids in a porous medium [129]. Therefor the relatively high water contact angle of Pellethane® in comparison to DegraPol® and hybrid scaffolds ($P < 0.05$) correlates to lower wettability of Pellethane® scaffolds and therefor most likely is also a contributing factor to the low permeability of the scaffolds.

3.3.3 Suture retention analysis

There was no significant difference in the mean suture retention strength of either Pellethane® or DegraPol® scaffolds between their longitudinal and circumferential directions ($p > 0.05$), however the same was not true for hybrid scaffolds ($p < 0.05$). The mean suture retention strength for Pellethane® was 3.38 ± 0.12 N longitudinally and 3.1 ± 0.16 N circumferentially. As shown in Figure 46 (*left*), this was roughly double that of hybrid and DegraPol® scaffolds at 1.68 ± 0.02 N and 1.53 ± 0.07 N longitudinally and 2.43 ± 0.23 N and 1.82 ± 0.22 N circumferentially.

Specimen thickness and the distance of the suture bite from the free edge of the specimen are the most influential geometrical parameters in determining suture retention strength [130]. Thus, Figure 46 (*right*) discusses suture retention strength measured in N/mm, as this takes specimen thickness into consideration. The average specimen thicknesses for Pellethane® were 0.21 ± 0.02 mm longitudinally and 0.18 ± 0.01 mm circumferentially, 0.24 ± 0.004 mm longitudinally and 0.41 ± 0.01 mm circumferentially for hybrid scaffolds and lastly, 0.22 ± 0.01 mm longitudinally and 0.31 ± 0.02 mm circumferentially for DegraPol® scaffolds.

Interestingly, during testing samples behaved differently at failure. Pellethane® and DegraPol® failure tears occurred straight through from the suture bite through to the specimen free edge, as in Figure 47A. Hybrid scaffolds, on the other hand, experienced failure tears at the suture bite, parallel with the specimen free edge, as in Figure 47B. The reason for this phenomenon could be attributed to the low resistance to tear strength of hybrid scaffolds, discussed in section 3.3.4.

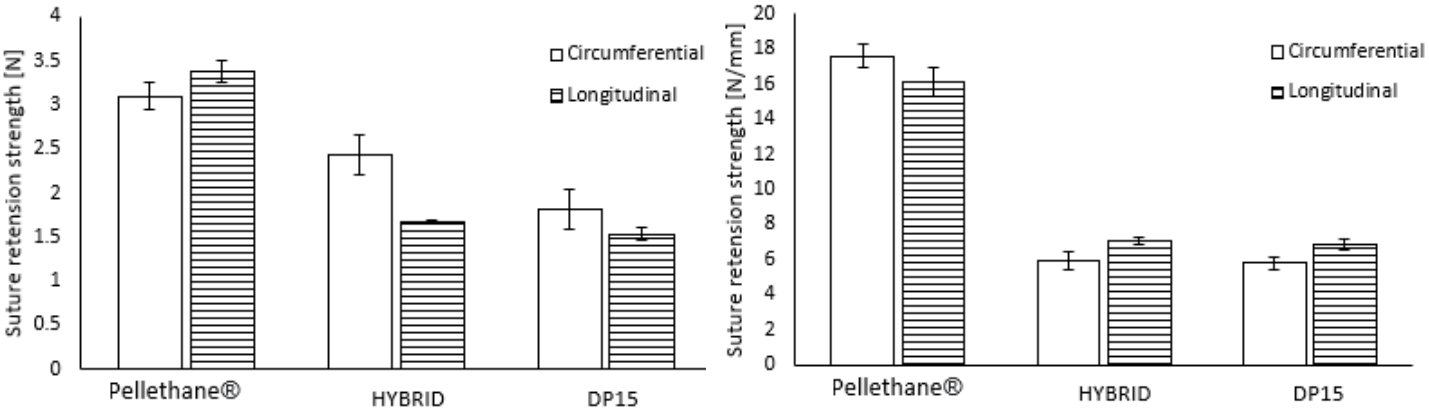

Figure 46 - Suture retention strength in (left) Newton, and (right) Newton/mm

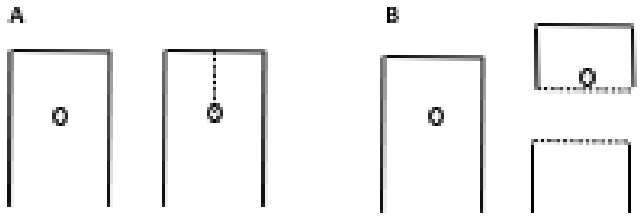

Figure 47 - Suture retention strength tearing modes

The suture retention strength of electrospun Pellethane® (3.38 ± 0.12 N longitudinally and 3.1 ± 0.16 N circumferentially) compares well to previously reported values of 2.8 ± 0.3 N circumferentially [131]. Additionally, the suture retention strength of electrospun bi-layered vascular grafts, fabricated from segmented polyester urethane and poly(L-lactic acid) through sequential electrospinning, has been reported as 1.55 ± 0.42 N, which correlates well with the suture retention strength recorded for both DegraPol® and hybrid scaffolds [132]. Notably, for certain mechanical characterisations, the properties of hybrid scaffolds fall roughly halfway between what was recorded for Pellethane® and DegraPol® scaffolds, while for other properties hybrid scaffolds more closely mimic the characteristics exhibited by DegraPol®. In the case of suture retention strength, the characteristics of DegraPol® are mimicked by hybrid scaffolds and the addition of Pellethane® seems to have little effect.

3.3.4 Resistance to tear analysis

The tear strength of all polymer groups is summarised in Figure 48 (left) in Newtons and Figure 48 (right) in Newton/mm to normalise the data against scaffold thicknesses so that the data is comparable. Pellethane® exhibited a significantly higher tear strength (13.53 ± 1.24 N/mm, $p < 0.05$ for all groups), close to three times higher than that of hybrid scaffolds (4.70 ± 0.29 N/mm) and roughly double that of DegraPol® scaffolds (5.82 ± 0.35 N/mm), with no significant difference between the tear strength of hybrid and DegraPol® scaffolds ($p > 0.05$).

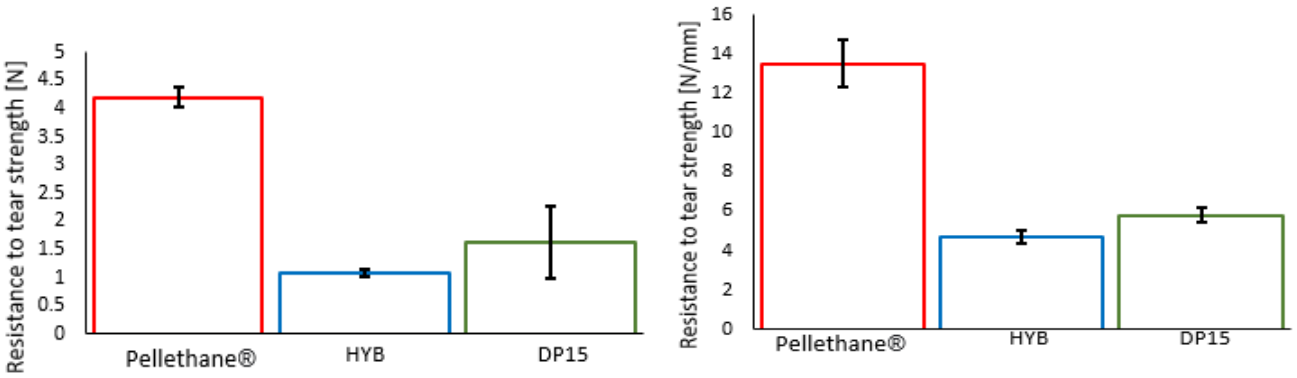

Figure 48 - Tear strength of electrospun scaffolds in (left) Newtons and (right) Newton/mm

The tear strength of electrospun PCL, a biodegradable polyester, has been reported to range between 4.7 ± 0.9 N to 10.6 ± 1.8 N, depending on the wt% of the solution [133]. This correlates well with the tear strength recorded for Pellethane® (4.2 ± 1.7 N) but is significantly higher than that of DegraPol® or hybrid scaffolds (1.62 ± 0.63 N and 1.08 ± 0.07 N, respectively).

In general, a combination of parameters affects the tear strength of textiles/scaffolds, including their basic weave construction or fibre deposition patterns and the adhesion of fibres. To ensure high tear strength values, fibres/filaments should not remain fixed but should be able so slide and move within the structure [134]. Therefore, it was not surprising to see that DegraPol® had a low resistance to tear strength, considering the inclusion of HFIP led to more fibre fusion, due to wet landing caused by the high vapour pressure of HFIP, which in turn leads to lower fibre mobility and thus tear strength. The low tear strength recorded for hybrid scaffolds could also be attributed to the same phenomenon, however it is interesting to note that the inclusion of Pellethane® has little to no effect on the tear strength, as in the case of suture retention strength. A study by Cacciola *et al.* which focused on synthetic fibre-reinforced heart valves found that the fibre-matrix interface determines the strength of the composite and that during tests perpendicular to the direction of reinforcing fibres, specimens broke at stresses lower than the stress required to break the matrix material without reinforcing fibres [135]. This could explain why hybrid scaffolds don't perform as expected for both suture retention and resistance to tear analysis, as the strength of the scaffolds during these tests could be reliant on the strength of the interfaces between DegraPol® and Pellethane® fibres.

3.3.5 Valve hydrodynamic testing

Table 14 in appendix A lists the results of the pulse duplicator tests for all valve prototypes designed. For a better appreciation of the test results, data for a St Jude mechanical valve with a diameter of 23 mm is used as comparison [136]. The effective orifice area (EOA), transaortic mean pressure and regurgitation fraction are summarised in Figures 49 - 51. All valves maintained integrity and suture retention under physiological pressures. In Figures 49-51 "DP" refers to DegraPol® valve leaflets, "P" to Pellethane® valve leaflets, and "H" to hybrid valve leaflets, with the numerical suffix used a unique identifier referring to how many of that valve type were manufactured. For example, H1 is the first hybrid valve manufactured. Due to constraints on both time and availability of specialised materials only two DegraPol® and two Pellethane® valves could be fabricated, while three hybrid valves were fabricated, as these valves were the focus of the study to provide a proof of principle.

All samples had large EOA's of close to 2 cm^2 and above. Overall, DegraPol® valves had the smallest EOA and Pellethane® valves the largest. Additionally, DegraPol® valves had the highest total regurgitant fraction, roughly double that of both hybrid and Pellethane® valves, while hybrid valves had the lowest. Lastly, DegraPol® and hybrid valves had similar transaortic mean pressures, both slightly higher than that of Pellethane®.

All valves surpassed ISO EOA requirements, with all valves exhibiting EOA's much larger than the required 1.25 cm^2 . All valves had total regurgitant fractions higher than the required 20%, however a portion of the regurgitant volume can be attributed to the scaffold permeability.

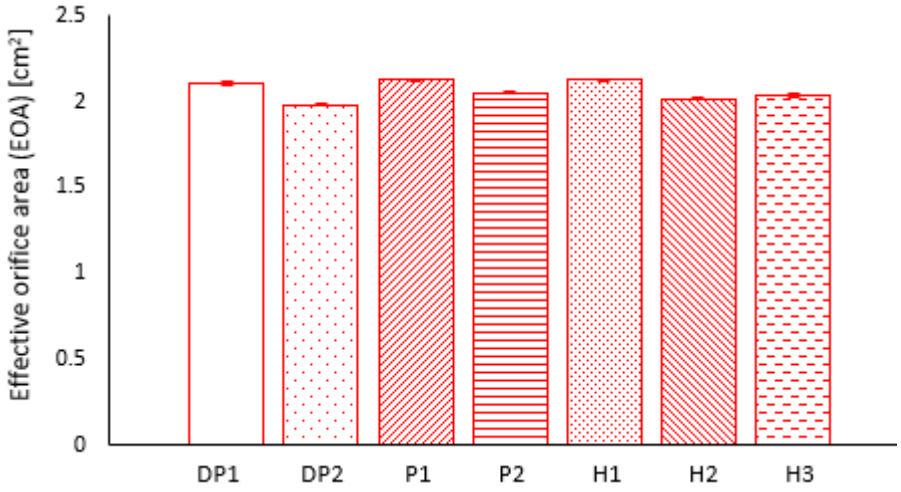

Figure 49 – Effective orifice area for all valve prototypes produced

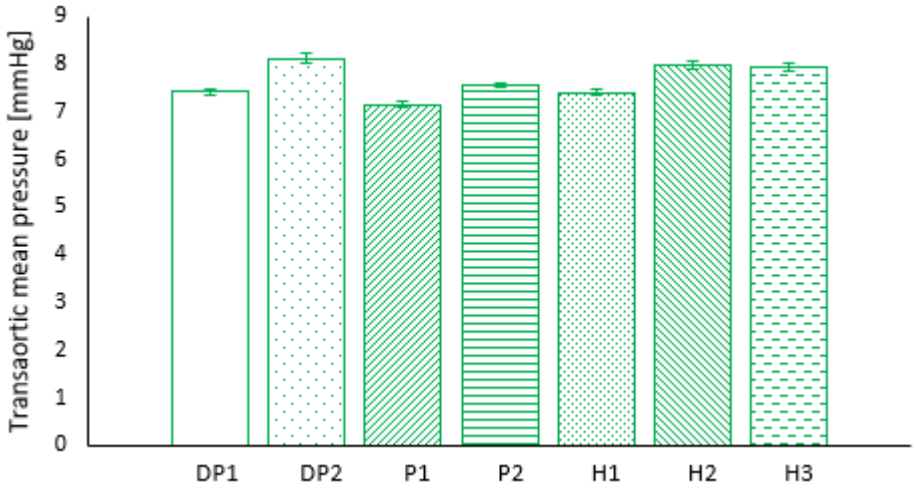

Figure 50 – Transaortic mean pressure for all valve prototypes produced

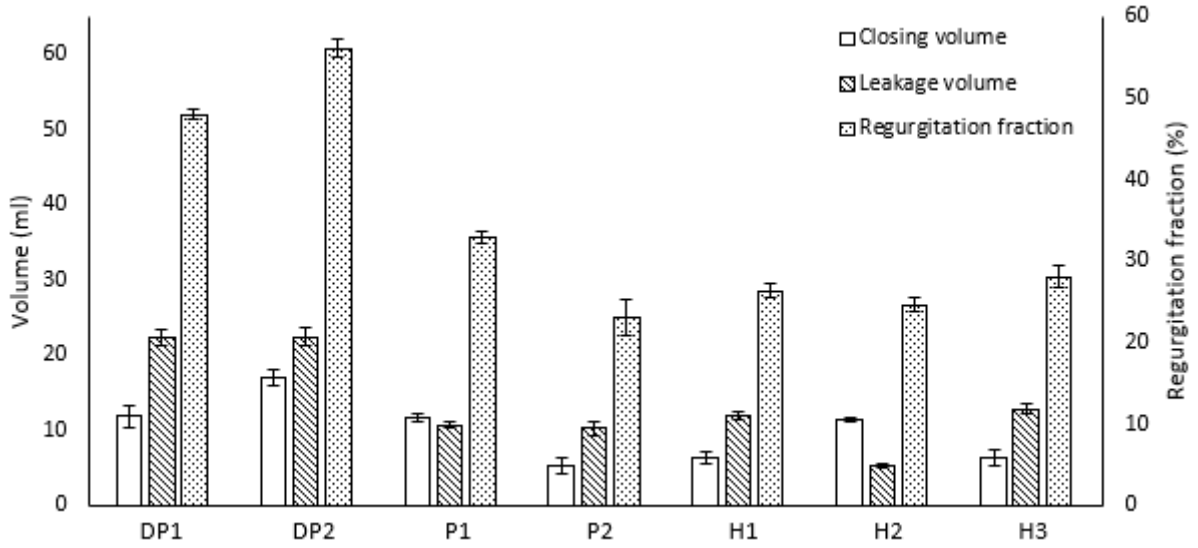

Figure 51 - Closing and leakage volume (ml) and corresponding regurgitation fraction (%) for all valve prototypes produced

The aortic regurgitation fraction is made up of both the aortic leakage volume and the aortic closing volume. DegraPol® valves exhibited both the highest closing volume and the highest leakage volume. The average closing volume of DegraPol® valves was 14.38 ± 0.72 ml, almost double that of Pellethane® (8.47 ± 0.58 ml, $p < 0.0001$) and hybrid valves (8.03 ± 0.49 ml, $p < 0.0001$) with no significant difference between the average closing volume of Pellethane® and hybrid valves ($p > 0.05$). Additionally, DegraPol® valves had an average leakage volume of 22.4 ± 0.82 ml, more than double that of Pellethane® (10.49 ± 0.4 ml) and hybrid (10.04 ± 0.39 ml) scaffolds ($p < 0.05$ for all pairings). The high closing and leakage volume exhibited by DegraPol® valves is validated when looking at the flow curve in Figure 53 in comparison to the flow curves shown for Pellethane® and hybrid scaffolds in Figures 55 and 57 respectively.

What is important to take into account is scaffold permeability as a large portion of the leakage volume experienced for all valve prototypes can be attributed to the permeability of the leaflet material. Figure 52 compares scaffold permeability to the average valve leakage volume and closing volume for all polymer groups. Importantly, the high leakage volume experienced by DegraPol® valves can be attributed to the high permeability of the material, however the closing volume of the valves still remain the highest. Interestingly, the permeability of hybrid scaffolds was significantly higher than of Pellethane® scaffolds, however the valves of both these groups had similar leakage volumes. The reason for this phenomenon is not known, however it is very beneficial to the valve's functioning.

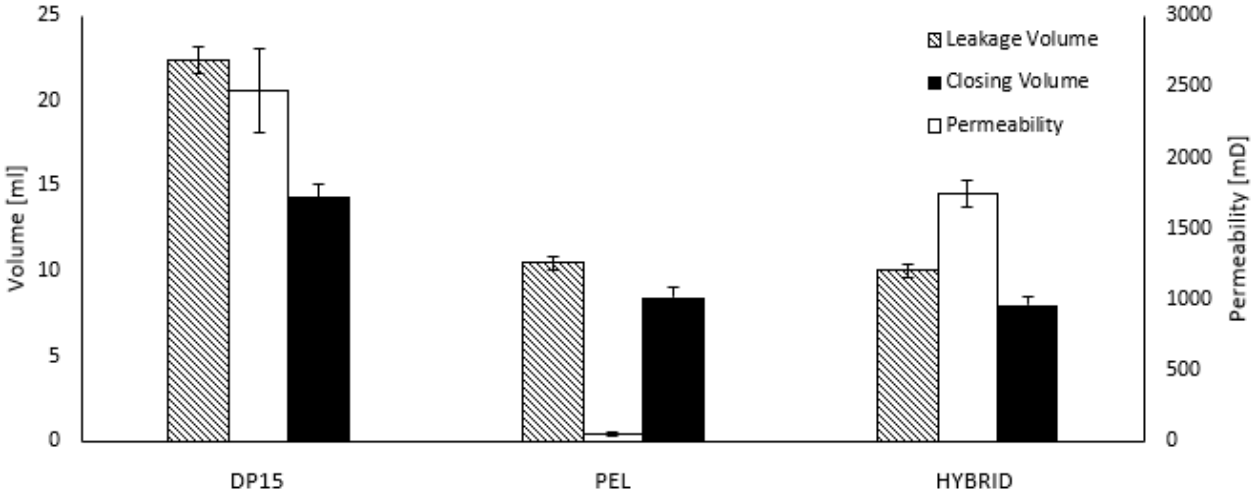

Figure 52 - Scaffold permeability in comparison with valve closing and leakage volume

On the other hand there is a lack of scientific understanding of the mechanisms of neo-tissue development as well as clinical success and failure with regards to tissue engineered heart valves [137]. One study on tissue engineered heart valves for transcatheter delivery showed successful function and endothelialisation after two weeks of implantation in a sheep model [138]. It is expected that blood will begin to clot the porous surface of leaflet scaffolds well before this two-week time point, however this provides an indication of how quickly cellular ingrowth into valves will occur and therefor it is expected that the leakage volume associated with hybrid and Pellethane® valves due to permeability will not be a concern for long in vivo.

The same can however not be said for DegraPol® valves that have both an extremely high leakage volume and closing volume. It is possible that DegraPol® valves have a higher leakage and closing volume due to a lack of stiffness inherent to the material and the high porosity and permeability associated with the electrospun scaffolds. Mimicking nature and increasing the thickness of the leaflet edges as well as the leaflet free edge length could mitigate this problem by increasing the coaptation area, serving as a sealing mechanism and enhancing the durability of the leaflets [135].

Table 12 lists the average leaflet thicknesses for all valves. After initial accelerated fatigue testing it was found that leaflet thickness had an effect on valve durability and therefor the effect of leaflet thickness on valve hydrodynamic performance was also assessed for hybrid valves. It was found that leaflet thickness affected hydrodynamic performance.

Leaflet thickness significantly affected valve EOA. H2 had a smaller EOA than H1 ($p < 0.0001$) which was expected due to the thinner leaflets of H1. This pattern followed through to H3 which also had a larger EOA than H2 ($p < 0.05$) coupled with thinner leaflets than H2. Interestingly H3 had a smaller EOA than H1 ($p < 0.0001$) even though the leaflet of H3 were much thinner than those of H1. This could be since both H1 and H3 were close to a maximum value for EOA that a 23 mm valve can possibly reach. These finding were supported by previous work where an association between reduced EOA for valves with thicker leaflets has been reported [139].

Furthermore, as can be seen from Figure 53, it was observed that H2 had a higher mean pressure gradient that H1 ($p < 0.0001$), which can again be contributed to the thicker leaflets of H2. However, again this trend did not carry through to H3 which had a higher pressure gradient than H1 ($p < 0.0001$) even though the valve had the thinnest leaflets.

Additionally, there was no significant difference ($p > 0.05$) between the pressure gradient of H2 and H3 even though there was a drastic difference in the leaflet thickness of the two valves. The observation that H2 had the highest transaortic mean pressure coupled with the thickest leaflets, even though not significant in terms of H3, is supported by previous work which concluded that the mean pressure gradient over the valve is expected to increase as the leaflet thickness increases [139]. A possible explanation for why H3 had a higher transaortic mean pressure than H1 and similar pressure to H2 while the leaflets of H3 were much thinner than both H1 and H2, could be attributed to a variety of factors such as the effect of leaflet stiffness which could have been altered by pulling the leaflet lugs further into the commissure posts or suturing further away from the edge of the belly of the leaflet.

With regards to the regurgitant fraction H2 had the lowest regurgitant fraction ($p < 0.05$ for all pairings) coupled with the thickest leaflets, while H3 had the highest regurgitant fraction ($p < 0.05$ for all pairings) coupled with the thinnest leaflets. These findings are supported by previous work which found that a reduction in regurgitant fraction is expected for valves with thicker leaflets [139].

Table 12 - Average leaflet thicknesses [mm]

DegraPol valves		**Pellethane valves**		**Hybrid valves**		
DP1	**DP2**	**PEL1**	**PEL2**	**H1**	**H2**	**H3**
0.38 ± 0.02	0.38 ± 0.01	0.38 ± 0.02	0.37 ± 0.01	0.36 ± 0.06	0.39 ± 0.02	0.30 ± 0.01

Bernacca *et al.* [140] performed an in vitro study to compare the effects of varying the elastic modulus vs. leaflet thickness on the hydrodynamics of a polyurethane trileaflet valve. Valve leaflets tested had an elastic modulus range from 5 – 63.3 MPa and a leaflet thickness range from 48 – 238 µm. They found that except for the highest elastic modulus (63.3 MPa), the choice of modulus over the range of 5 – 32.5 MPa did not significantly affect the hydrodynamic performance of the valve with regards to regurgitation, leakage, energy loss, and mean pressure differential. However, in accordance with beam theory, the leaflet thickness was a much greater determinant of hydrodynamic performance [141]. This could explain why, with the exception of the regurgitation fraction due to permeability, even with the large difference in elastic modulus between polymer groups, the transaortic mean pressure and EOA readings produced during pulse duplicator tests are more or less similar for all valve prototypes.

Figures 53 to 58 display pulse duplicator data on flow (Q(t)), aortic pressure (AO) and ventricular pressure (VE) for two pulses for all valve groups, along with images of valves at peak systole and diastole to compare the shape of fully open and closed valves. From these images it can be seen that all valves had a complete circular opening corresponding to the relatively large EOA values recorded. Additionally, all valves had relatively low transaortic mean pressure readings which can be seen in the small difference between curves for aortic pressure and ventricular pressure at peak pressure values in Figures 53,55 and 57. This is indicative of good valve functioning, as higher pressures are a result of greater force required to open the valve which is associated with higher energy loss across the valve [141]. The snapshots of the valves completely closed also indicate good coaptation, which supports the assumption that a large portion of the valve regurgitation fraction recorded can be attributed to slow through the valve leaflet due to material permeability. This is further supported by the flow curves which depict an especially large closing and leakage volume for DegraPol® valves (Figure 53) in comparison to Pellethane® (Figure 55) and hybrid (Figure 57) valves.

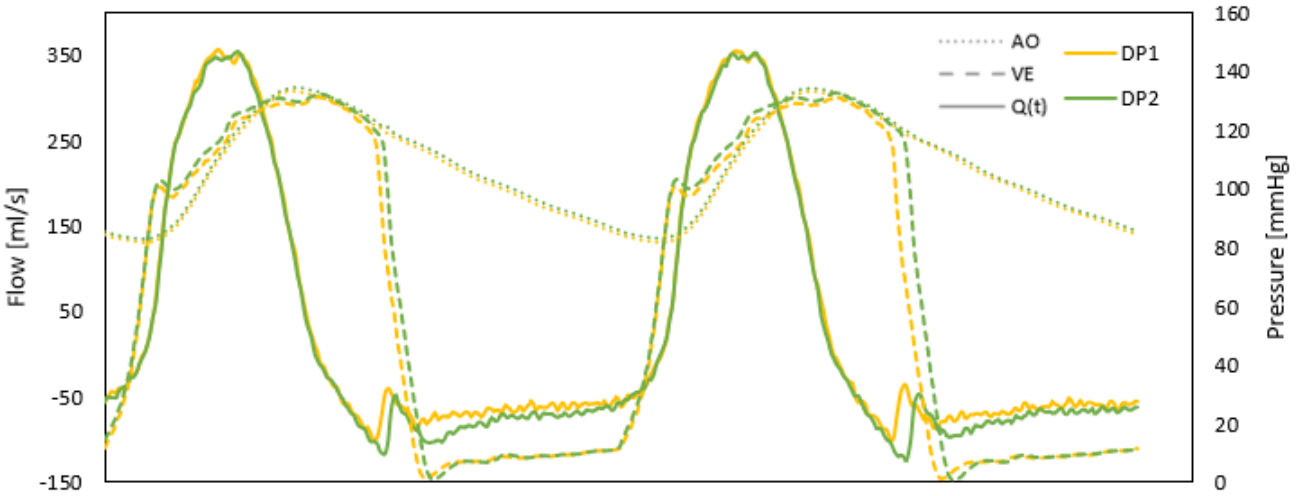

Figure 53 - Pulse duplicator results for both DegraPol® valve prototypes (DP1 & DP2)

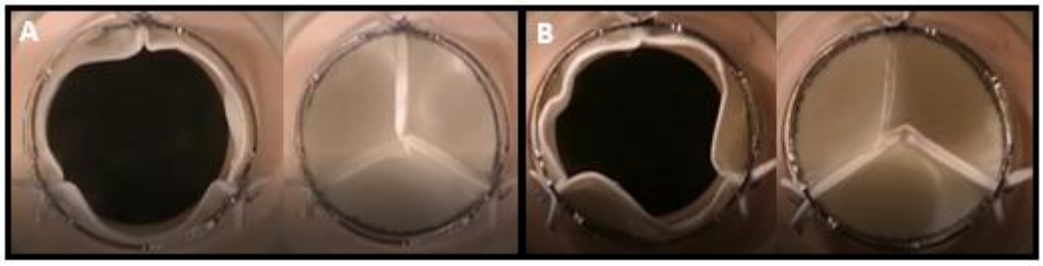

Figure 54 - Snapshots of peak systole and diastole for DegraPol® valves (A) D1 & (B) D2

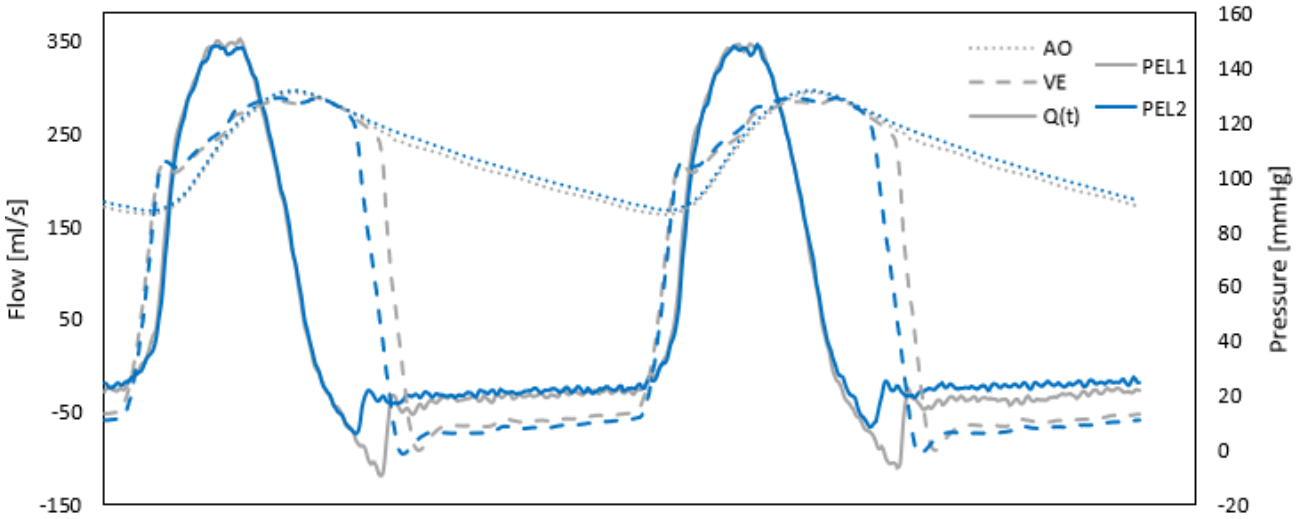

Figure 55 - Pulse duplicator results for both Pellethane® valve prototypes (PEL1 & PEL2)

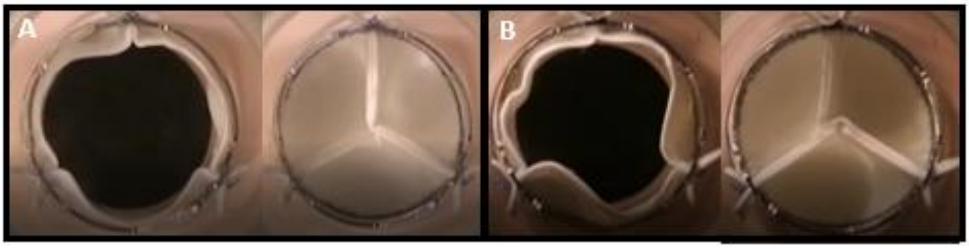

Figure 56 - Snapshots of peak systole and diastole for Pellethane® valves (A) PEL1 & (B) PEL2

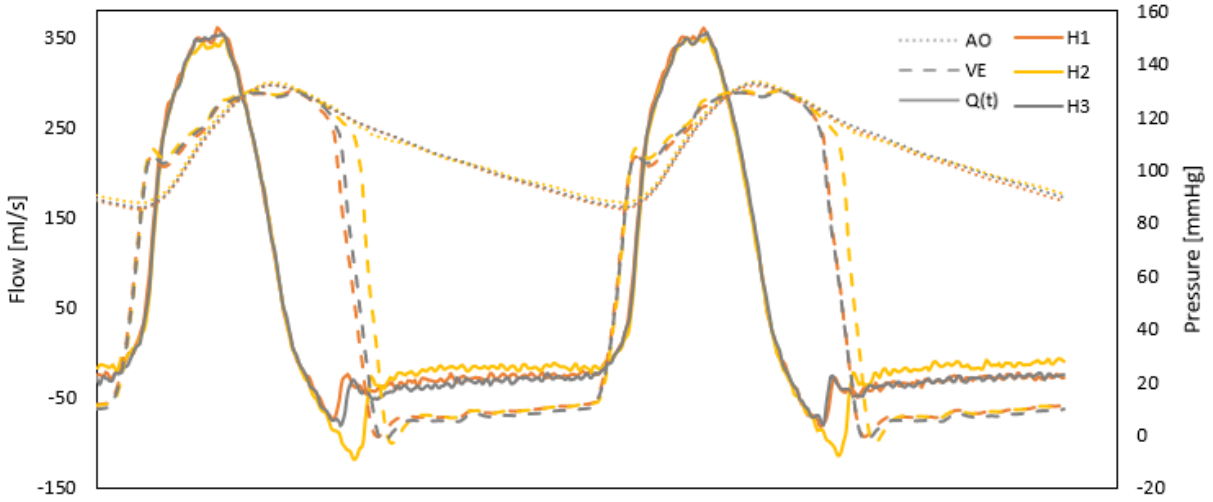

Figure 57 - Pulse duplicator results for Hybrid valve prototypes (H1 & H2 & H3)

Figure 58 - Snapshots of peak systole and diastole for (A) H1 & (B) H2 & (C) H3

3.3.6 Valve durability analysis

DegraPol® valves survived hydrodynamic testing at left heart pressures but failed before adequate testing pressures could be reached in the fatigue tester. Both DegraPol® valves failed through the formation of a vertical tear at a commissure post, which continued down the leaflet suture line (Figure 59A). Both Pellethane® valves on the other hand had reached ±40 million cycles by the end of the project which translates to a 1-year equivalence in vivo and were removed before failure.

The first hybrid valve fabricated (H1) reached ±4 320 000 cycles before failure. The valve had an average leaflet thickness of 0.36 ± 0.06 mm, however one of the leaflets was substantially thinner than the remaining two leaflets, as can be seen in the relatively large standard deviation of the average leaflet thickness. This inconsistency in leaflet thickness led to premature opening and closing on the thinner leaflet and thus induced increased stresses on the leaflet. The valve failed due to a vertical tear at the commissure post of the thinned leaflet, which continued down to the suture line of the leaflet (Figure 59B). Importantly all failure tears which occurred at the commissure posts of valves occurred on leaflets which were positioned to overlap a neighbouring leaflet, as previously explained. Additionally, some fraying was also noted at the free edge of the leaflet (Figure 59C).

Valve leaflet thicknesses varied slightly as can be seen in Table 14, where H2 had thicker leaflets (0.39 ± 0.02 mm) than H1 and failed after ±6 700 000 cycles, while H3 had thinner leaflets (0.30 ± 0.01 mm) than H1 and failed after ±10 000 000 cycles. Both H2 (Figure 59D) and H3 (Figure 59F) developed small vertical tears in their leaflets at ±4 800 000 cycles which slowly enlarged until valves were removed due to what was deemed improper functioning due to the enlargement of the tears, with H2 also developing a small vertical tear at a commissure post as well as free edge leaflet fraying of one leaflet (Figure 59E).

Thus, of all the hybrid valves, only H3 did not exhibited free edge leaflet fraying or commissure post tears which promotes the use of thinner leaflet for hybrid valves.

Table 13 - Valve prototype leaflet thickness and durability

Leaflet polymer	Valve number	Average leaflet thickness (mm)	Cycles to failure	Failure mode
Pellethane®	**P1**	0.38 ± 0.02	±40 000 000	No failure
	P2	0.37 ± 0.01	±40 000 000	No failure
Hybrid	**H1**	0.36 ± 0.06	±4 320 000	Tear at commissure post
	H2	0.39 ± 0.02	±6 700 000	Removed due to leaflet tears
	H3	0.30 ± 0.01	±10 000 000	Removed due to leaflet tears
DegraPol®	**DP1**	0.38 ± 0.02	± 0	Tear at commissure post
	DP2	0.38 ± 0.01	± 0	Tear at commissure post

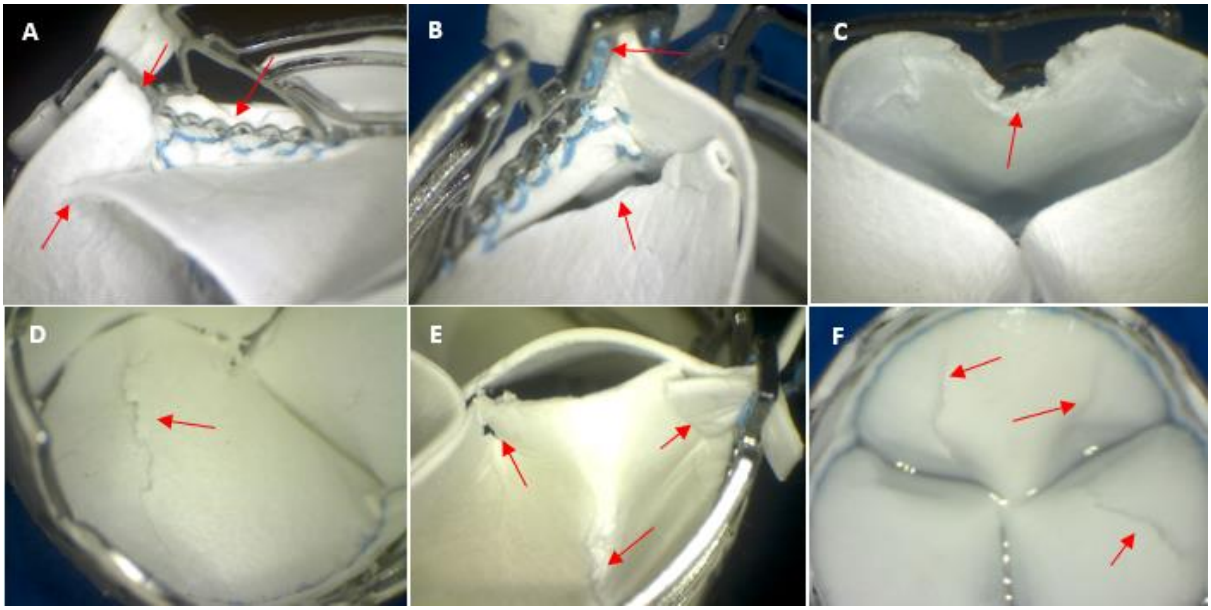

Figure 59 - Valve failure sites (indicated to with red arrows). (A) D1 commissure post tears and leaflet tear along suture line. (B) H1 commissure post tear and vertical leaflet tear next to suture line. (C) H1 leaflet fraying at free edge. (D) H2 vertical tears in leaflet from outflow side. (E) H2 commissure post tear, vertical leaflet tear and leaflet free edge fraying. (F) H3 vertical tears in leaflets.

It can be said that there was significant variation between the durability of leaflets for each of the polymer groups with the durability of valve prototypes tested according to ISO standard 5840. The premature failure of DegraPol® after surviving pulse duplicator testing at left heart pressures was unexpected. However, studies have shown that cyclic loading at physiological pressure can have a cumulative effect, resulting in elongation of the leaflet or residual strain. This leaflet elongation is necessarily accompanied by localised thinning, which leads to increased stresses and reduced fatigue life [141]. Thus, it is expected that the loading and unloading cycles of the durability tester, during initial testing to get the system up to pressure, was so rapid that the DegraPol® leaflets were not able to fully recover before the next cycle, leading to cumulative residual strain and essentially leaflet creep leading to thinning and leaflet tears.

This also coincides with the positioning of failure tears which were at the commissure posts of the valves, which have been reported as high stress areas [142].

The increased durability of fibre reinforced valves (hybrid valves) in comparison to DegraPol® valves was expected as studies have shown that these reinforced prototypes have a longer lifetime [135]. However, the vertical tears exhibited by hybrid valves were unexpected. As discussed in section 3.3.4, a resistance to tear analysis showed that hybrid scaffolds have the lowest resistance to tear strength of the three scaffold groups. The exact reason for this could possibly be attributed to interaction between the two polymer group fibres from which the scaffold is made up. It could be hypothesized that the fibre fusion points between DegraPol® and Pellethane® fibres are not as strong as the fusion points between like fibres, resulting in the low resistance to tear strength and suture retention strength of hybrid scaffolds. A study by De Hart *et al.* on a fibre reinforced aortic valve prosthesis stated that the failure of a fibre-reinforced prosthesis is most likely to be caused by debonding between fibre and matrix, and tearing and perforation of the matrix material [112]. Although heart valves in De Hart's study were not homogenously reinforced such as the hybrid valves of this study, the findings of De Hart et al.'s study support the notion that bonds between non-like fibres (matrix and reinforcing fibres) are weaker than the bonds between like fibres.

Additionally, the vertical tears in hybrid scaffolds increased in size at a very slow rate. This could be since tears potentially propagated in areas with more DegraPol® fibres and could only spread until they reached areas with more Pellethane® (reinforcing fibres) [143]. Thus, the initiation of tears did not render the valve function improper.

It is important to note that the leaflet tears of both H2 and H3 only occurred after ±4 800 000 cycles, at which it would be expected that recellularization would have initiated in vitro or in vivo. Previous research states that 30 days in vivo (±3 330 000 cycles) should provide adequate time for the recellularization process to begin [144]. Another study conducted to assess tissue formation rate in relation to the degradation rate of a scaffold, utilised both seeded and unseeded scaffolds of PGA-P4HB and PCL which were cultured for up to six weeks. The study found that PCL scaffolds, which degrade at a slower rate than PGA-P4HB scaffolds, resulted in the most tissue formation which also increased the stiffness of the scaffolds. Additionally, the tissue that formed on the PCL scaffolds contained ECM components in amounts similar to those in native leaflets [145]. The study concluded that slow-degrading scaffold materials, such as the developed hybrid scaffolds, are favoured over fast-degrading materials to create organised ECM-rich tissues in vitro [146]. Thus, it can be reasonably expected that cellular ingrowth into the hybrid scaffolds would increase the stiffness of the leaflets providing additional mechanical strength, ultimately avoiding leaflets tears. Regardless of the leaflet tears which occurred in hybrid valves, all hybrid valves lasted longer than DegraPol® valves in the fatigue tester, although they did not last as long as Pellethane® valves.

4 Conclusion

The following conclusions were formulated based on the investigations performed in this study to develop and analyse the characteristics of reinforced hybrid scaffolds for an application in transcatheter aortic heart valve tissue engineering.

Novel hybrid scaffolds comprising of DegraPol15® and Pellethane® could be and were successfully produced through dual electrospinning and confirmed through degradation analysis and SEM imaging. Optimised dual scaffolds with similar DP15 and Pellethane® fibre diameters were produced by increasing the polymer concentration (wt%) to maximise Pellethane® fibre diameter and adding HFIP to DP15 solutions to decrease DegraPol® fibre sizes. The integration of the two polymers resulted in scaffolds with intermediate mechanical properties. This concept is advantageous in tissue engineering applications that require a partially degradable scaffold that contains a non-degradable component which can serve as a permanent reinforcing structure for cell ingrowth and ECM deposition.

DP15 and Pellethane® were cast to determine the mechanical properties of the materials, as opposed to the structure/material combination as in the case of electrospun scaffolds. The ultimate tensile strength of Pellethane® films was measured to be approximately four times larger than that of DegraPol® films, while the maximum elongation of cast DegraPol® films was roughly double that of Pellethane® . The Young's modulus of cast Pellethane® films was found to be nearly five times that of DegraPol® films. Comparing these properties to the measured mechanical properties of electrospun scaffolds showed that electrospun scaffolds do have reduced mechanical properties for both ultimate tensile strength and Young's modulus. However, although high strength of the material itself is important for valve durability, the introduction of degradability into polyurethanes is often associated with a compromise in other mechanical properties. This was one of the driving factors for this research, where using a combination of the two polymers allows one to achieve both structural strength and degradability which is key in tissue engineering scaffolds.

DP15, Pellethane® and hybrid scaffolds were successfully electrospun. The hydrolytic degradation of electrospun samples led to sample mass decrease with incubation time, and this led to a decrease in the mechanical properties of the samples (i.e., UTS and ε_{max}). Interestingly, although not significant, hybrid samples exhibited the most mass loss, but not the most significant decrease in mechanical properties. DP15 scaffolds saw the largest decrease in UTS and extensibility in both the circumferential and longitudinal directions ($p < 0.05$) and Pellethane® scaffolds the least. The Young's modulus of all groups was not significantly affected by degradation, except for Pellethane® scaffolds in the longitudinal direction and hybrid scaffolds in the circumferential direction. The significant mass loss exhibited by hybrid scaffolds is advantageous for cellular ingrowth into the electrospun scaffolds for tissue engineering purposes. This is especially advantageous when coupled with the fact that the hybrid scaffolds did not show the most significant reduction in strength, thus the scaffolds should continue to provide adequate mechanical properties for proper valve functioning. These two factors place hybrid scaffolds in a promising light for use as tissue engineering scaffolds.

In the case of suture retention strength and resistance to tear strength, dual spinning DegraPol15® and Pellethane® did not result in the expected tuneable intermediate material properties. For both of these properties Pellethane® scaffolds were superior. Hybrid scaffolds had the weakest resistance to tear and similar suture retention strength to DegraPol® as it is expected these properties rely on the strength of the bonds between fibres, which are stronger between like fibres than non-like fibres. Further investigation is required to fully characterise this behaviour.

Scaffold permeability was successfully characterised with Pellethane® scaffolds exhibiting the lowest permeability and DegraPol® scaffolds the highest. This was expected as the pore size of Pellethane® is roughly half that of DegraPol® and hybrid scaffolds. The small pore size of Pellethane® scaffolds could be associated with a reduction in the interconnectivity of pores as well as tortuosity, ultimately leading to the lower scaffold permeability recorded.

Electrospun DegraPol® and Pellethane® scaffolds exhibited a much higher water contact angle than their hydrophilic cast film counterparts, with all electrospun scaffolds exhibiting hydrophobic water contact angles on both their luminal and abluminal surfaces. DegraPol® and hybrid scaffolds exhibited similar contact angles on both their luminal and abluminal surfaces, while Pellethane® scaffolds did not. This is attributed to surface roughness as the luminal surfaces of Pellethane® scaffolds were noticeably smoother than the abluminal surfaces. Considering some researchers suggest hydrophobic electrospun surfaces are unfavourable for tissue engineering, the hydrophobic nature of hybrid scaffolds surfaces is still not optimised for tissue engineering purposes. Altering the hydrophobic nature of all scaffold surfaces might be a necessary future development to appropriate hydrophilic functionalisation to improve the contact angles for tissue engineering.

All valves maintained integrity and suture retention under physiological pressures, with all valves surpassing ISO EOA requirements, with EOA's much larger than the required 1.25 cm^2 . All valves had total regurgitant fractions higher than the ISO required 20%, however a portion of the regurgitant volume can be attributed to the scaffold permeability. Overall, DegraPol® valves had the smallest EOA and Pellethane® valves the largest. Additionally, DegraPol® valves had the highest total regurgitant fraction, close to double that of hybrid and Pellethane® valves, while hybrid valves had the lowest regurgitant fraction regardless of the scaffold's high permeability. Lastly, DegraPol® and hybrid valves had similar transaortic mean pressures, both slightly higher than that of Pellethane®, however all valves had relatively low transaortic mean pressures indicative of good valve functioning. It was found that for hybrid valves, leaflet thickness affected hydrodynamic performance. This indicates that hybrid valves are a promising solution in the field of tissue engineering as they have a closing volume similar to that of Pellethane® valves and the regurgitant fraction present in hybrid valves is not expected to be a concern for long in vivo, as it is expected that blood will begin to clot the porous leaflet surface shortly after implantation. Thus, hybrid valves are expected to have very low leakage volumes coupled with good EOA's as per ISO requirements. This is indicative of effective heart valve functioning for hybrid leaflet valves, where sufficient blood is allowed to flow through the valve at low transaortic mean pressures, while minimal blood is allowed to leak back through the valve.

DegraPol® valves survived hydrodynamic testing at left heart pressures but failed before adequate testing pressures could be reached in the fatigue tester. Both Pellethane® valves reached ±40 million cycles by the end of the study, translating to 1 year equivalence in vivo, and were removed before failure. Hybrid valves all lasted longer than the DegraPol® valves during durability testing, however they did not last as long as the Pellethane® valves. The aim of the study was thus partially achieved, as the addition of the non-degradable fibres improved the durability of the valves, but not to the full extent desired, most likely as the degradable fibres that bonded to themselves and the stable Pellethane fibres failed, leading to failure of the scaffold. Further iterations of hybrid valves all failed due to small, slow growing, vertical tears which propagated in the valve leaflets. These tears only initiated in leaflets after a substantial number of cycles, at which point in vivo some cellular ingrowth would be expected which would theoretically provide mechanical support to avoid the propagation of these tears. Therefor hybrid scaffolds show great promise as leaflet material for tissue engineered heart valves due to their improved mechanical properties and durability along with adequate hydrodynamic performance.

5 Limitations and Recommendations

The following recommendations are made as suggestions for the continuation of the current research in order to improve on techniques or expand our understanding of specific sub-topics focused towards developing hybrid scaffolds for an application in heart valve tissue engineering.

1. Due to constraints on both time and availability of specialised materials only two DegraPol® and two Pellethane® valves could be fabricated, while three hybrid valves were fabricated as these valves were the focus of the study to provide a proof of principle. It is recommended that in future more valves in each of the polymer groups should be fabricated to confirm these initial results.

2. Time constraints also affected the maximum length of time used in the degradation experiments. Additional (longer) timepoints should be used in future work on this topic. The 3- and 6 week timepoints are however important as the loss of mechanical strength is much more rapid than the mass loss experienced within this time frame, and it is consistent with the initial ingrowth period of cells in tissue engineering applications.

3. Improving the stent coating method of stents is suggested to improve control over the coating thickness and uniformity.
4. Studying various ratios of degradable to non-degradable fibres in hybrid scaffolds to determine critical points of reinforcement and cellular ingrowth, as hybrid scaffolds with maximal degradable fibres would be beneficial for tissue engineering applications.
5. Improving mandrel charge distribution, which is currently only supplied from one side of the mandrel, to potentially allow better fibre distribution and thus more homogenous scaffold thickness.
6. Charged plates could be utilised for dual spinning to improve the yield of evenly distributed fibres along the mandrel.
7. Investigating a way to clog scaffold pores, without unduly altering the mechanical properties of the scaffold, to reduce the leakage volume through leaflets during pulse duplicator testing. In vivo blood will clot these surfaces almost instantaneously however currently we have no way of simulating this in a pulse duplicator to give a more accurate understanding of valve performance after implantation.
8. Conducting a study on water absorption of scaffolds could be beneficial in further understanding the variation in degradation rates between dual spun and single spun scaffolds, as scaffolds with high water absorption properties show higher degradation rates.
9. It is highly recommended to conduct further research on bonds between non-like fibres and like fibres at fibre interfaces, to determine which scaffolds properties will rely on fibre strength and which on the strength of the bonds between fibres. This will allow a better understanding, and hopefully improvement, of characteristics such as resistance to tear and suture retention of hybrid scaffolds.

6 References

1. *HiCycle System User Manual*, in *HiTest Version 5.0*. ViVitro Labs Inc. p. 106.
2. Hülk, V.M., *Electrospun Tissue Engineered Vascular Grafts (Thesis)*, in *Department of Human Biology*. 2019, University of Cape Town.
3. Van den Bergh, W.J.W., *Drug eluting electrospun scaffolds for tissue regeneration (Thesis)*. 2018, University of Cape Town.
4. Forsberg, P. and M.T. DeSancho, *Role of Novel Anticoagulants for Patients with Mechanical Heart Valves.* Current Atherosclerosis Reports, 2014. **16**(11): p. 448.
5. Jones, B.M., A. Krishnaswamy, E.M. Tuzcu, S. Mick, W.A. Jaber, L.G. Svensson, and S.R. Kapadia, *Matching patients with the ever-expanding range of TAVI devices.* Nature Reviews Cardiology, 2017. **14**(10): p. 615-626.
6. Voorneveld, J., A. Oosthuysen, T. Franz, P. Zilla, and D. Bezuidenhout, *Dual electrospinning with sacrificial fibers for engineered porosity and enhancement of tissue ingrowth.* Journal of biomedical materials research. Part B, Applied biomaterials, 2016. **105**.
7. Sahay, R., V. Thavasi, and S. Ramakrishna, *Design Modifications in Electrospinning Setup for Advanced Applications.* Journal of Nanomaterials, 2011.
8. Goodwin, R.L. and S.V. Biechler, *Chapter 1 - Clinical anatomy and embryology of heart valves*, in *Principles of Heart Valve Engineering*, A. Kheradvar, Editor. 2019, Academic Press. p. 1-12.
9. Byrne, J., G. Eksteen, and C. Crickmore, *Cardiovascular Disease Statistics Reference Document*. 2016, Heart and Stroke Foundation South Africa (HSFSA).
10. Kitsara, M., O. Agbulut, D. Kontziampasis, Y. Chen, and P. Menasche, *Fibers for hearts: A critical review on electrospinning for cardiac tissue engineering.* Acta Biomater, 2017. **48**: p. 20-40.
11. Huntley, G.D., J.J. Thaden, and V.T. Nkomo, *Chapter 3 - Epidemiology of heart valve disease*, in *Principles of Heart Valve Engineering*, A. Kheradvar, Editor. 2019, Academic Press. p. 41-62.
12. Dina M. Ibrahim, A.K., Nageh K. Allam, *Recent advances on electrospun scaffolds as matrices for tissueengineered heart valves.* Materials Today Chemistry, 2017.
13. Lung, B., G. Baron, E. Butchart, F. Delahaye, C. Gohlke-Bärwolf, O. Levang, P. Tornos, J.-L. Vanoverschelde, F. Vermeer, E. Boersma, P. Ravaud, and A. Vahanian, *A prospective survey of patients with valvular heart disease in Europe: The Euro Heart Survey on Valvular Heart Disease.* European heart journal, 2003. **24**.
14. Schultz, W.M., J.C. Lisko, T. Varghese, J. Shen, P. Sandesara, A. Quyyumi, A.H. Taylor, M. Gulati, J.G. Harold, J.H. Mieres, K.C. Ferdinand, G.A Mensah, *Socioeconomic Status and Cardiovascular Outcomes - Challenges and Interventions.* Circulation, 2018: p. 2166–2178.
15. Carapetis, J.R., A.C. Steer, E.K. Mulholland, and M. Weber, *The global burden of group A streptococcal diseases.* The Lancet Infectious Diseases, 2005. **5**(11): p. 685-694.
16. Miller, S. and B.C. Flynn, *Valvular Heart Disease and Postoperative Considerations.* Seminars in Cardiothoracic and Vascular Anesthesia, 2015. **19**(2): p. 130-142.
17. Engel, M.E., A. Haileamlak, L. Zuhlke, C.E. Lemmer, S. Nkepu, M. van de Wall, W. Daniel, M. Shung King, and B.M. Mayosi, *Prevalence of rheumatic heart disease in 4720 asymptomatic scholars from South Africa and Ethiopia.* Heart, 2015. **101**(17): p. 1389-94.
18. Monroe, M., A. Zhu, and K.J. Grande-Allen, *Chapter 2 - Heart valves' mechanobiology*, in *Principles of Heart Valve Engineering*, A. Kheradvar, Editor. 2019, Academic Press. p. 13-39.
19. Jana, S., B.J. Tefft, D.B. Spoon, and R.D. Simari, *Scaffolds for tissue engineering of cardiac valves.* Acta Biomater, 2014. **10**(7).

20. Zhang, B.L., R.W. Bianco, and F.J. Schoen, *Preclinical Assessment of Cardiac Valve Substitutes: Current Status and Considerations for Engineered Tissue Heart Valves.* Front Cardiovasc Med, 2019. **6**: p. 72.
21. Rippel, R., H. Ghanbari, and A. Seifalian, *Tissue-Engineered Heart Valve: Future of Cardiac Surgery.* World journal of surgery, 2012. **36**.
22. Pibarot, P. and G. Dumesnil Jean, *Prosthetic Heart Valves.* Circulation, 2009. **119**(7): p. 1034-1048.
23. Kaiser, N. and K. Coulombe, *Physiologically inspired cardiac scaffolds for tailored in vivo function and heart regeneration.* Biomedical Materials, 2015. **10**.
24. Li, R.L., J. Russ, C. Paschalides, G. Ferrari, H. Waisman, J.W. Kysar, and D. Kalfa, *Mechanical considerations for polymeric heart valve development: Biomechanics, materials, design and manufacturing.* Biomaterials, 2019. **225**.
25. Yoganathan, A., Z. He, and S. Jones, *Fluid Mechanics of Heart Valves.* Annual review of biomedical engineering, 2004. **6**.
26. Musumeci, L., N. Jacques, A. Hego, A. Nchimi, P. Lancellotti, and C. Oury, *Prosthetic Aortic Valves: Challenges and Solutions.* Front Cardiovasc Med, 2018. **5**: p. 46.
27. Phillips, E.H. and C.J. Goergen, *Chapter 4 - Surgical heart valves*, in *Principles of Heart Valve Engineering*, A. Kheradvar, Editor. 2019, Academic Press. p. 63-84.
28. Zilla, P., P. Human, and D. Bezuidenhout, *Bioprosthetic heart valves: The need for a quantum leap.* Biotechnology and applied biochemistry, 2004. **40**: p. 57-66.
29. *Bioprosthetic surgical aortic valve (SAV) construction*. 04/08/2021]; Available from: https://www.pcronline.com/Cases-resources-images/TAVI-Atlas/Techniques/Valve-in-valve/Bioprosthetic-surgical-aortic-valve-SAV-construction.
30. Bagur, R., P. Pibarot, and C. Otto, *Importance of the valve durability-life expectancy ratio in selection of a prosthetic aortic valve.* Heart, 2017. **103**.
31. Sarraf, M., E.M. Groves, and A. Kheradvar, *Chapter 5 - Transcatheter heart valves*, in *Principles of Heart Valve Engineering*, A. Kheradvar, Editor. 2019, Academic Press. p. 85-122.
32. Fioretta, E., S. Motta, V. Lintas, S. Loerakker, K. Parker, F. Baaijens, V. Falk, S. Hoerstrup, and M. Emmert, *Next-generation tissue-engineered heart valves with repair, remodelling and regeneration capacity.* Nature reviews. Cardiology, 2020.
33. Bezuidenhout, D., D.F. Williams, and P. Zilla, *Polymeric heart valves for surgical implantation, catheter-based technologies and heart assist devices.* Biomaterials, 2015. **36**: p. 6-25.
34. Dandeniyage, L., R. Adhikari, M. Bown, R. Shanks, B. Adhikari, C. Easton, T. Gengenbach, D. Cookson, and T. Gunatillake, *Morphology and surface properties of high strength siloxane poly(urethane-urea)s developed for heart valve application.* Journal of Biomedical Materials Research Part B: Applied Biomaterials, 2018. **107**.
35. Dandeniyage, L., T. Gunatillake, R. Adhikari, M. Bown, R. Shanks, and B. Adhikari, *Development of high strength siloxane poly(urethane-urea) elastomers based on linked macrodiols for heart valve application.* Journal of Biomedical Materials Research Part B: Applied Biomaterials, 2017. **106**.
36. Rotman, O., B. Kovarovic, W.-C. Chiu, M. Bianchi, G. Marom, M. Slepian, and D. Bluestein, *Novel Polymeric Valve for Transcatheter Aortic Valve Replacement Applications: In Vitro Hemodynamic Study.* Annals of Biomedical Engineering, 2018. **47**.
37. Scherman, J., D. Bezuidenhout, C. Ofoegbu, D.F. Williams, and P. Zilla, *TAVI for low to middle income countries.* European Heart Journal, 2017. **38**(16): p. 1182-1184.

38. Legg, M., E. Mathews, and R. Pelzer, *The design and development of a stented tissue mitral and aortic heart valve replacement for human implantation.* Cardiovascular journal of Africa, 2012. **23**(3): p. 126-130.
39. Mackay, T.G., D.J. Wheatley, G.M. Bernacca, A.C. Fisher, and C.S. Hindle, *New polyurethane heart valve prosthesis: design, manufacture and evaluation.* Biomaterials, 1996. **17**(19): p. 1857-1863.
40. Rahmani, B., S. Tzamtzis, H. Ghanbari, G. Burriesci, and A.M. Seifalian, *Manufacturing and hydrodynamic assessment of a novel aortic valve made of a new nanocomposite polymer.* Journal of Biomechanics, 2012. **45**(7): p. 1205-1211.
41. Rahmani, B., S. Tzamtzis, R. Sheridan, M.J. Mullen, J. Yap, A.M. Seifalian, and G. Burriesci, *A new transcatheter heart valve concept (the TRISKELE): feasibility in an acute preclinical model.* EuroIntervention, 2016. **12**(7).
42. Jansen, J. and H. Reul, *A synthetic three-leaflet valve.* J Med Eng Technol, 1992. **16**(1): p. 27-33.
43. Oveissi, F., S. Naficy, A. Lee, D.S. Winlaw, and F. Dehghani, *Materials and manufacturing perspectives in engineering heart valves: a review.* Materials Today Bio, 2020. **5**.
44. Leat, M.E. and J. Fisher, *The influence of manufacturing methods on the function and performance of a synthetic leaflet heart valve.* Proc Inst Mech Eng H, 1995. **209**(1): p. 65-9.
45. Heineken, F.G. and R. Skalak, *Tissue Engineering: A Brief Overview.* Journal of Biomechanical Engineering, 1991. **113**(2): p. 111-112.
46. Shinoka, T., C.K. Breuer, R.E. Tanel, G. Zund, T. Miura, P.X. Ma, R. Langer, J.P. Vacanti, and J.E. Mayer, *Tissue engineering heart valves: Valve leaflet replacement study in a lamb model.* The Annals of Thoracic Surgery, 1995. **60**: p. 513-516.
47. De Gaetano, F., P. Bagnoli, A. Zaffora, A. Pandolfi, M. Serrani, J. Brubert, J. Stasiak, G. Moggridge, and M. Costantino, *A Newly Developed Tri-Leaflet Polymeric Heart Valve Prosthesis.* Journal of Mechanics in Medicine and Biology, 2015. **15**.
48. Coulter, F., M. Schaffner, J. Faber, A. Rafsanjani, R. Smith, H. Appa, P. Zilla, D. Bezuidenhout, and A. Studart, *Bioinspired Heart Valve Prosthesis Made by Silicone Additive Manufacturing.* 2019. **1**: p. 266-279.
49. Rotman, O.M., M. Bianchi, R.P. Ghosh, B. Kovarovic, and D. Bluestein, *Principles of TAVR valve design, modelling, and testing.* Expert review of medical devices, 2018. **15**(11): p. 771-791.
50. Rotman, O., B. Kovarovic, M. Bianchi, M. Slepian, and D. Bluestein, *In Vitro Durability and Stability Testing of a Novel Polymeric Transcatheter Aortic Valve Replacement Valve.* ASAIO journal (American Society for Artificial Internal Organs : 1992), 2019. **66**.
51. Rahmani, B., S. Tzamtzis, R. Sheridan, M. Mullen, J. Yap, A. Seifalian, and G. Burriesci, *In Vitro Hydrodynamic Assessment of a New Transcatheter Heart Valve Concept (the TRISKELE).* Journal of cardiovascular translational research, 2017. **10**.
52. Rotman, O.M., B. Kovarovic, W.-C. Chiu, M. Bianchi, G. Marom, M.J. Slepian, and D. Bluestein, *Novel Polymeric Valve for Transcatheter Aortic Valve Replacement Applications: In Vitro Hemodynamic Study.* Annals of biomedical engineering, 2019. **47**(1): p. 113-125.
53. Bhardwaj, N. and S.C. Kundu, *Electrospinning: A fascinating fiber fabrication technique.* Biotechnology Advances, 2010. **28**(3): p. 325-347.
54. Boffito, M., S. Sartori, and G. Ciardelli, *Polymeric scaffolds for cardiac tissue engineering: Requirements and fabrication technologies.* Polymer International, 2014. **63**.
55. Lin, T. and J. Fang, *2. Electrospinning*, in *Fundamentals of Electrospinning & Electrospun Nanofibers*. DEStech Publications.

56. Tucker, N., J. Stanger, M. Staiger, and K. Hofman, *The History of the Science and Technology of Electrospinning from 1600 to 1900*. 2013.
57. Meher, A.K. and Y.-C. Chen, *Electrospray Modifications for Advancing Mass Spectrometric Analysis.* Mass spectrometry (Tokyo, Japan), 2017. **6**.
58. Pillay, V., C. Dott, Y. Choonara, C. Tyagi, L. Tomar, P. Kumar, L. du Toit, and P.D.V. Ndesendo, *A Review of the Effect of Processing Variables on the Fabrication of Electrospun Nanofibers for Drug Delivery Applications.* Journal of Nanomaterials, 2013.
59. Taylor, G., *Disintegration of Water Drops in an Electric Field.* Proceedings of the Royal Society of London. Series A, Mathematical and Physical Sciences, 1964. **280**: p. 383-397.
60. Yarin, A.L., S. Koombhongse, and D. Reneker, *Taylor Cone and Jetting from Liquid Droplets in Electrospinning of Nanofibers.* Journal of Applied Physics, 2001. **90**: p. 4836-4846.
61. Cooley, J.F., *Apparatus for Electrically Dispersing Fluids*. 1900.
62. Doshi, J. and D.H. Reneker, *Electrospinning process and applications of electrospun fibers.* Journal of electrostatics, 1995. **35**(2-3): p. 151-160.
63. Ramakrishna, S., K. Fujihara, W.-E. Teo, T. Yong, Z. Ma, and R. Ramaseshan, *Electrospun nanofibers: solving global issues.* Materials Today, 2006. **9**(3): p. 40-50.
64. Baker, B.M., A.O. Gee, R.B. Metter, A.S. Nathan, R.A. Marklein, J.A. Burdick, and R.L. Mauck, *The potential to improve cell infiltration in composite fiber-aligned electrospun scaffolds by the selective removal of sacrificial fibers.* Biomaterials, 2008. **29**(15): p. 2348-2358.
65. Reneker, D. and I.J.N. Chun, *Nanometre diameter fibres of polymer, produced by electrospinning.* 1996. **7**: p. 216-223.
66. Demir, M.M., I. Yilgor, E. Yilgor, and B. Erman, *Electrospinning of polyurethane fibers.* Polymer, 2002. **43**(11): p. 3303-3309.
67. Zhang, C., X. Yuan, L. Wu, Y. Han, and J. Sheng, *Study on morphology of electrospun poly(vinyl alcohol) mats.* European Polymer Journal, 2005. **41**(3): p. 423-432.
68. Casasola, R., N.L. Thomas, A. Trybala, and S. Georgiadou, *Electrospun poly lactic acid (PLA) fibres: Effect of different solvent systems on fibre morphology and diameter.* Polymer, 2014. **55**(18): p. 4728-4737.
69. Smallwood, I., *Handbook of Organic Solvent Properties.* 1996.
70. Du, J. and Y.-L. Hsieh, *PEGylation of chitosan for improved solubility and fiber formation via electrospinning.* Cellulose, 2007. **14**: p. 543-552.
71. Li, R.L., J. Russ, C. Paschalides, G. Ferrari, H. Waisman, J.W. Kysar, and D. Kalfa, *Mechanical considerations for polymeric heart valve development: Biomechanics, materials, design and manufacturing.* Biomaterials, 2019. **225**.
72. Khan, I., N. Smith, E. Jones, D.S. Finch, and R.E. Cameron, *Analysis and evaluation of a biomedical polycarbonate urethane tested in an in vitro study and an ovine arthroplasty model. Part I: materials selection and evaluation.* Biomaterials, 2005. **26**(6): p. 621-631.
73. Kucinska-Lipka, J., I. Gubanska, H. Janik, and M. Sienkiewicz, *Fabrication of polyurethane and polyurethane based composite fibres by the electrospinning technique for soft tissue engineering of cardiovascular system.* Materials Science and Engineering: C, 2015. **46**: p. 166-176.
74. Saad, B., G. Ciardelli, S. Matter, M. Welti, G.K. Uhlschmid, P. Neuenschwander, and U.W. Suter, *Degradable and highly porous polyesterurethane foam as biomaterial: Effects and phagocytosis of degradation products in osteoblasts.* Journal of Biomedical Materials Research, 1998. **39**(4): p. 594-602.

75. Borkenhagen, M., R.C. Stoll, P. Neuenschwander, U.W. Suter, and P. Aebischer, *In vivo performance of a new biodegradable polyester urethane system used as a nerve guidance channel.* Biomaterials, 1998. **19**(23).
76. Lendlein, A., P. Neuenschwander, and U.W. Suter, *Tissue-compatible multiblock copolymers for medical applications, controllable in degradation rate and mechanical properties.* Macromolecular Chemistry and Physics, 1998. **199**(12).
77. Ladd, M.R., S.J. Lee, J.D. Stitzel, A. Atala, and J.J. Yoo, *Co-electrospun dual scaffolding system with potential for muscle–tendon junction tissue engineering.* Biomaterials, 2011. **32**(6): p. 1549-1559.
78. Driessen-Mol, A., M.Y. Emmert, P.E. Dijkman, L. Frese, B. Sanders, B. Weber, N. Cesarovic, M. Sidler, J. Leenders, R. Jenni, J. Grünenfelder, V. Falk, F.P.T. Baaijens, and S.P. Hoerstrup, *Transcatheter Implantation of Homologous "Off-the-Shelf" Tissue-Engineered Heart Valves With Self-Repair Capacity: Long-Term Functionality and Rapid In Vivo Remodeling in Sheep.* Journal of the American College of Cardiology, 2014. **63**(13): p. 1320-1329.
79. Kluin, J., H. Talacua, A.I.P.M. Smits, M.Y. Emmert, M.C.P. Brugmans, E.S. Fioretta, P.E. Dijkman, S.H.M. Söntjens, R. Duijvelshoff, S. Dekker, M.W.J.T. Janssen-van den Broek, V. Lintas, A. Vink, S.P. Hoerstrup, H.M. Janssen, P.Y.W. Dankers, F.P.T. Baaijens, and C.V.C. Bouten, *In situ heart valve tissue engineering using a bioresorbable elastomeric implant – From material design to 12 months follow-up in sheep.* Biomaterials, 2017. **125**: p. 101-117.
80. Emmert, M.Y., B. Weber, P. Wolint, L. Behr, S. Sammut, T. Frauenfelder, L. Frese, J. Scherman, C.E. Brokopp, C. Templin, J. Grünenfelder, G. Zünd, V. Falk, and S.P. Hoerstrup, *Stem Cell–Based Transcatheter Aortic Valve Implantation: First Experiences in a Pre-Clinical Model.* JACC: Cardiovascular Interventions, 2012. **5**(8): p. 874-883.
81. Emmert, M.Y., B. Weber, L. Behr, T. Frauenfelder, C.E. Brokopp, J. Grünenfelder, V. Falk, and S.P. Hoerstrup, *Transapical Aortic Implantation of Autologous Marrow Stromal Cell-Based Tissue-Engineered Heart Valves: First Experiences in the Systemic Circulation.* JACC: Cardiovascular Interventions, 2011. **4**(7): p. 822-823.
82. Emmert, M.Y., B. Weber, L. Behr, S. Sammut, T. Frauenfelder, P. Wolint, J. Scherman, D. Bettex, J. Grünenfelder, V. Falk, and S.P. Hoerstrup, *Transcatheter aortic valve implantation using anatomically oriented, marrow stromal cell-based, stented, tissue-engineered heart valves: technical considerations and implications for translational cell-based heart valve concepts.* European Journal of Cardio-Thoracic Surgery, 2014. **45**(1): p. 61-68.
83. Lintas, V., E. Fioretta, S. Motta, P. Dijkman, M. Pensalfini, E. Mazza, E. Caliskan, H. Rodriguez Cetina Biefer, M. Lipiski, M. Sauer, N. Cesarovic, S. Hoerstrup, and M. Emmert, *Development of a Novel Human Cell-Derived Tissue-Engineered Heart Valve for Transcatheter Aortic Valve Replacement: an In Vitro and In Vivo Feasibility Study.* Journal of Cardiovascular Translational Research, 2018. **11**.
84. Emmert, M.Y., B.A. Schmitt, S. Loerakker, B. Sanders, H. Spriestersbach, E.S. Fioretta, L. Bruder, K. Brakmann, S.E. Motta, V. Lintas, P.E. Dijkman, L. Frese, F. Berger, F.P.T. Baaijens, and S.P. Hoerstrup, *Computational modeling guides tissue-engineered heart valve design for long-term in vivo performance in a translational sheep model.* Science Translational Medicine, 2018. **10**(440).
85. Miyazaki, Y., O. Soliman, M. Abdelghani, A. Katsikis, C. Naz, S. Lopes, B. Warnack, M. Cox, Y. Onuma, and P. Serruys, *Acute performance of a novel restorative transcatheter aortic valve: Preclinical results.* EuroIntervention : journal of EuroPCR in collaboration with the Working Group on Interventional Cardiology of the European Society of Cardiology, 2017. **13**.

86. Morales, D.L., C. Herrington, E.A. Bacha, V.O. Morell, Z. Prodán, T. Mroczek, S. Sivalingam, M. Cox, G. Bennink, and F.M. Asch, *A Novel Restorative Pulmonary Valve Conduit: Early Outcomes of Two Clinical Trials.* 2021. **7**(367).
87. Horst, M., V. Milleret, S. Nötzli, S. Madduri, T. Sulser, R. Gobet, and D. Eberli, *Increased porosity of electrospun hybrid scaffolds improved bladder tissue regeneration.* Journal of biomedical materials research. Part A, 2014. **102**.
88. Ding, B., E. Kimura, T. Sato, S. Fujita, and S. Shiratori, *Fabrication of blend biodegradable nanofibrous nonwoven mats via multi-jet electrospinning.* Polymer, 2004. **45**(6): p. 1895-1902.
89. Moreira, R., T. Velz, N. Alves, V.N. Gesche, A. Malischewski, T. Schmitz-Rode, J. Frese, S. Jockenhoevel, and P. Mela, *Tissue-Engineered Heart Valve with a Tubular Leaflet Design for Minimally Invasive Transcatheter Implantation.* Tissue Engineering Part C: Methods, 2014. **21**(6): p. 530-540.
90. Sanders, B., S. Loerakker, E.S. Fioretta, D.J.P. Bax, A. Driessen-Mol, S.P. Hoerstrup, and F.P.T. Baaijens, *Improved Geometry of Decellularized Tissue Engineered Heart Valves to Prevent Leaflet Retraction.* Annals of Biomedical Engineering, 2016. **44**(4): p. 1061-1071.
91. Shin, J.-w., H. Shin, S.-J. Heo, Y. Lee, Y. Hwang, D.-H. Kim, J. Kim, and J. Shin, *Hybrid nanofiber scaffolds of polyurethane and poly(Ethylene oxide) using dual-electrospinning for vascular tissue engineering*. 2007. p. 692-695.
92. Milleret, V., B. Simona, P. Neuenschwander, and H. Hall, *Tuning electrospinning parameters for production of 3D-fiberfleeces with increased porosity for soft tissue engineering applications.* European cells & materials, 2011. **21**: p. 286-303.
93. Stalder, A.F., T. Melchior, M. Müller, D. Sage, T. Blu, M. Unser, *Low-Bond Axisymmetric Drop Shape Analysis for Surface Tension and Contact Angle Measurements of Sessile Drops*, in *Colloids And Surfaces A: Physicochemical And Engineering Aspects*. September, 2010.
94. Raheem, Z., *Standard Test Method for Tensile Properties of Plastics 1*. 2019.
95. Sharma, S. and D.A. Siginer, *Permeability Measurement Methods in Porous Media of Fiber Reinforced Composites.* Applied Mechanics Reviews, 2010. **63**(2).
96. Voorneveld, J., *High Porosity Electrospun Scaolds for Small Diameter Vascular Graft Applications*, in *Department of Human Biology*. 2015, University of Cape Town: Cape Town. p. 143.
97. Yalcinkaya, F., O. Jirsak, and R. Gemci, *Effect of Polymer Concentration on Electrospinning System*. 2010.
98. Nezarati, R.M., M.B. Eifert, and E. Cosgriff-Hernandez, *Effects of humidity and solution viscosity on electrospun fiber morphology.* Tissue engineering. Part C, Methods, 2013. **19**(10): p. 810-819.
99. Luo, C.J., E. Stride, and M. Edirisinghe, *Mapping the influence of solubility and dielectric constant on electrospinning polycaprolactone solutions.* Macromolecules, 2012.
100. Gu, X., X. Song, C. Shao, P. Zeng, X. Lu, X. Shen, and Q. Yang, *Electrospinning of poly(butylene-carbonate): Effect of Solvents on the Properties of the Nanofibers Film.* International Journal of Electrochemical Science, 2014. **9**: p. 8045-8056.
101. Du, L., H. Xu, Y. Zhang, and F. Zou, *Electrospinning of polycaprolatone nanofibers with DMF additive: The effect of solution proprieties on jet perturbation and fiber morphologies.* Fibers and Polymers, 2016. **17**: p. 751-759.
102. Sill, T. and H. Recum, *Electrospinning: Applications in Drug Delivery and Tissue Engineering.* Biomaterials, 2008. **29**: p. 1989-2006.

103. Amariei, N., L. Manea, A. Bertea, A. Bertea, and P. Alexandru, *The Influence of Polymer Solution on the Properties of Electrospun 3D Nanostructures.* IOP Conference Series: Materials Science and Engineering, 2017. **209**.
104. Wang, Z., Y. Cui, J. Wang, X. Yang, Y. Wu, K. Wang, X. Gao, D. Li, Y. Li, X.-L. Zheng, Y. Zhu, D. Kong, and Q. Zhao, *The effect of thick fibers and large pores of electrospun poly(ε-caprolactone) vascular grafts on macrophage polarization and arterial regeneration.* Biomaterials, 2014. **35**(22): p. 5700-5710.
105. Megelski, S., J. Stephens, D. Chase, and J. Rabolt, *Micro- and Nanostructured Surface Morphology on Electrospun Polymer Fibers.* Macromolecules, 2002. **35**.
106. Jung, J.H., M. Ree, and H. Kim, *Acid- and base-catalyzed hydrolyses of aliphatic polycarbonates and polyesters.* Catalysis Today, 2006. **115**(1): p. 283-287.
107. Hong, Y., *19 - Electrospun fibrous polyurethane scaffolds in tissue engineering*, in *Advances in Polyurethane Biomaterials*, S.L. Cooper and J. Guan, Editors. 2016, Woodhead Publishing. p. 543-559.
108. Buschmann, J., M. Calcagni, G. Meier, E. Bonavoglia, P. Neuenschwander, V. Milleret, and P. Giovanoli, *Synthesis, characterization and histomorphometric analysis of cellular response to a new elastic DegraPol® polymer for rabbit Achilles tendon rupture repair: Comparison of classic and new elastic electrospun DegraPol® polymers.* Journal of tissue engineering and regenerative medicine, 2012. **9**.
109. `Pírková, M., J. Hodan, L. Kobera, J. Kredátusova, D. Kubies, L. Machová, R. Por ba, M. Serkis, A. Zhigunov, J.J.P.D. Kotek, and Stability, *The influence of the length of the degradable segment on the functional properties and hydrolytic stability of multi-component polyurethane elastomeric films.* 2017. **137**: p. 216-228.
110. Henry, J., M. Simonet, A. Pandit, and P. Neuenschwander, *Characterization of a slowly degrading biodegradable polyesterurethane for tissue engineering scaffolds.* Journal of biomedical materials research. Part A, 2007. **82**.
111. Mondal, S. and D. Martin, *Hydrolytic degradation of segmented polyurethane copolymers for biomedical applications.* Polymer Degradation and Stability, 2012. **97**: p. 1553–1561.
112. Hart, J.D., G. Cacciola, P.J.G. Schreurs, and G.W.M. Peters, *A three-dimensional analysis of a fibre-reinforced aortic valve prosthesis.* Journal of Biomechanics, 1998. **31**(7): p. 629-638.
113. Stella, J.A., J. Liao, and M.S. Sacks, *Time-dependent biaxial mechanical behavior of the aortic heart valve leaflet.* Journal of Biomechanics, 2007. **40**(14): p. 3169-3177.
114. Hasan, A., K. Ragaert, W. Swieszkowski, S. Selimović, A. Paul, G. Camci-Unal, M.R. Mofrad, and A. Khademhosseini, *Biomechanical properties of native and tissue engineered heart valve constructs.* J Biomech, 2014. **47**(9).
115. McClure, M., S. Sell, D. Simpson, and G. Bowlin, *Electrospun Polydioxanone, Elastin, and Collagen Vascular Scaffolds: Uniaxial Cyclic Distension.* Journal of Engineered Fibers and Fabrics, 2009. **4**: p. 18-25.
116. Limbert, G., R. Omar, H. Krynauw, D. Bezuidenhout, and T. Franz, *The anisotropic mechanical behaviour of electro-spun biodegradable polymer scaffolds: Experimental characterisation and constitutive formulation.* Journal of the Mechanical Behavior of Biomedical Materials, 2016. **53**: p. 21-39.
117. Lendlein, A., M. Colussi, P. Neuenschwander, U.J.M.C. Suter, and Physics, *Hydrolytic Degradation of Phas… Segregated Multiblock Copoly(ester urethane)s Containing Weak Links.* 2001. **202**: p. 2702-2711.

118. Loh, X.J., K.K. Tan, X. Li, and J. Li, *The in vitro hydrolysis of poly(ester urethane)s consisting of poly[(R)-3-hydroxybutyrate] and poly(ethylene glycol).* Biomaterials, 2006. **27**(9): p. 1841-1850.
119. Wang, W., Y. Guo, and J. Otaigbe, *Synthesis and characterization of novel biodegradable and biocompatible polyurethane thin films prepared by homogeneous solution polymerization.* Polymer, 2008. **49**: p. 4393–4398.
120. Hafeman, A.E., K.J. Zienkiewicz, A.L. Zachman, H.-J. Sung, L.B. Nanney, J.M. Davidson, and S.A. Guelcher, *Characterization of the degradation mechanisms of lysine-derived aliphatic poly(ester urethane) scaffolds.* Biomaterials, 2011. **32**(2): p. 419-429.
121. Wang, W., Y. Guo, and J.J.P. Otaigbe, *Synthesis, characterization and degradation of biodegradable thermoplastic elastomers from poly(ester urethane)s and renewable soy protein isolate biopolymer.* 2010. **51**: p. 5448-5455.
122. Wang, C. and M. Wang, *Dual-source dual-power electrospinning and characteristics of multifunctional scaffolds for bone tissue engineering.* Journal of materials science. Materials in medicine, 2012. **23**.
123. Salam, A., M.Q. Khan, T. Hassan, N. Hassan, A. Nazir, T. Hussain, M. Azeem, and I.S. Kim, *In-vitro assessment of appropriate hydrophilic scaffolds by co-electrospinning of poly(1,4 cyclohexane isosorbide terephthalate)/polyvinyl alcohol.* Scientific Reports, 2020. **10**(1).
124. Evrova, O., J. Houska, M. Welti, E. Bonavoglia, M. Calcagni, P. Giovanoli, V. Vogel, and J. Buschmann, *Bioactive, Elastic, and Biodegradable Emulsion Electrospun DegraPol Tube Delivering PDGF-BB for Tendon Rupture Repair.* Macromolecular Bioscience, 2016. **16**(7): p. 1048-1063.
125. Chernonosova, V., A. Gostev, I. Murashov, B. Chelobanov, A. Karpenko, and P. Laktionov, *Assessment of Electrospun Pellethane-Based Scaffolds for Vascular Tissue Engineering.* Materials (Basel, Switzerland), 2021. **14**(13).
126. Tamada, Y. and Y. Ikada, *Effect of Preadsorbed Proteins on Cell Adhesion to Polymer Surfaces.* Journal of Colloid and Interface Science, 1993. **155**(2): p. 334-339.
127. Niemczyk-Soczynska, B., A. Gradys, and P. Sajkiewicz, *Hydrophilic Surface Functionalization of Electrospun Nanofibrous Scaffolds in Tissue Engineering.* Polymers (Basel), 2020. **12**(11).
128. Sell, S., C. Barnes, D. Simpson, and G. Bowlin, *Scaffold permeability as a means to determine fiber diameter and pore size of electrospun fibrinogen.* Journal of biomedical materials research. Part A, 2008. **85**.
129. Anderson, W.G., *Wettability Literature Survey Part 5: The Effects of Wettability on Relative Permeability.* Journal of Petroleum Technology, 1987. **39**(11): p. 1453-1468.
130. Pensalfini, M., S. Meneghello, V. Lintas, K. Bircher, A.E. Ehret, and E. Mazza, *The suture retention test, revisited and revised.* Journal of the Mechanical Behavior of Biomedical Materials, 2017. **77**.
131. Bergmeister, H., C. Schreiber, C. Grasl, I. Walter, R. Plasenzotti, M. Stoiber, D. Bernhard, and H. Schima, *Healing characteristics of electrospun polyurethane grafts with various porosities.* Acta Biomaterialia, 2013. **9**(4): p. 6032-6040.
132. Montini Ballarin, F., D. Calvo, P. Caracciolo, F. Rojo, P. Frontini, G. Abraham, and G. Guinea-Totuero, *Mechanical behavior of bilayered small-diameter nanofibrous structures as biomimetic vascular grafts.* Journal of the Mechanical Behavior of Biomedical Materials, 2016. **60**.
133. Ebersole, G.C., E.G. Buettmann, M.R. MacEwan, M.E. Tang, M.M. Frisella, B.D. Matthews, and C.R. Deeken, *Development of novel electrospun absorbable polycaprolactone (PCL) scaffolds for hernia repair applications.* Surg Endosc, 2012. **26**(10).

134. Patti, A., F. Costa, M. Perrotti, D. Barbarino, and D. Acierno, *Polyurethane Impregnation for Improving the Mechanical and the Water Resistance of Polypropylene-Based Textiles.* Materials (Basel), 2021. **14**(8).
135. Cacciola, G., G.W.M. Peters, and F.P.T. Baaijens, *A synthetic fiber-reinforced stentless heart valve.* Journal of Biomechanics, 2000. **33**(6): p. 653-658.
136. Grabow, N., K. Schmohl, A. Khosravi, M. Philipp, M. Scharfschwerdt, B. Graf, C. Stamm, A. Haubold, K.-P. Schmitz, and G. Steinhoff, *Mechanical and Structural Properties of a Novel Hybrid Heart Valve Scaffold for Tissue Engineering.* Artificial organs, 2004. **28**.
137. Zakko, J., K.M. Blum, J.D. Drews, Y.-L. Wu, H. Hatoum, M. Russell, S. Gooden, M. Heitkemper, O. Conroy, J. Kelly, S. Carey, M. Sacks, K. Texter, E. Ragsdale, J. Strainic, M. Bocks, Y. Wang, L.P. Dasi, A.K. Armstrong, and C. Breuer, *Development of Tissue Engineered Heart Valves for Percutaneous Transcatheter Delivery in a Fetal Ovine Model.* 2020. **5**(8): p. 815-828.
138. Syedain, Z.H., A.C. Jenson, P.S. Patel, C. Feagler, L. Bahmer, R. Faizer, and R.T. Tranquillo, *Tissue-engineered transcatheter vein valve.* Biomaterials, 2019. **216**.
139. Stasiak, J.R., M. Serrani, E. Biral, J.V. Taylor, A.G. Zaman, S. Jones, T. Ness, F. De Gaetano, M.L. Costantino, V.D. Bruno, S. Suleiman, R. Ascione, and G.D. Moggridge, *Design, development, testing at ISO standards and in vivo feasibility study of a novel polymeric heart valve prosthesis.* Biomater Sci, 2020. **8**(16): p. 4467-4480.
140. Bernacca, G.M., B. O'Connor, D.F. Williams, and D.J. Wheatley, *Hydrodynamic function of polyurethane prosthetic heart valves: influences of Young's modulus and leaflet thickness.* Biomaterials, 2002. **23**(1): p. 45-50.
141. Li, R., J. Russ, C. Paschalides, G. Ferrari, H. Waisman, J. Kysar, and D. Kalfa, *Mechanical considerations for polymeric heart valve development: Biomechanics, materials, design and manufacturing.* Biomaterials, 2019. **225**.
142. Martin, C. and W. Sun, *Simulation of long-term fatigue damage in bioprosthetic heart valves: effects of leaflet and stent elastic properties.* Biomechanics and modeling in mechanobiology, 2014. **13**(4): p. 759-770.
143. Kütting, M., J. Roggenkamp, U. Urban, T. Schmitz-Rode, and U. Steinseifer, *Polyurethane heart valves: past, present and future.* Expert Rev Med Devices, 2011. **8**(2): p. 227-233.
144. Choe, J., S. Jana, B. Tefft, R. Hennessy, J. Go, D. Morse, A. Lerman, and M. Young, *Biomaterial Characterization of Off-the-Shelf Decellularized Porcine Pericardial Tissue for use in Prosthetic Valvular Applications.* Journal of Tissue Engineering and Regenerative Medicine, 2017. **12**.
145. Nachlas, A.L.Y., S. Li, and M.E. Davis, *Developing a Clinically Relevant Tissue Engineered Heart Valve—A Review of Current Approaches.* Advanced Healthcare Materials, 2017. **6**(24).
146. Brugmans, M.M.C.P., R.S. Soekhradj-Soechit, D. van Geemen, M. Cox, C.V.C. Bouten, F.P.T. Baaijens, and A. Driessen-Mol, *Superior Tissue Evolution in Slow-Degrading Scaffolds for Valvular Tissue Engineering.* Tissue Engineering Part A, 2015. **22**(1-2): p. 123-132.

7 Appendices

A – Pulse duplicator results for valve prototypes

Table 14 - Pulse duplicator results for all valves tested

	D1	D2	H1	H2	H3	P1	P2	St. Jude [136]
Trans aortic mean pressure [P] (mmHg)	7.42 ±0.06	8.12 ±0.1	7.41 ±0.08	7.98 ±0.09	7.95 ±0.09	7.15 ±0.06	7.56 ±0.05	±8
Pump stroke volume (ml)	75.01 ±0	74.99 ±0	75.09 ±0	75.06 ±0.04	74.99 ±0.04	74.97 ±0.04	75.02 ±0.05	49.6
Systolic percent of cycle	36.41 ±1.04	36.72 ±0.41	36.33 ±0.96	36.6 ±0.67	36.88 ±0.33	36.8± 0.68	36.8 ±0.75	
Aortic forward volume (ml)	65.72 ±0.17	64.7 ±0.27	63.96 ±0.16	62.59 ±0.22	63.28 ±0.32	62.93 ±0.17	62.23 ±0.43	
Aortic closing volume (ml)	-11.81 ±1.36	-16.943 ±1.01	-6.25 ±0.75	-11.44 ±0.33	-6.41 ±1.07	-11.68 ±0.57	-5.26 ±0.96	-2.0
Aortic leakage volume (ml)	-22.39 ±1.1	-22.4 ±1.28	-12 ±0.58	-5.28± 0.34	-12.84 ±0.78	-10.72 ±0.38	-10.27 ±0.98	-5.0
Total Aortic regurgitation fraction (%)	52.04 ±0.65	60.81 ±1.25	28.53 ±0.93	26.71 ±0.93	30.42 ±1.44	35.6 ±0.76	24.96 ±2.29	±14
Aortic orifice area [P] (cm^2)	2.1 ±0.01	1.98 ±0.01	2.12 ±0.01	2.02 ±0.01	2.03 ±0.01	2.12 ±0.01	2.05 ±0.01	